The interactomes of ALS/FTD associated poly-GR/PR link protein translation to disease pathogenesis

Dissertation zum Erwerb des Doktorgrades der Naturwissenschaften an der Medizinischen Fakultät der Ludwig-Maximilians-Universität München im Jahr 2019

vorgelegt von M.Sc.

Hannelore Hartmann

geboren am 22. Oktober 1988 in Iaşi

Gedruckt mit der Genehmigung der Medizinischen Fakultät der Universität München

Betreuer: Prof. Dr. rer. nat. Dr. h. c. Christian Haass

                                       _____

Zweitgutachterin: PD Dr. Florence Bareyre

Dekan: Prof. Dr. med. dent. Reinhard Hickel

Datum der mündlichen Prüfung: 03. Dezember 2019

Eidesstattliche Versicherung

<u>Hartmann, Hannelore</u>

Name, Vorname

Ich erkläre hiermit an Eides statt,

dass ich die vorliegende Dissertation mit dem Thema „*The interactomes of ALS/FTD associated poly-GR/PR link protein translation to disease pathogenesis*" selbständig verfasst, mich außer der angegebenen keiner weiteren Hilfsmittel bedient und alle Erkenntnisse, die aus dem Schrifttum ganz oder annähernd übernommen sind, als solche kenntlich gemacht und nach ihrer Herkunft unter Bezeichnung der Fundstelle einzeln nachgewiesen habe.

Ich erkläre des Weiteren, dass die hier vorgelegte Dissertation nicht in gleicher oder in ähnlicher Form bei einer anderen Stelle zur Erlangung eines akademischen Grades eingereicht wurde.

<u>München, den 28.02.2020</u>

Ort, Datum

<u>Hannelore Hartmann</u>

Unterschrift Doktorandin/Doktorand

SUMMARY

The (GGGGCC)$_n$ repeat expansion within the first intron of the *C9orf72* gene is the most common known genetic cause of amyotrophic lateral sclerosis (ALS) and frontotemporal dementia (FTD). So far, three non-exclusive potential mechanisms underlying *C9orf72*-mediated neurodegeneration are described. First, reduced expression of the mutated *C9orf72* allele may impair the physiological function of the C9orf72 protein. Second, the repeat-containing RNA accumulates in nuclear foci and sequesters RNA-binding proteins, which might trigger a loss-of-function mechanism. And third, unconventional repeat associated non-ATG (RAN) translation of the expanded repeat results in aggregation-prone dipeptide repeat (DPR) proteins, namely, poly-GA, poly-GP, poly-GR, poly-PR, and poly-PA, which are potentially toxic. These DPR proteins are found in cytoplasmic inclusions throughout the patient brain. While poly-GA is the most abundant species, poly-GR and poly-PR expression is most toxic in many model systems. Although extensive *in vitro* work has been done on the characterization of DPR proteins, their role in disease pathogenesis remains unclear. In order to elucidate potential toxic mechanisms underlying the arginine-rich DPR proteins poly-GR and poly-PR, I analyzed their interactome in primary neurons and HEK293 cells and validated the results in patient tissue.

I identified close to 600 GFP-(GR)$_{149}$ and (PR)$_{175}$-GFP interacting proteins in primary neurons with significant overlap, particularly in RNA-binding proteins. Analysis revealed that interactors are especially enriched for components of stress granules, the nucleolus, the ribosome, and the splicing machinery. Stress granules are cellular membrane-less compartments which form upon cellular stress and mainly contain stalled translation pre-initiation complexes. The nucleolus represents the site of ribosome biogenesis, while the ribosome itself is a complex molecular machinery responsible for protein synthesis. The interactomes of poly-GR and poly-PR in HEK293 corroborate the pathways and compartments identified in neurons.

In order to validate individual interactors, I performed overexpression experiments with over 30 interacting proteins. I mainly tested interactors associated with stress granules, the nucleolus, and the ribosome and their effect on poly-GR/poly-PR localization as well as expression and *vice versa*. Under control conditions, poly-GR is expressed in the nucleolus and diffusely distributes in the cytoplasm, whereas poly-PR mainly localizes to the nucleolus in HEK293 cells. In neurons, poly-GR is mainly found in the cytoplasm and poly-PR exclusively localizes to the nucleolus. To assess the role of stress granules, I co-expressed the poly-GR/PR interacting stress granule proteins STAU1, STAU2, and YBX1 together

with poly-GR/poly-PR in both cell systems. Interestingly, all tested stress granule proteins rerouted poly-GR/PR into large cytoplasmic granules which were positive for the stress granule marker G3BP1. Importantly, STAU2 colocalizes with poly-GR in *C9orf72* patient brains suggesting it is a disease-relevant interactor. Moreover, closer examination of the nucleolus revealed that poly-PR expression disrupts uniform distribution of nucleolar proteins such as NOP56 and Fibrillarin suggesting that also nucleolar functions, such as assembly of ribosomes, might be comprised. In addition, expression of the nucleolar component NPM1 recruited otherwise cytoplasmic poly-$(GR)_{149}$ into the nucleolus. Regarding the ribosome, expression of toxic nucleolar poly-$(PR)_{175}$, but not cytoplasmic poly-$(GR)_{149}$, significantly reduced levels of several ribosomal subunits which was accompanied by a comparable reduction in overall protein synthesis. Surprisingly, truncated poly-GR versions localized to the nucleolus and inhibited translation – like poly-PR. In accordance, boosting protein synthesis by overexpression of MEK1 blunted poly-GR/PR toxicity. Most importantly, I detected ribosomal proteins in poly-GR/PR inclusions in *C9orf72* ALS/FTD brains. This direct interaction between poly-GR/PR and the ribosome was confirmed *in vitro*.

In summary, this study provides the first poly-PR/GR interactome in primary neurons and identifies ribosomes as a direct link between the toxicity of poly-GR/PR *in vitro* and in *C9orf72* patients. It shows that the two arginine-rich DPR proteins alter stress granule formation, disrupt nucleolar organization and reduce ribosomal subunits as well as protein synthesis. Together these findings suggest that impaired ribosome biogenesis and/or function may drive acute neurotoxicity underlying poly-GR and poly-PR expression *in vitro* and contribute to chronic toxicity *in vivo*. These intriguing findings might pave ways for new therapeutic strategies targeting *C9orf72*-mediated ALS/FTD.

ZUSAMMENFASSUNG

Eine Verlängerung der (GGGGCC)$_n$ Repeatsequenz im nicht-kodierenden Bereich des *C9orf72*-Gens ist als die häufigste genetische Ursache Amyotropher Lateralsklerose (ALS) und Frontotemporaler Demenz (FTD) bekannt. Umfangreiche Forschungsarbeiten konnten bisher drei mögliche nicht-exklusive Mechanismen der *C9orf72*-assoziierten Neurodegeneration aufdecken. Erstens, wird das mutierte *C9orf72* Allel geringer exprimiert, so dass die physiologische C9orf72-Funktion beeinträchtigt sein könnte. Zweitens, könnte die Akkumulation der Repeat-RNA in nukleäre Foci, durch die Sequestrierung von RNA-bindenden Proteinen, zu Neurodegeneration führen. Drittens, entstehen durch unkonventionelle Translation der Repeatsequenz fünf aggregationsanfällige Dipeptid Repeat (DPR)-Proteine, genauer poly-GA, poly-GP, poly-GR, poly-PR und poly-PA, welche neuronale zytoplasmatische Einschlüsse bilden und ebenfalls zu neuronalem Zelltod beitragen könnten. Während poly-GA die am häufigsten vorkommende DPR-Protein-Spezies ist, gelten poly-GR und poly-PR allgemein als die toxischsten Aggregat-Typen in vielen Modelsystemen. Obwohl intensiv an der Charakterisierung von DPR-Proteinen und deren Auswirkungen gearbeitet wird, bleibt ihre exakte Rolle im Krankheitsverlauf weiterhin unklar. Um den Beitrag der Arginin-reichen DPR Proteine poly-GR und poly-PR zur zellulären Toxizität zu entschlüsseln, habe ich in dieser Arbeit umfangreiche Interaktom-Studien in primären Neuronen und HEK293 Zellen durchgeführt und die Ergebnisse in Patientengewebe validiert.

Ich konnte nahezu 600 GFP-(GR)$_{149}$- und (PR)$_{175}$-GFP-interagierende Proteine in primären Neuronen identifizieren und zeigen, dass die beiden DPR-Proteine zahlreiche RNA-bindende Interaktoren gemeinsam haben, darunter Splicing-, Stress Granule-, Nukleoli- und Ribosomkomponenten. Sogenannte Stress Granules sind zelluläre membranlose Kompartimente, welche sich aufgrund von zellulärem Stress bilden und hauptsächlich aus blockierten Translationskomplexen bestehen. Der Nukleolus stellt den Ort der Ribosombiogenese dar und das Ribosom ist die molekulare Maschine, welche für die Proteinsynthese zuständig ist. In den poly-GR/PR-Interaktomen von HEK293-Zellen waren Proteine mit Funktionen in ähnlichen zellulären Vorgängen und Kompartimenten angereichert.

Um verschiedene Interaktoren individuell zu validieren, führte ich Überexpressionsexperimente mit über 30 poly-GR- und poly-PR-bindenden Proteinen durch. Dabei untersuchte ich hauptsächlich Proteine aus Stress Granules, dem Nukleolus und Ribosomen. Unter Kontroll-Bedingungen war poly-GR in HEK293-Zellen im Nukleolus und diffus im Zytoplasma zu finden, während poly-PR primär im

Nukleolus lokalisierte. In Neuronen verteilte sich poly-GR gleichmäßig im Zytoplasma. Poly-PR lokalisierte ausschließlich im Nukleolus. Um die Rolle der Stress Granules in poly-GR/PR-vermittelter Toxizität aufzudecken, ko-exprimierte ich die Stress Granule-Proteine STAU1, STAU2 und YBX1 zusammen mit poly-GR/poly-PR in beiden Zellsystemen. Interessanterweise führte dies zu der Bildung großer zytoplasmatischer Einschlüsse, in welchen nicht nur die jeweiligen Stress Granule-Proteine, sondern auch poly-GR und poly-PR akkumulierten. Darüber hinaus kolokalisierte STAU2 mit poly-GR-Einschlüssen in *C9orf72*-ALS/FTD-Patienten und wurde so auch im menschlichen Gewebe als Interaktor validiert. Weiterhin ergab die Untersuchung des Nukleolus in Neuronen, dass poly-PR die ansonsten gleichmäßige Verteilung nukleolärer Proteine wie NOP56 oder Fibrillarin erheblich stört und somit auch nukleoläre Funktionen, wie die Zusammensetzung der Ribosomen, beeinträchtig sein könnten. Zudem wurde zytoplasmatisches poly-$(GR)_{149}$ von NPM1, einem Protein, welches Aufgaben in der Ribosombiogenese übernimmt, in den Nukleolus rekrutiert. Anschließend ergab die detaillierte Analyse ribosomaler Proteine, dass die Expression des toxischen, nukleolären poly-$(PR)_{175}$, aber nicht die des zytoplasmatischen poly-$(GR)_{149}$, die Proteinmenge von mehreren ribosomalen Untereinheiten in Neuronen herabsetzt und dies mit vergleichbarer Reduktion der Proteinsynthese einhergeht. Interessanterweise wurden ähnliche Effekte mit einer verkürzten poly-GR-Version erzielt, welche im Nukleolus lokalisierte und nachweislich toxisch war. Steigerung der Proteinsynthese durch MEK1 reduzierte die zelluläre DPR-Toxizität. Die bedeutendste Beobachtung dieser Arbeit jedoch ist, dass ribosomale Untereinheiten in poly-GR/PR Einschlüssen in *C9orf72*-ALS/FTD Gehirnen zu finden sind. Diese direkte Interaktion konnte ich auch *in vitro* bestätigen.

Insgesamt enthält diese Arbeit die erste poly-PR/GR-Interaktom-Studie in primären Neuronen und identifiziert Ribosomen als direkte Verbindung zwischen poly-GR/PR-Toxizität *in vitro* und in *C9orf72*-Patienten. Sie zeigt, dass die beiden Arginin-reichen DPR-Proteine Stress Granules beeinflussen, die Organisation des Nukleolus stören und sowohl Ribosom-Menge als auch Proteinsynthese reduzieren. Zusammen implizieren diese Beobachtungen, dass eine beeinträchtigte Ribosombiogenese und/oder -funktion die Ursache von poly-GR- und poly-PR-vermittelter Neurotoxizität sind. Diese Erkenntnisse könnten zu neuen Therapiestrategien für *C9orf72*-ALS/FTD führen.

Table of Content

1. INTRODUCTION

1.1. Amyotrophic lateral sclerosis and frontotemporal dementia

Amyotrophic lateral sclerosis (ALS) and frontotemporal lobar dementia (FTD) are two devastating neurodegenerative diseases with no available cure or causal therapy so far. Both diseases are rapidly progressing with a typical onset at ~55 and <65 years, respectively (Chio et al., 2013; Vieira et al., 2013). With an incidence of 5.4/100,000 per year, ALS is considered the most common neurological disorder affecting the upper and lower motor neurons (Chio et al., 2013). FTD occurs with an incidence of 2.7-4.1 per 100,000 and represents the third most common form of dementia following Alzheimer's disease and Lewy bodies-associated dementia (Onyike and Diehl-Schmid, 2013; Vieira et al., 2013). Over the years it became clear that ALS and FTD are linked by overlapping clinical symptoms, pathology and genetics and thereby represent two extremes in a disease spectrum.

1.1.1. Clinical features of ALS and FTD

In 1869, Jean-Martin Charcot described ALS as a separate disease for the first time. The French neurologist observed progressive paralysis with and without contractures as well as muscle atrophy in affected individuals and linked these symptoms to motor neurons in the brain and spinal cord (Kumar et al., 2011). Today, hyperreflexia, spasticity, progressive muscle weakness and atrophy are considered the major symptoms of ALS. Disease often starts in the limbs, rapidly spreads to other muscle groups and ultimately leads to respiratory failure (Van Damme and Robberecht, 2009) defining ALS as a relentlessly progressive disease (Talbot, 2009). After symptom onset, 50% of patients die within 30 months and about 20% of patients survive 5 years. After 10 years, only a small percentage of patients is alive.

In FTD, first described by Arnold Pick, three different variants are distinguished based on the predominant clinical symptoms, namely behavioral variant FTD (bvFTD) and primary progressive aphasia (PPA). The latter is subdivided in semantic dementia (SD) and progressive non-fluent aphasia (PNFA). The most common form of FTD, bvFTD, is characterized by changes in social conduct and personality expressed by apathy, inappropriate or ritualistic behaviors, inertia or loss of sympathy emerging from degeneration in the frontal lobe. (Bang et al., 2015). The most pronounced symptoms of SD are impaired naming and word comprehension resulting from early asymmetrical degeneration of anterior temporal lobes and amygdala (Josephs et al., 2008; Seeley et al., 2005). Lastly, patients with PNFA show slow, effortful and halted speech production as well as agrammatism. Over time, all three

FTD syndromes converge and lead to global cognitive impairment. The bed-ridden patients usually die from pneumonia or secondary infections (Bang et al., 2015).

Interestingly, 15% of FTD diagnosed patients are estimated are estimated to develop symptoms consistent with a typical definition of ALS (Goldman et al., 2005; Rosso et al., 2003) and *vice versa*, up to 50% of ALS patients present some FTD-like symptoms (Abrahams et al., 2004; Mackenzie and Feldman, 2005) providing evidence that ALS and FTD are two distinct ends of a broad disease spectrum. Therefore, patients representing both ALS and FTD symptoms are referred to as ALS/FTD patients.

1.1.2. Pathological features and genetics of ALS/FTD

Pathologically, ALS shows loss of upper motor neurons, located in the cerebral cortex, and lower motor neurons, found in the brainstem and spinal cord while FTD is associated with degeneration of the frontal and temporal lobe. Nonetheless, in both disorders, common pathological protein inclusions are found in different areas of the brain which are thought to eventually cause cell death (Ferrari et al., 2011). In ALS, the pathological hallmarks are mainly transactive response (TAR) DNA binding protein (TDP-43), superoxide dismutase (SOD1) and Fused in sarcoma (FUS) inclusions being present in 97%, 2% and <1% of patient brains, respectively (Ling et al., 2013). In FTD, 45% of cases display TDP-43 aggregates and another 45% have mainly hyperphosphorylated TAU inclusions. FUS aggregates account for 9% of FTD cases, the remaining 1% show aggregates that can only be stained with markers for the ubiquitin proteasome system. Together, TDP-43 and FUS pathological inclusions are most abundant in both ALS and FTD (Figure 1-1**A** and **B**).

However, ALS and FTD do not only share similar types of neuropathological inclusions, but also show overlapping genetic features. Although most ALS and FTD cases are sporadic, familial ALS (fALS) and FTD (fFTD) caused by mutations in various genes, account for approximately 10% and 40% of patients, respectively, and are mostly inherited in an autosomal-dominant manner (Boylan, 2015; Rohrer et al., 2009). In the last years, a variety of genes was linked to either pure ALS, pure FTD or mixed ALS/FTD. *SOD1* is the gene which is most strongly associated with pure ALS and is found to be mutated in up to 20% of familial and up to 2% of sporadic cases (Al-Chalabi et al., 2012). Also mutations in the genes *TARDBP*, encoding for TDP-43, and *FUS* are connected specifically to ALS in 9% of familial patients (Renton et al., 2014). As both TDP-43 and FUS harbor RNA-binding domains and have important functions in RNA processing, genetics suggests that RNA homeostasis might be dysfunctional in ALS disease pathogenesis.
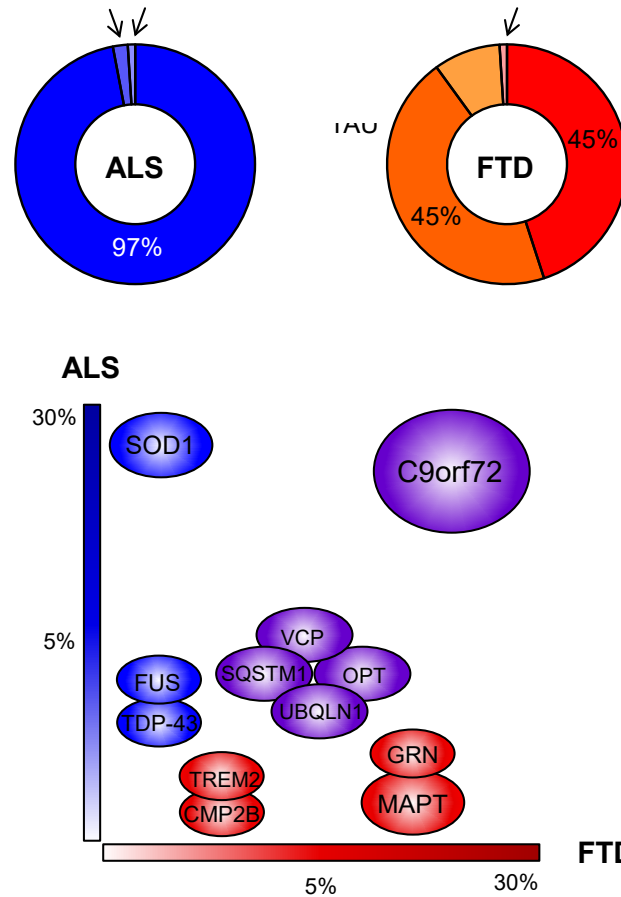
Figure 1-1: ALS and FTD are two ends of a disease spectrum - schematic illustration of neuropathological inclusions and genes associated with ALS and FTD.

(A, B) Neuropathological inclusions found in ALS and FTD classified according to the main accumulated protein. TDP-43 and FUS represent common inclusions **(C)** The ALS and FTD phenotypes are presented along the Y- and X-axis. Genetic mutations in *SOD1*, *TDP-43* and *FUS* result in a pure ALS phenotype, *TREM2, CHMP2B, GRN* and *MAPT* in a pure FTD one. Genes depicted in violet result in ALS/FTD. The more the gene is located towards the end of the axis, the more frequent the mutation is. The most frequent gene mutated in both ALS and FTD is *C9orf72. Adapted from Ling et al. (2013).*

Genes associated with pure FTD are microtubule-associated protein Tau (*MAPT*) and progranulin (*GRN*) as well as charged multivesicular body protein 2b (*CHMP2B*) and triggered receptor expressed on myeloid cells 2 (*TREM2*) (Borroni et al., 2014; Isaacs et al., 2011; Le Ber, 2013; Rayaprolu et al., 2013). Beyond the mutations linked to either ALS or FTD, several genes provide a direct molecular link between the two disorders. Among others, mutations in sequestosome 1 (*SQSTM1*), optineurin (*OPT*), valosin-containing protein (*VCP*) and ubiquilin 2 (*UBQLN2*) were identified in both diseases. Since all of the commonly affected proteins are involved in major clearance pathways of the cell, impairment of protein homeostasis is suggested to be a shared toxic mechanism of ALS and FTD. Most importantly, mutations in chromosome 9 open reading frame 72 (*C9orf72*) were discovered to be highly abundant in patients with ALS, FTD, and ALS/FTD. The *C9orf72* mutation can explain up to 40% of fALS and 25% of fFTD (Majounie et al., 2012) thereby representing the most common known causal mutation in both neurological disorders (Figure 1-1**C**).

1.2. The *C9orf72* nucleotide repeat expansion

The hexanucleotide GGGGCC repeat expansion within the non-coding region of the *C9orf72* gene was first discovered in 2011 (DeJesus-Hernandez et al., 2011; Renton et al., 2011). Depending on which of the three C9orf72 transcript variants is formed, the repeat is located either in the first intron between exon 1a and 1b or in the promoter region of the gene. While the sequence only harbors up to 23 repeats in healthy individuals, the repeat in *C9orf72*-mediated ALS/FTD cases is expanded to hundreds or even thousands of base pairs (DeJesus-Hernandez et al., 2011; Renton et al., 2011). However, the exact repeat length is not inherited as it has been shown that the GGGGCC sequence is unstable at a length above 20 repeats and might shrink or expand during germline or somatic transmission (Beck et al., 2013). Since most people harbor either very short (2-3) or very long repeats (>400), an exact cutoff for pathogenicity is not known. Surprisingly, there is no strong correlation between repeat length and clinical phenotype (Beck et al., 2013; Gijselinck et al., 2016).

1.2.1.   Clinical and pathological representation of *C9orf72*-mediated ALS/FTD

Nonetheless, independent of repeat length, patients carrying the *C9orf72* mutation show an earlier age of onset, shorter survival and a higher decline of cognitive and behavior functions compared to ALS/FTD cases without *C9orf72* expansion (Byrne et al., 2012; Chio et al., 2012) underlining the importance of the expansion in disease progression. Although patients harboring the *C9orf72* repeat expansion initially present highly heterogeneous clinical symptoms, the mutation typically leads to ALS and FTD in the end – an observation which differs from non-*C9orf72* ALS and FTD patients (Byrne et al., 2012; Stewart et al., 2012).

Nearly all *C9orf72* mutation carriers show TDP-43 cytoplasmic inclusions in the frontal and temporal or motor cortex, as well as the spinal cord reflecting the main regions of neurodegeneration (Hsiung et al., 2012; Stewart et al., 2012). In addition to TDP-43 pathology, other neuronal cytoplasmic inclusions were found which are positive for markers of the UPS system, such as p62, but are TDP-43 negative. These inclusions are present in the cerebellar cortex, hippocampus and, all neocortical regions and are unique to patient brains with the *C9orf72* mutation (Al-Sarraj et al., 2011). The nature of these p62-positive/TDP-43-negative inclusions will be discussed in more detail in 1.2.4.2.

1.2.2.   **Toxic mechanisms underlying the *C9orf72* repeat expansion**

Currently, three main non-exclusive mechanisms are suspected to cause *C9orf72*-associated neurodegeneration. The first potential pathomechanism implies that the C9orf72 protein loses its function due to decreased transcription and therefore expression of the repeat containing gene (haploinsufficiency). The second mechanism infers that the $(GGGGCC)_n$ expansion might gain toxic function upon transcription and accumulation of repeat RNA which potentially sequesters RNA-binding proteins (RBPs)(RNA mediated toxicity). Finally, it has been shown that unconventional bi-directional transcription and translation of the *C9orf72* repeat leads to expression of aggregation-prone dipeptide repeat (DPR) proteins. These proteins are toxic in various model systems and may interfere with several cellular pathways (protein mediated toxicity) (**Fehler! Verweisquelle konnte nicht gefunden werden.**). In the following chapters, these three mechanisms are described in more detail.
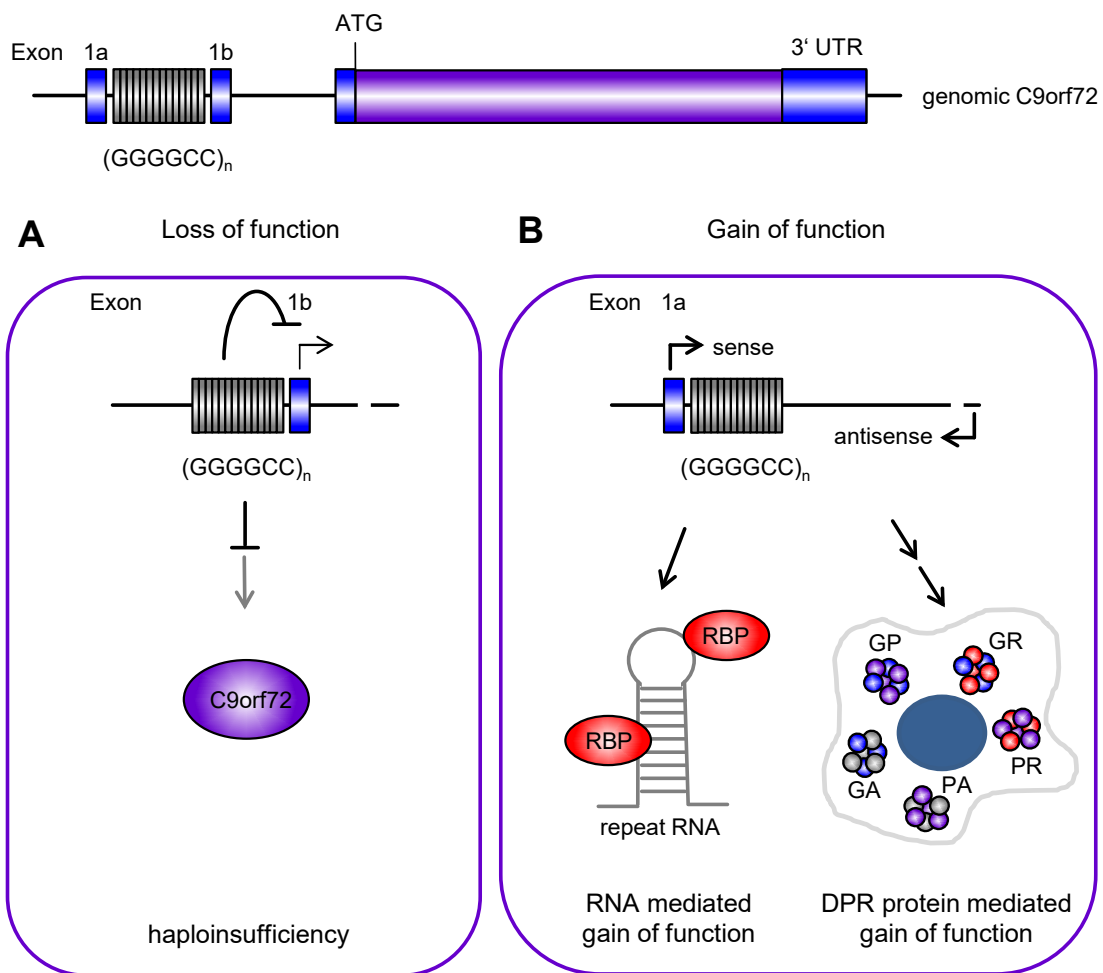
Figure 1-2: Postulated pathomechanisms underlying *C9orf72*-mediated ALS/FTD.

Schematic illustrations with overview of three potential mechanisms how the *C9orf72* repeat might cause neurodegeneration. The *C9orf72* repeat is depicted in grey, the non-coding region in blue and the coding region in violet. **(A)** The *C9orf72* repeat expansion hinders transcription of the gene which may impair C9orf72 protein function (haploinsufficiency). **(B)** Two gain of function mechanisms are postulated: The repeat RNA is forming secondary structures and binds RNA-binding proteins (RBPs, in red) (RNA mediated gain of function) or the repeat RNA is translated (in sense and antisense direction) into aggregation-prone DPR proteins, namely poly-GA, poly-GP, poly-GR, poly-PR and poly-PA (DPR protein mediated gain of function).

1.2.3. *C9orf72* loss of function

Alternative splicing of the *C9orf72* transcript results in three transcript variants with variant 1 encoding a short protein isoform and variants 2 and 3 encoding the full-length isoform (Figure 1-3). Already the initial report of the *C9orf72* mutation showed that the repeat expansion leads to reduced variant 2 *C9orf72* transcript levels in the frontal cortex and lymphoblast cells of individuals harboring the repeat (DeJesus-Hernandez et al., 2011).
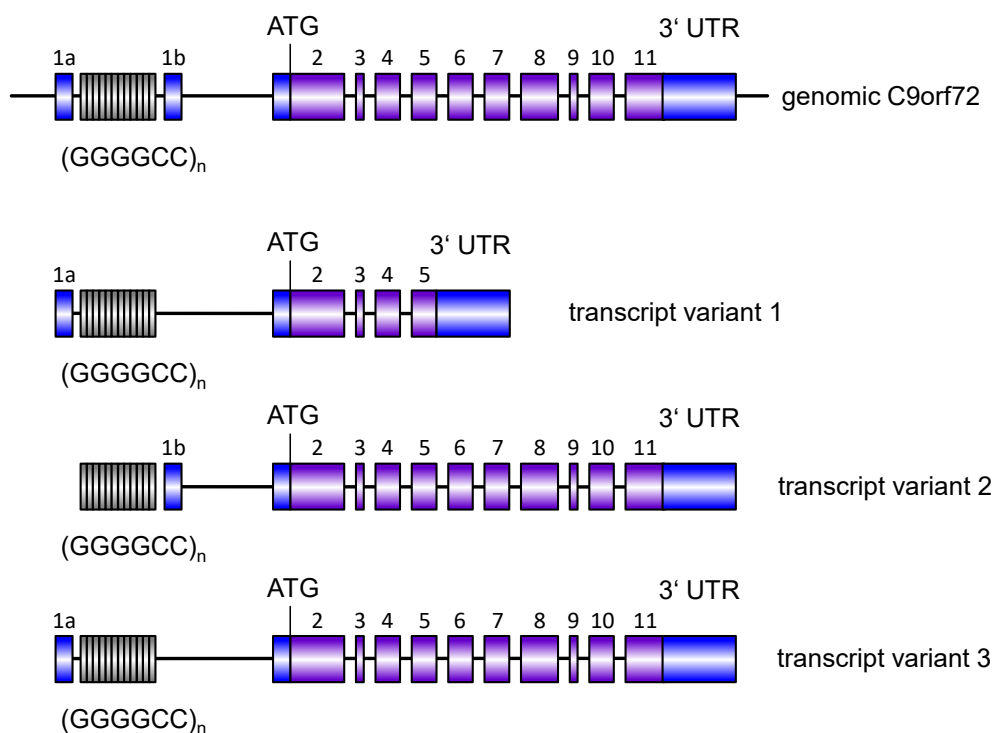
Figure 1-3: Scheme of genomic C9orf72 structure and its pre-mRNA splicing products.

Transcript variant 1 encodes for the short C9orf72 isoform, whereas transcript variant 2 and 3 encode for the long C9orf72 isoforms. Blue boxes represent noncoding and violet boxes represent coding exons. Positions of the $(GGGGCC)_n$ repeat (grey), the start codon (ATG) and the 3'UTR are indicated.

Others confirmed decreased *C9orf72* transcript as well as protein levels in affected brain tissues and cultured cells of mutation carriers (Belzil et al., 2013; Frick et al., 2018; Gijselinck et al., 2016; Renton et al., 2011). This reduction in *C9orf72* expression suggests haploinsufficiency may play a role in disease pathogenesis. However, the exact function of the C9orf72 protein is just emerging.

C9orf72 is most closely related to the DENN (differentially expressed in normal and neoplastic cells) domain containing proteins. Therefore, it is predicted to have functions as a GDP/GTP exchange factor (GEF) that activates Rab-GTPases (Levine et al., 2013; Zhang et al., 2012). In line with this, it was reported that C9orf72 activates Rab1a thereby mediating trafficking of the ULK1 autophagy initiation

complex to the phagophore (Webster et al., 2016; Yang et al., 2016). In addition, C9orf72 forms a complex with SMRC8 and WDR41 directly linking it to the autophagy pathway (Jung et al., 2017; Sellier et al., 2016; Yang et al., 2016). Concomitantly, depletion of C9orf72 *in vitro* mitigates autophagy leading to build-up of p62-positive inclusions as well as TDP-43 (Sellier et al., 2016; Webster et al., 2016) suggesting that loss of C9orf72 plays a role in disease development. Knockdown of *C9orf72* in zebrafish, for example, mediated by injection with antisense morpholino oligonucleotides, leads to altered axonal branching and locomotion impairment further strengthening this hypothesis (Ciura et al., 2013). Furthermore, Shi and colleagues confirm that reduced C9orf72 protein levels are sufficient to cause neurodegeneration by accumulation of glutamate receptors leading to excitotoxicity (Shi et al., 2018)

Conversely, in mice, neither knockdown nor knockout of *C9orf72* results in neurodegeneration or ALS/FTD-related phenotype such as TDP-43 pathology (Atanasio et al., 2016; Burberry et al., 2016; O'Rourke et al., 2016). Instead, these mice show enlarged spleens and lymph nodes linking the C9orf72 protein to the immune system (Atanasio et al., 2016). Also, *C9orf72* knockout in mice leads to an altered immune response of microglia (O'Rourke et al., 2016). However, instead of showing a more severe phenotype, the clinical symptoms of a patient homozygous for the *C9orf72* repeat expansion does not differ from the ones in heterozygote patients (Fratta et al., 2013). Taken together, the observations made in mice and diseased human individuals strongly indicate that loss of *C9orf72* is not sufficient to trigger full disease pathology including neurodegeneration.

1.2.4.   *C9orf72* gain of function

A second way how the *C9orf72* nucleotide repeat expansion might contribute to disease pathogenesis is through gain of toxic function of repeat containing RNA or dipeptide repeat proteins.

1.2.4.1.   *RNA mediated toxicity*

One pathological feature typical for many diseases associated with repeat expansions is the formation of RNA foci containing the repeat RNA. Also in myotonic dystrophy, RNA foci emerging from the CTG nucleotide repeat are toxic as they interfere with normal cellular functions of several RNA binding factors, such as the muscleblind-like proteins (Miller et al., 2000). An initial study shows that these foci also accumulate in nuclei within the cortex and spinal cord of *C9orf72*-associated FTD patients (DeJesus-Hernandez et al., 2011). Subsequently, RNA foci, which form after transcription of the sense and antisense strand, were found in neurons, but also astrocytes, microglia and oligodendrocytes of ALS/FTD patients as well as cell culture models expressing the repeat (Cooper-Knock et al., 2015; Donnelly et al., 2013; Gendron et al., 2013; Lagier-Tourenne et al., 2013; Mizielinska et al., 2013; Mori et al., 2013a; Sareen et al., 2013; Zu et al., 2013). Here, RNA foci predominantly localize to the nucleus

but are also found in the cytoplasm of patient derived fibroblasts (Donnelly et al., 2013; Lagier-Tourenne et al., 2013; Sareen et al., 2013). Generally, these RNA foci are highly stable as they form secondary and tertiary structures, which may include G-quadruplexes and hairpins.

The repeat containing RNA foci might cause toxicity similar to sequestration of muscleblind-like protein 1 (MBNL1) by $(CUG)_n$ RNA in myotonic dystrophy type 1. The $(GGGCC)_n$ repeat may sequester essential RNA-binding proteins (RBPs) leading to impairment of their normal function in various molecular cascades such as RNA processing, RNA localization or translation. One major protein family trapped by the GGGGCC and CCCCGG repeat are the heterogeneous nuclear ribonucleoproteins (hnRNPs) (Cooper-Knock et al., 2015; Cooper-Knock et al., 2014; Lee et al., 2013; Mori et al., 2013b). Additional proteins which are found to colocalize with *C9orf72* RNA foci including the splicing factors ALYREF (Cooper-Knock et al., 2015; Cooper-Knock et al., 2014) and SRSF2 (Cooper-Knock et al., 2015; Cooper-Knock et al., 2014), the transcriptional regulator Pur-α (Sareen et al., 2013; Xu et al., 2013), the nucleolar protein Nucleolin (NCL) (Haeusler et al., 2014) and RanGAP1 (Zhang et al., 2015), a protein involved in nucleocytoplasmic transport. Although dysregulation of splicing and alternative polyadenylation have been reported in *C9orf72* patient brains (Conlon et al., 2016; Prudencio et al., 2015), none of the RNA interactors have been connected to neuronal injury and it remains to be elucidated whether loss of one or more of the sequestered RBPs contributes to disease pathology.

1.2.4.2. *Protein mediated toxicity*

As mentioned earlier, abundant p62-positive/TDP-43-negative inclusions are found in *C9orf72* patient brains. These inclusions remained uncharacterized until it was found that the repeat is being transcribed and translated. The ability of repeat containing RNA to form secondary structures such as hairpins enables the transcript to undergo so-called repeat-associated non-ATG (RAN) translation. This type of unconventional translation was first identified in the microsatellite expansion disease spinocerebellar ataxia type 8 (SCA8) and was found to occur in absence of an ATG start codon (Zu et al., 2011).

RAN translation of the hexanucleotide repeat in *C9orf72* gives rise to five different dipeptide repeat (DPR) protein species from six different reading frames. Translation of the sense transcript results in poly-glycine-proline (poly-GP), poly-glycine-alanine (poly-GA) and poly-glycine-arginine (poly-GR) peptides and translation of the antisense strand leads to poly-proline-arginine (poly-PR), poly-proline-alanine (PA) and further poly-glycine-proline (poly-GP) peptides (Ash et al., 2013; Mori et al., 2013a; Mori et al., 2013c; Zu et al., 2013). The DPR proteins are prone to aggregation and accumulate throughout the brain of *C9orf72* mutation carriers showing highest abundance in the cerebellum, hippocampus, thalamus, amygdala, and the motor, temporal and frontal cortex (Figure 1-4). They show only moderate pathology in subcortical areas and are infrequent in lower motor

neurons of the spinal cord (Ash et al., 2013; Mackenzie et al., 2013; Mori et al., 2013a; Zu et al., 2013). This neuroanatomical distribution is highly consistent among *C9orf72* positive cases irrespective of clinical symptoms. Notably, there is no correlation observed between DPR expression and areas of neurodegeneration (Mackenzie et al., 2013). However, one has to keep in mind that DPR proteins are also present in soluble forms and may, therefore, be difficult to visualize in patient tissue. Additionally, highly toxic DPRs might not be detectable anymore due to loss of degenerating neurons.
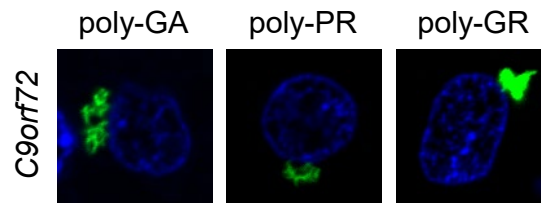
Figure 1-4: Dipeptide repeat proteins in the human cortex of *C9orf72* brains tissue

Immunofluorescence images of three different dipeptide repeat protein species in the human brain of *C9orf72* patients. Poly-GA, poly-PR and poly-GR aggregates are depicted in green. The nuclei are stained with DAPI in blue.

DPR proteins form typical star- or dot-shaped neuronal inclusions positive for p62 but show little colocalization with phospho-TDP-43 aggregates (Mackenzie et al., 2013; Mann et al., 2013; Mori et al., 2013a; Mori et al., 2013c). Furthermore, it has been shown that although the majority of DPR proteins is found in large cytoplasmic inclusions in post-mortem tissue they can also be sparsely detected in p62-negative para-nucleolar aggregates (Schludi et al., 2015a).

How individual DPR species contribute to cellular toxicity and thereby neurodegeneration is still under intense debate. In the following sections, the specific DPR proteins are examined in more detail.

1.2.4.3. *Poly-GA is the most abundant DPR species in patients*

Among the five DPR species in *C9orf72*-ALS/FTD, only poly-GA is found in nearly all TDP-43 negative inclusions. Short poly-GA peptides form amyloid-like structures containing characteristic cross-β sheets (Chang et al., 2016). Cryo-electron tomography of poly-GA inclusions in cultured neurons revealed densely packed twisted ribbons that are highly enriched in 26S proteasome, linking poly-GA to impaired proteasomal degradation (Guo et al., 2018). Supporting this connection, poly-GA also sequesters several proteasome-linked proteins *in vitro*, with p62 and UBQLN1 among them (May et al., 2014; Schludi et al., 2015a). Thus, disruption of the ubiquitin-proteasome system (UPS) might trigger the toxicity seen in cell culture and flies upon poly-GA expression (May et al., 2014; Mizielinska et al., 2014; Yamakawa et al., 2015; Zhang et al., 2014). Consistent with the toxicity observed in cellular models, mice expressing GFP-(GA)$_{50}$ show neuronal loss and astrogliosis along with motor and cognitive deficits (Zhang et al., 2016). Furthermore, poly-GA expression shortens life span in transgenic flies (Mizielinska et al., 2014)

Besides UPS impairment, poly-GA aggregation causes mislocalization of nuclear pore components such as Pom121 and RanGAP1 *in vivo* (Zhang et al., 2016)*. In addition, we have shown that poly-GA expression hinders nuclear import of a fluorescent reporter containing the TDP-43 nuclear localization (NLS) signal. Importantly, expression of poly-$(GA)_{175}$ significantly shifted predominantly nuclear TDP-43 into small cytoplasmic TDP-43 granules in primary neurons further indicating that poly-GA impairs nucleocytoplasmic transport (Khosravi et al., 2017). Importantly, with these findings, we and others could causally connect two major aggregating proteins, namely TDP-43 and poly-GA, in *C9orf72*-mediated ALS/FTLD disease.

Taken together, poly-GA is the most abundant DPR protein species in brains and spinal cord of *C9orf72* mutation carriers and may contribute to human disease by inhibiting the UPS or nucleocytoplasmic transport.

1.2.4.4. *Poly-GR and poly-PR are the most toxic DPR species in model systems*

Although there is a general agreement that poly-GA is toxic in several biological systems (May et al., 2014; Zhang et al., 2014), the arginine-rich DPR proteins poly-GR and poly-PR show significantly higher toxicity in side by side comparisons. In fact, they induce toxicity in multiple cell culture and animal models including U2OS cells, human astrocytes (Kwon et al., 2014), HEK293T cells, NSC34 cells (Kanekura et al., 2016; Tao et al., 2015), primary cortical and motor neurons (Wen et al., 2014), neurons derived from induced pluripotent stem cells (iPSCs) (Lopez-Gonzalez et al., 2016; Wen et al., 2014) and *Drosophila* (Boeynaems et al., 2016; Freibaum et al., 2015; Lee et al., 2016a; Mizielinska et al., 2014; Wen et al., 2014). In the majority of cellular systems, both poly-GR and poly-PR localize to the nucleolus, the assembly site of ribosomes. However, in *C9orf72*-ALS/FTD patient brains poly-GR and poly-PR are predominantly found in compact cytoplasmic inclusions and to a lesser extent in para-nucleolar compartments. When looking at the overall distribution of the two DPR species within the brain, poly-GR and poly-PR are most abundant in the frontal, occipital and motor cortex as well as the thalamus, hippocampus, and the cerebellar regions. Of note, poly-PR inclusions have been noted to be extremely rare and represent about 1% of DPR protein inclusions (Mackenzie et al., 2013; Schludi et al., 2015a).

So far, little is known about the effects of poly-GR and poly-PR on cellular function and the mechanisms underlying poly-GR/PR toxicity are just emerging. Initial reports describe how the two arginine-rich DPR protein species might interfere with the physiology of the cell in different cell culture systems. These findings are described in the next paragraphs.

Poly-GR/PR expression impairs the dynamics of membrane-less organelles

In order to approach the mechanisms contributing to poly-GR and poly-PR associated neurodegeneration, Lee and colleagues performed a proteomic study in poly-GR and poly-PR expressing HEK293 cells. Analysis revealed that poly-GR/PR interactors are enriched in RNA-binding proteins containing low complexity domains (LCDs). While only 35.8% of human proteins harbor LCDs, up to 67.9% of poly-GR/PR interactors contained low complexity sequences (Lee et al., 2016a). LCDs show low amino acid diversity and often harbor mainly glycine and serine interspersed with aromatic and charged residues (Uversky et al., 2015). Proteins with LCDs can undergo low-affinity interactions which are important for them to become rapidly and reversibly concentrated in discrete spots within the cell. These interactions are crucial in the formation and function of membrane-less organelles such as nuclear speckles, the nuclear pore complex (NPC), stress granules, and the nucleolus which represent sites of splicing, nucleocytoplasmic transport, stalled translation complexes, and ribosome biogenesis, respectively. Under certain conditions, these intermolecular biophysical interactions, however, drive phase separation of the LCD containing proteins and clustering in liquid droplets which have the property to propagate into hydrogels comprised of amyloid-like fibers. This process is called liquid-liquid phase separation (LLPS).

Liquid phase transition has been shown to occur in a variety of poly-GR and poly-PR interactors with NPM1, TIA1 or FUS being among them (Lee et al., 2016a; Lin et al., 2016). Moreover, the ALS-linked RBPs hnRNPA1 and TDP-43 are able to assemble into protein-rich droplets by LLPS (Molliex et al., 2015). Thus, several proteins aggregating in ALS/FTD patients are found to undergo LLPS *in vitro*. As disease-causing mutations in these genes are mostly located within LCDs (Taylor et al., 2016) and have the ability to disturb their biophysical properties it is proposed that LLPS is a general disease mechanism.

Both poly-GR and poly-PR are highly charged, basic and polar due to the incorporation of arginine residues and have a disordered nature. Thus, they are expected to form flexible structures that remain soluble. *In vitro*, the two DPR species induce liquid droplet formation of NPM1, hnRNPA1, and TIA1, proteins found in the nucleolus and SGs, when applied in the right ratios suggesting that poly-GR/PR disturb low-affinity interactions. Also, poly-$(GR)_{20}$ and poly-$(PR)_{20}$ do phase separate by themselves *in vitro* following the addition of a molecular crowder (Boeynaems et al., 2017).

Thus, a complementary mechanism how poly-GR and poly-PR might contribute to *C9orf72* pathogenesis is by disruption of the assembly and dynamics of membrane-less organelles such as nuclear speckles, the NPC, stress granules or the nucleolus through disturbance of the LLPS properties of their resident proteins. However, all approaches so far were performed *in vitro*, with pure proteins and/or in high molecular ranges and no co-aggregation was reported in patient tissue. Consequently,

further experiments are needed in order to prove that these relations occur under physiological conditions.

Poly-GR and poly-PR lead to aberrant splicing in cell culture systems

Another putative mechanism by which the two DPR species might lead to toxicity is their effect on mRNA splicing. The first study describing altered splicing *in vitro* was by Kwon and colleagues who exposed human astrocytes to PR_{20} synthetic peptide and subsequently analyzed the extracted RNA by deep sequencing. Analysis revealed ~5,000 mis-spliced RNA transcripts resulting from altered RNA processing such as exon skipping or intron retention (Kwon et al., 2014). In concordance, classification analysis of the interactome of poly-PR_{20} in treated NSC34 cells revealed mRNA splicing as the second most enriched gene ontology category (Kanekura et al., 2016). This was also true for a more recent study with GR_{20} or PR_{20} peptides in which mostly the U2 snRNP complex was enriched. In line with the findings *in vitro*, also in *C9orf72* patient cerebella and cortices, U2-dependent exons, mostly linked to mitochondrial functions, were preferentially mis-spliced (Yin et al., 2017). Together with the widespread transcriptome changes found in familial and sporadic ALS patient brains (Prudencio et al., 2015) splicing could further be shown to be deregulated in *C9orf72*-mediated ALS/FTD, but it is not known whether poly-GR and poly-PR play a role in disruption of this process in patients.

Poly-GR and poly-PR cause oxidative and ER stress *in vitro*

Poly-GR and poly-PR have also been associated with toxic effects in mitochondria and the endoplasmic reticulum (ER). As mentioned above, transcripts of mitochondrial genes were found to undergo aberrant splicing, including *COX16* and *TIMM9* and the mitochondrial ribosomal proteins *MRPL52* and *MRPS31* suggesting that mitochondrial function may be comprised. And indeed, mitochondria in patient-derived *C9orf72* iPSC motor neurons and neurons expressing poly-$(GR)_{80}$ show increased membrane potential accompanied by elevated production of reactive oxygen species (ROS) and increase in DNA damage (Lopez-Gonzalez et al. 2016) suggesting a role of poly-GR in oxidative stress. Whether these defective mitochondria also show altered mitochondrial respiration or morphology has not been addressed. Additionally, these *in vitro* effects have not been validated in patient tissue.

Besides oxidative stress, also ER stress was linked to cellular toxicity in $(GR)_{20}$/$(PR)_{20}$ peptide treated human cells and mouse primary cortical neurons. In a CRISPR/Cas9 knockout screen, Kramer *et al* identified ER-resident proteins and almost all members of the ER-membrane to modulate poly-GR/PR toxicity, with transmembrane thioredoxin protein (TMX2) being the strongest protective hit. Knock-down of TMX2, a protein enriched at the mitochondria-associated membrane of the ER, decreased Caspase 3/7 activity and increased ATP levels in poly-PR_{20} treated neuronal cells suggesting

a role of ER stress in DPR-mediated toxicity in cell culture (Kramer et al., 2018). Although IRE1 signaling positively correlates with TDP-43 pathology in familial *C9orf72*-ALS cases (Lee et al., 2016b), there is no evidence for a connection between ER stress and poly-GR/poly-PR in patients so far.

Nucleocytoplasmic transport is comprised in poly-GR/PR expressing cells

Recently, the nuclear pore complex was linked to poly-GR and poly-PR toxicity. Jovičić *et al*. identified modifier genes involved in nucleocytoplasmic transport in a gain and loss of function screen in yeast. In this study, poly-(PR)$_{50}$ toxicity was mainly modified by nuclear import receptors, NPC components and regulators of the Ran-GTPase cycle (Jovicic et al., 2015). To validate hits *in vivo*, an RNAi screen was performed in *Drosophila* expressing a poly-PR version with 25 repeats. Also here, similar proteins were found to be modifiers of poly-PR toxicity (Boeynaems et al., 2016). In line with these findings, flies expressing 58 repeats of the GGGGCC expansion showed an abnormal nuclear envelope. Next to the defects in architecture of the nuclear envelope, disruption of the Ran-GTP gradient between nucleus and cytoplasm was observed in patient derived iPSC neurons. (Freibaum et al., 2015).

Overall, these data indicate that the nuclear pore is at least partly dysfunctional in cell culture systems harboring the hexanucleotide repeat. In *C9orf72*-associated ALS motor cortex, RanGAP1, a protein that stimulates Ran to hydrolase GTP to GDP, and Nup205, an extremely long-lived NPC scaffold protein, exhibit mislocalization (Zhang et al., 2015). However, if these phenotypes ultimately lead to nucleocytoplasmic trafficking defects also in patients and if DPR proteins are contributors to these findings has not been addressed.

Poly-GR and poly-PR impair stress granule and nucleolus dynamics

Stress granules (SGs) are membrane-less cytoplasmic compartments with a very dynamic nature which form in response to cellular stress. Upon stress, translational control allows for the regulation of mRNA expression and is the mechanism by which the cell protects itself from environmental changes. After phosphorylation of the translation initiation factor eIF2α, a variety of proteins, such as RNA-binding proteins, transcription factors, and RNA helicases, as well as mRNA accumulate. Binding of the RNPs to the mRNA transcripts subsequently prevents translation initiation. These translation inhibition complexes are routed into SGs and thus, translational programming is closely linked to SG assembly (Anderson and Kedersha, 2009). Importantly, cytoplasmic TDP-43 was found to be trapped in SGs. This was validated by colocalization with SG markers (TIA-1, eIF3) in postmortem brains from ALS and FTD patients linking SGs to disease (Liu-Yesucevitz et al., 2010). With the finding that mutations in TIA-1 (Mackenzie et al., 2017) and Ataxin 2 (Elden et al., 2010), two important components of SGs, increase the risk for ALS, evidence exists linking *C9orf72*-mediated toxicity to stress granules also *in vivo*.

Nucleoli are distinct subnuclear components associated with ribosome biogenesis that consist of three separate regions. The fibrillar center (FC) is surrounded by a dense fibrillar component (DFC) where pre-ribosomal RNA transcripts are spliced and modified. FC and DFC are both enclosed by the granular component (GC) where ribosomal proteins and the ribosomal RNA (rRNA) are assembled (Boisvert et al., 2007).

Although SGs and the nucleolus are in a rapid dynamic equilibrium with the cytoplasm, poly-GR, as well as poly-PR, have the property to impair this dynamic and stabilize molecular interactions as suggested by fluorescence recovery after photobleaching (FRAP) experiments (Figure 1-5**A** and **B**). Here, nucleolin (NCL), an important protein involved in pre-rRNA transcription and ribosome assembly and nucleophosmin 1 (NPM1), connected with ribosome biogenesis and nucleolar export, exhibit reduced mobility upon poly-$(GR)_{20}$/$(PR)_{20}$ expression (Lee et al., 2016a). Whether these poly-GR/PR dependent changes in dynamics affect SG and nucleolar function, such as translational control and ribosome assembly, respectively, has not been addressed.
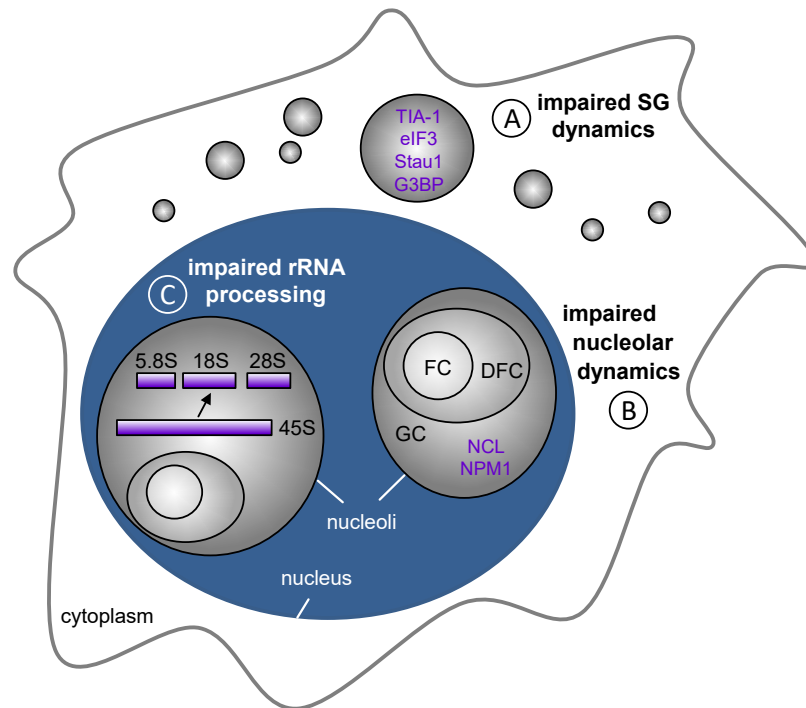
Figure 1-5: Scheme of the impact of poly-GR and poly-PR expression on SGs and the nucleolus *in vitro*.

(A) The expression of poly-GR_{20} and poly-PR_{20} results in impaired stress granule dynamics as suggested by FRAP experiments with SG markers such as TIA-1, eIF3, Stau1 or G3BP. **(B)** The nucleolus is subdivided into three separate regions – the fibrillary center (FC), the dense fibrillar component (DFC) and the granular component. The letter contains several proteins involved in ribosome biogenesis or rRNA processing with NCL and NPM1 among them. These two proteins are less mobile upon poly-GR/PR expression. **(C)** The pre-ribosomal 45S rRNA is processed into mature 5.8S, 18S and 28S rRNA in the nucleolus. Poly-GR and poly-PR expressing cells show reduced levels of mature rRNAs suggesting disturbed rRNA processing.

Interestingly, overexpressed poly-PR exclusively localizes within the nucleolus and poly-GR is seen in both, nucleolus and cytoplasm in all *in vitro* model systems regardless of whether the DPR proteins are expressed from a vector or added as synthetic peptides (Boeynaems et al., 2017; Kramer

et al., 2018; Kwon et al., 2014; Lee et al., 2016a; Schludi et al., 2015a; Tao et al., 2015; Wen et al., 2014; Zhang et al., 2018b). Super-resolution fluorescent imaging revealed that GFP-(GR)$_{50}$ is recruited to the GC and the DFC, while poly-(PR)$_{50}$ is solely found in the GC (Lee et al., 2016a). Thus, both poly-GR and poly-PR are localized to the outer layer of the nucleolus where ribosome assembly takes place (Lee et al., 2016a).

However, so far, none of the DPR protein species was detected in stress granules or the nucleolus in patients and therefore validation experiments are needed in order to link poly-GR/PR to the two compartments in *C9orf72*-ALS/FTD pathogenesis.

Poly-GR and poly-PR alter rRNA processing

One of the first studies linking DPR protein toxicity to the ribosome showed that administration of the PR$_{20}$ peptide to human astrocytes alters RNAs encoding ribosomal proteins and indeed impairs processing of the pre-ribosomal 45S rRNA (Kwon et al., 2014). In eukaryotic cells, rRNA processing is a tightly regulated process in which the 45S rRNA precursor is first methylated and subsequently cleaved and processed into mature 18S, 5.8S, and 28S rRNA. These rRNAs then serve as a scaffold for the assembly of ribosomal proteins and execute catalytic functions in translation initiation, elongation, and termination (Henras et al., 2015). In poly-PR treated cells, the levels of 5.8S rRNA are reduced by 70% providing evidence that altered rRNA processing is underlying DPR toxicity (Kwon et al., 2014). Likewise, 18S and 28S rRNA is remarkably decreased upon poly-GR/PR expression in NSC-34 cells (Tao et al., 2015). Thus, these findings indicate, that poly-GR and poly-PR comprise rRNA processing *in vitro* (Figure 1-5**C**). However, many open questions remain: Does this reduction in rRNA processing products lead to overall impairment of ribosome biogenesis and if yes, is also protein synthesis altered? Would restorage of rRNA processing products rescue poly-GR/PR-mediated toxicity? Is the ribosome also affected in *C9orf72*-ALS/FTD?

Taken together, the exact mechanism(s) by which the arginine-rich DPR proteins poly-GR and poly-PR induce toxicity in *C9orf72* pathogenesis are still not quite understood. So far, alternative splicing, oxidative and ER stress, mitochondrial and NPC dysfunction, alterations in nucleolus and SG dynamics, as well as reduced rRNA processing, have been implicated, nevertheless, detailed analysis of these putative toxic mechanisms is missing. Most importantly, all experiments have been performed in cellular or animal models and thus, there is no evidence for the significance of these mechanisms in *C9orf72*-ALS/FTD patients yet.

1.2.4.5. *The role of poly-GP and poly-PA*

Poly-GP and poly-PA are two DPR species translated from the antisense *C9orf72* transcript. While poly-GP inclusions are highly abundant in *C9orf72*-associated ALS/FTD brains, poly-PA inclusions are rare. Under individual expression *in vitro*, poly-GP localization is mainly cytoplasmic and poly-PA is localized to the nucleus as well as the cytoplasm. Following poly-GP/PA expression or treatment, NCS-34 and HEK93 cells, cultured neurons and yeast as well as flies show similar survival as their respective controls (Jovicic et al., 2015; Lee et al., 2016a; May et al., 2014; Tao et al., 2015; Wen et al., 2014; Yamakawa et al., 2015). Only in zebrafish, poly-PA with a repeat length of 1000 shows an effect on larvae survival (Swaminathan et al., 2018). Due to their amino acid residues, these DPR proteins have an uncharged nature and might therefore not undergo strong interactions with endogenous cellular proteins (Lee et al., 2016a). Therefore, poly-GP and pol-PA are thought to contribute the least to toxicity.

1.2.5. **Biomarkers in *C9orf72*-associated ALS/FTD**

Although there is general agreement that DPR proteins contribute to toxicity in cellular and animal models, their overall significance in *C9orf72*-mediated ALS/FTD remains unresolved. To better address their role in *C9orf72*-ALS/FTD pathogenesis it is crucial to monitor individual DPR proteins in patients over time. As studies in post mortem tissue cannot provide temporal information, a DPR dependent biomarker could serve as a useful tool. Interestingly, in patients with *C9orf72*-FTD, widespread accumulation of DPR proteins within neurons occurs much earlier than TDP-43 pathology (Baborie et al., 2015). Thus, it is possible that DPR proteins already exist early in disease or even before its onset and therefore might be used as pharmacodynamic biomarkers.

So far, poly-GP has been discovered as a potential biomarker candidate as it was shown to be readily detectable in the cerebrospinal fluid (CSF) in a small case series of symptomatic ALS patients harboring the *C9orf72* mutation (Su et al., 2014). Recently, two larger studies built up on this finding and showed that poly-GP can indeed be detected in immunoassays and thus serve as a biomarker signaling the onset and progression of *C9orf72*-ALS/FTD. Importantly, poly-GP levels were already measurable in asymptomatic *C9orf72* mutation carriers and thus can be used to detect target engagement of applied *C9orf72*-directed drugs (Gendron et al., 2017a; Lehmer et al., 2017). In contrast, phosphorylated neurofilament heavy chain (pNFH), a marker for axonal damage, was only elevated in the symptomatic patients and showed similar levels in ALS cases with or without *C9orf72* mutation. Nonetheless, pNFH levels predict disease progression of ALS patients over time (Gendron et al., 2017b) and thus serve as an additional, DPR-independent and prognostic biomarker.

As poly-GR and poly-PR show far greater toxicity than poly-GP *in vitro* and *in vivo*, it is of great importance to develop immunoassays also monitoring their protein levels in patients. This may help to clarify the defined role of poly-GR and poly-PR in *C9orf72*-disease progression.

1.2.6. *C9orf72* repeat expansion-directed therapies

Although the exact mechanisms underlying *C9orf72*-mediated ALS/FTD are not quite understood, gain-of-function of the repeat-containing RNA is likely essential for pathogenesis as not only potentially toxic RNA foci, but also DPR proteins can emerge from it. Therefore, reduction of the repeat-containing RNA is a therapeutic option. However, lowering of global *C9orf72* transcripts in order to treat RNA-dependent toxic mechanisms might be disadvantageous in case haploinsufficiency significantly contributes to disease pathogenesis.

Therefore, antisense oligonucleotides (ASOs), which can be designed to target and inactivate specific mRNA sequences, are suitable for therapeutic treatment. Recently, ASOs have been proven to be safe in humans and are already applied for therapy of spinal muscular atrophy (Chiriboga et al., 2016). In a study from April 2018, Liu and colleagues could show that their *C9orf72*-ASO sequence preferentially reduced repeat-containing transcripts in patient-derived iPSC neurons and fibroblasts and validated their promising results in *C9orf72* BAC transgenic mice. Here, they observed a reduction of both RNA foci and DPR proteins without affecting total C9orf72 levels (Liu et al. 2018). Further investigation will be needed for their ASO treatment to be approved for therapy as correct targeting, efficacy, and efficiency remain to be confirmed also in patients.

Another therapeutic approach might emerge from targeting secondary structures occurring in repeat containing RNA or specifically inhibit RAN-translation by other means. Here, structure-specific small molecules recognize and bind to nucleotides with a defined RNA conformation, such as RNA hairpins or G-quadruplexes, as seen in the *C9orf72* hexanucleotide repeat transcript. Most recently, it was shown that application of compounds binding to the *C9orf72* repeat RNA reduced RNA foci and poly-GP expression in iPSC-derived spinal motor neurons, cortical neurons, and flies (Simone et al., 2018). However, it remains an open question whether these compounds might also bind off target or inhibit ATG-initiated translation of regular repetitive RNA. Even so, Simone and colleagues pave the way for new *C9orf72*-associated treatment opportunities and provide a serious therapy option to ASOs which, in contrast to small molecules, require invasive application.

Although ASOs, RNA-targeting small molecules or other compounds might be viable treatment options for *C9orf72*-ALS/FTD, only clinical trials can show their suitability and efficacy in patients. Ultimately, patients can only profit from the fast evolving *C9orf72* research field which shows great interest in *C9orf72*-associated therapies.

1.3. Translation deregulation in human disease

The ribosome is one of the most accurately constructed and most complex molecular machines of the cell. It is the workplace for protein synthesis which itself is a finely tuned process. Translation factors, transfer RNAs (tRNAs) and ribosomes need to be coordinated precisely in order to translate the information contained in mRNA into a polypeptide chain. Thus, the ribosome, as well as the process of translation, are both highly susceptible to malfunction on multiple levels. Consequently, a variety of human diseases exist which are linked to ribosome structure and biogenesis, ribosome assembly, tRNA modifications, tRNA synthetases and other proteins involved in protein translation (Figure 1-6).

1.3.1.   Ribosomopathies

Alterations in ribosomal structure and function can lead to a heterogeneous class of disease termed ribosomopathies. Usually, the ribosome is built up of four rRNAs and a large number of ribosomal proteins forming a ribonucleoprotein. It comprises two subunits of different size that work as one: the small 40S subunit, which binds to the mRNA template, and the large 60S subunit, which binds to the tRNA and the amino acids. In eukaryotes, the biogenesis of ribosomes occurs in the nucleolus. For transcription of ribosomal proteins, ribosome maturation, rRNA modification, folding and processing (described in 'Poly-GR and poly-PR alter rRNA processing') as well as ribosome assembly, a plethora of factors are needed (Fromont-Racine et al., 2003; Henras et al., 2008; Kressler et al., 2010). Mutations in these factors or in ribosomal proteins themselves might result in genetic ribosomopathy.

In 1999 for example, a mutation in the RPS19 gene was discovered to account for 25% of patients suffering from Diamond-Backfan Anemia (DBA) (Draptchinskaia et al., 1999). Since then, more mutations have been identified to lead to DBA – 50% to 70% of those affected genes encoding ribosomal proteins (Gerrard et al., 2013). The deficiencies in ribosomal proteins result in impaired ribosome assembly and decreased translation in cells of both hematopoietic and non-hematopoietic lineage, although the disease is characterized by low red cell count (Gazda et al., 2006). Similarly, also the 5q-syndrome, which shares clinical and pathologic features with DBA including anemia, is linked to haploinsufficiency of another ribosomal protein, namely RPS14 (Ebert et al., 2008). Mutations in *DKC1* and *TCOF1*, both involved in ribosome biogenesis, play a role in X-linked Dyskeratosis Congenita (Heiss et al., 1998) and the Treacher-Collins Syndrome (Dixon, 1996), respectively.
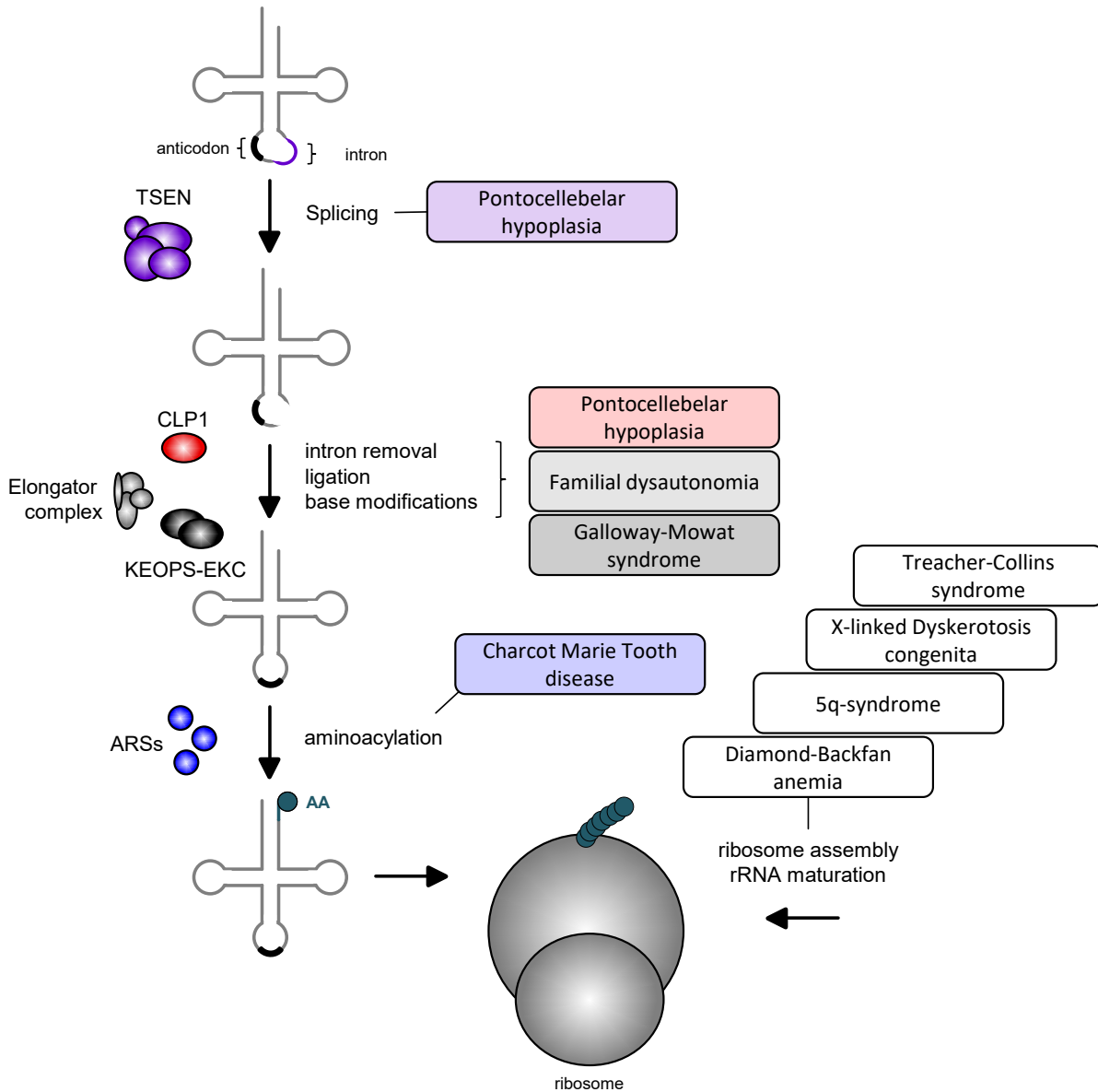
Figure 1-6: **Scheme of translation deregulation in human disease.**

Translation deregulation in human disease can occur on multiple levels. Disrupted tRNA maturation, dysfunctional aminoacyl tRNA synthases or impaired ribosome assembly can all result in disease. Pontocerebellar hypoplasia, for example, is caused by defective tRNA splicing due to mutations in components of the tRNA-splicing endonuclease (TSEN) complex and in the polynucleotide kinase CLP1 (also part of TSEN). Uridine and adenosine bases are modified by the Elongator Complex and the KEOPS-EKC proteins, respectively. Mutations in these proteins cause familial dysautonomia and the Galloway-Mowat syndrome. Mutated ARSs result in disease in two ways: either by non-functional synthase activities (Charcot Marie Tooth disease) or non-functional proof-reading activities leading to amino acid (AA) misincorporation and misfolded proteins. Ribosomopathies like Diamond-Backfan anemia and the Treacher-Collins syndrome are defined by mutations in either ribosomal proteins themselves or proteins associated with ribosome biogenesis such as DKC1 and TCOF1.

1.3.2. Deregulation of tRNA function is often connected to neurodegenerative diseases

tRNAs are the adaptor molecules between the information encoded by nucleic acids and the information on a protein level. They show a highly conserved as well as complex secondary and tertiary structure which is crucial to ensure efficient translation by correct codon-anticodon interactions. tRNA

biogenesis involves a multistep maturation process with a cascade of enzymatic reactions. Currently, 93 post-transcriptional modifications are known (Cantara et al., 2011). These are executed by a variety of modulators such as endo- and exonucleases, ligases, kinases, and transferases. The functionality of these factors is of major importance as their modifications can lead to enormous tRNA structural rearrangements and with it tRNA dysfunction. Mutations in tRNA modifying factors lead to several human disorders.

For example, pontocerebellar hypoplasia (PCH) is a spectrum of early onset neurodegenerative diseases commonly characterized by impaired brain development, muscle weakness and motor deficits (Ryan et al., 2000). It is caused by mutations in proteins of the tRNA splicing endonuclease complex (TSEN) with *TSEN54, TSEN34, TSEN15*, and *TSEN2* among them (Breuss et al., 2016; Budde et al., 2008). Also homozygous mutations in *CLP1*, an additional factor required for tRNA intron removal and ligation, are reported in individuals with PCH (Karaca et al., 2014; Schaffer et al., 2014). These mutations result in reduced affinity of individual components of the complex which leads to altered enzymatic activity and defects in tRNA splicing. Schaffer *et al*. suggest a subsequent accumulation of tRNA fragments including 'half' tRNAs which are known to inhibit protein translation (Sobala and Hutvagner, 2013). Further neurodegenerative diseases associated with dysfunctional tRNA include Familial Dysautonomia (mutation in the Elongator complex which is in charge of uridine modifications) (Anderson et al., 2001) and Galloway-Mowat syndrome (mutation in the KEOPS-EKC complex which is in charge of adenosine modifications) (Braun et al., 2017).

1.3.3. Mutant aminoacyl tRNA synthetases cause disease in multiple ways

Aminoacyl tRNA synthetases (ARS) are the enzymes that ligate amino acids (AAs) to their corresponding tRNA. These multidomain proteins catalyze the covalent attachment of the AAs to the tRNA in a two-step reaction. To ensure the correct translation of mRNA, accurate function of the ARS catalytic, as well as editing, activity is necessary (Pang et al., 2014). Predominantly mutations in glycyl-tRNA, tyrosyl-tRNA, and alanyl-tRNA synthetase have been reported to cause Charcot Marie Tooth (CMT) disease (Antonellis et al., 2003; Jordanova et al., 2006; Latour et al., 2010). CMT is the most common heritable disorder of the peripheral nervous system and patients suffer from progressive muscle weakness and wasting as well as loss of touch sensation. It is hypothesized that the common underlying pathogenic mechanism of ARS mutations is inhibition of translation (Storkebaum, 2016).

Not only translational inhibition but also misincorporation of false AAs into the nascent poly-peptide chain can be an outcome of mutations in ARS. Lee *et al.* report a mutation within the active site of the alanyl-ARS editing domain. Normally, mischarged tRNAs would be cleared by the editing function of ARS, however, this ARS mutant shows proofreading defects. The subsequent AA misincorporation during protein synthesis leads to misfolded or unfolded proteins which accumulate

and stress the proteostasis system. Concomitant with the knowledge that protein aggregation commonly leads to neuron loss, the most prominent phenotype in their mouse model is neurodegeneration (Lee et al., 2006).

1.3.4. Evidence for protein translation defects in ALS and FTD

Experiments in cellular models of ALS/FTD point to a role of in these diseases. TDP-43 knockdown, for example, results in alternative splicing of SKAR, an exon junction complex. Subsequently, S6 kinase activity is enhanced which in turn leads to increased translation and cell size. Thus, mutant TDP-43 might regulate translation on a global level (Fiesel et al., 2012). Interestingly, the lysyl-ARS binds to mutant but not wild type SOD1, further connecting ALS to translation. In this scenario, lysyl-ARS might co-aggregate with mutant SOD1 and thereby be impaired in performing its normal function (Kunst et al., 1997). Whether also the DPR proteins poly-GR and poly-PR contribute to alterations in protein translation remains elusive. As so far only altered rRNA processing has been implicated, more evidence is needed to link the two arginine rich DPR protein species to translation deregulation.

Taken together, disorders associated with deregulation of protein translation often belong to the group of neurodegenerative diseases. It would be rewarding for the ALS/FTD field to elucidate whether altered protein synthesis also contributes to neurodegeneration in these patients.

2. AIM OF THIS WORK

Despite several proposed pathomechanisms, it is still largely unclear how the *C9orf72* repeat expansion and in particular the individual dipeptide repeat (DPR) proteins mediate toxicity ultimately leading to neurodegeneration in patients. Several studies showed that poly-GA impairs the ubiquitin proteasome system and interferes with nucleocytoplasmic transport (Guo et al., 2018; Khosravi et al., 2017; May et al., 2014; Mizielinska et al., 2014; Yamakawa et al., 2015). However, while poly-GA is the most abundant DPR species in patient brains, poly-GR and poly-PR are more toxic in cell culture and animal models (Kanekura et al., 2016; Kwon et al., 2014; Lee et al., 2016a; Lopez-Gonzalez et al., 2016; Tao et al., 2015; Wen et al., 2014). When I started my dissertation in the Edbauer lab, little was known about the role of arginine-rich DPR proteins in relation to neurodegeneration. At that time, only two groups had published their results on the mechanistic contribution of poly-GR/PR to disease pathology. Their studies revealed that the two DPR protein bind nucleoli, induce stress granule formation, impair mRNA splicing and disrupt rRNA processing *in vitro* (Kwon et al., 2014; Wen et al., 2014).

Based on these findings, the major aim of my work was to further elucidate by which mechanisms poly-GR and poly-PR contribute to cellular toxicity and determine their relevance in *C9orf72* patients. An extensive interactome study based on mass spectrometry in primary neurons and HEK293 cells should identify the major proteins sequestered by the arginine-rich DPR proteins. In parallel, the global effects of poly-GR/PR on the neuronal proteome should be monitored. A system level enrichment analysis of the protein networks should be used to prioritize specific interactors from key cellular compartments for individual detailed analysis using a variety of methods including validation of co-aggregation in patient tissue. Finally, specific interactors and common identified pathways should be tested for modulation of poly-GR and poly-PR toxicity.

Since my aim was to reveal potential pathogenic disease mechanisms, the used models should resemble the disease context in *C9orf72*-ALS/FTD patients as closely as possible. Therefore, it was of great importance to conduct the interactome study as well as the subsequent validation experiments in primary hippocampal and cortical neurons. Validation of poly-GR/PR interactors directly in patient tissue was critical to connect cell culture models to human disease.

Another aim was to address the importance of subcellular localization of poly-GR/PR toxicity as several groups reported poly-GR as well as poly-PR to be predominantly localized to the nucleolus *in vitro*, while both proteins are almost exclusively found in cytoplasmic inclusions in patient brains.

Taken together, the mechanisms of poly-GR and poly-PR toxicity should be investigated *in vitro* and subsequently be linked to *C9orf72* disease pathogenesis in patients starting with an interactome study in primary neurons.

3. MATERIALS

3.1. Instruments, devices and equipment

3.1.1. General equipment

Equipment	Supplier
scale BP3100S	Sartorius
Certomat BS-1 incubator	B. Braun Biotech International
developing machine Cawomat 2000 IR	CaWo
filter trap slot blot	Hoefer Scientific Instruments
forceps	FST
freezer (-20°C)	Liebherr
freezer (-80°C) HFU-T Series	Hareus
fridge	Liebherr
glassware	VWR, Hirschmann
incubator for bacteria	Binder
liquid Nitrogen tank	Messer Griesheim
microwave inverter	Sharp
MilliQ plus filtration system QPod	Merck Millipore
multichannel pipettes	VWR
multichannel pipettes - automated	Rainin
NanoPhotometer^{TM}	Implen
pH meter Five Easy	Mettler-Toledo
pipette boy	Brand
pipettes	Gilson, Rainin
scanner V700 Photo	Epson
shaker	Edmund Bühler
Thermomixer® comfort	Eppendorf
vortex-Genie 2	Scientific Industries

3.1.2.   **Centrifuges**

(a) Beckman Coulter Ultracentrifuge Optima XpN90 with SW28 rotor; (b) Heraeus Multifuge 3 SR with a swing-out rotor for Falcon Tubes and 96-well plates; (c) Heraeus Megafuge 16; (d) Heraeus Megafuge 40R (e) Eppendorf Centrifuge 5427R for centrifugation of 1.5 and 2 mL reaction tubes at 4°C or RT; (f) Eppendorf Centrifuge 5417R for centrifugation of 1.5 and 2 mL reaction tubes at 4°C or RT.

3.1.3.   **Microscope equipment**

(a) BioTek Cytation 3 imaging reader; (b) Hund Wetzlar Light Microscope WilovertS Mikro; (c) Olympus CKX41 Fluorescent Microscope with (d) Olympus RFL-T Mercury Burner MSH-1030L; (e) Zeiss LSM 710 Confocal Laser Scanning Microscope; with (f) LASOS RMC 7812 Z2 remote control; (g) Zeiss Illuminator HXP 120 V; (h) Zeiss Stage Controller XY CD MC 2008; (i) Zeiss Objective Plan Apochromat 40x/1.4 oil DIC; (j) Zeiss Objective Plan Apochromat 63x/1.4 oil DIC.

3.1.4.   **Devices for (qRT-)PCR experiments**

(a) Bio Rad PowerPac Basic Power Supply; (b) Bio Rad CFX384 Touch^{TM} Real-Time PCR Detection System; (c) Eppendorf PCR thermal cycler nexus (gradient eco) (d) INTAS UV Transilluminator; (e) Mitsubishi P93D printer (f) peqlab and owl separation systems gel chambers and combs; (g) Rainin EDP3 Multichannel Pipette E3-8-20.

3.1.5.   **Cell culture**

(a) Agilent Seahorse XF96 extracellular flux analyzer; (b) Agilent Seahorse XF prep station; (c) GFL waterbath; (d) Heraeus Hera cell culture hood Safe2020; (e) Heraeus Hera incubator Safe Cell 150; (f) Heraeus Bunsen burner; (g) LifeTechnologies Countess II.

3.1.6.   **Protein biochemistry**

(a) Bio-Rad glass plates for electrophoresis gels; (b) Bio-Rad electrophoresis gel casting system; (c) Bio-Rad Mini-PROTEAN Tetra Cell Electrophoresis system; (d) Bio-Rad Mini-PROTEAN Trans-Blot Transfer Cell; (e) Bio-Rad foam pads; (f) Branson Digital Sonifier 250; (g) Fuji X-ray films; (h) G. Kisker X-ray film chamber.

3.1.7.   **Mass spectrometry**

(a) Maisch GmbH Inhouse 1.9 µm C18 particle packed columns with 75µm inner diameter and 20 cm length; (b) Thermo Fisher Easy-nLC 1000 HPLC system; (c) Thermo Fisher Orbitrap Elite.

3.2. Software

(a) Adobe Systems Incorporated - Adobe Acrobat Pro; (b) Bio Rad – CFX Manager for qRT-PCR data analysis; (c) CLC bio – CLC Main Workbench for DNA, RNA, and protein analysis; (d) Ensemble online data base (http://www.ensembl.org/index.html); (e) Fiji for image processing; (f) Graphpad Software, Inc. – GraphPad PRISM for statistical analysis; (g) Microsoft Corporation – Microsoft Office 2016; (h) Primer 3 online tool for qPCR primer design (http://bioinfo.ut.ee/primer3/); (i) NCBI online data base (http://www.ncbi.nlm.nih.gov/); (j) Thomson Reuters - EndNote X8.

3.3. Services

(a) DNA Sequencing: GATC Biotech; (b) Oligonucleotide Synthesis: Sigma-Aldrich.

3.4. Consumable supplies

3.4.1. General consumables

equipment	supplier
Biosphere® Filtertips	Sarstedt
gloves (Latex)	Semperit
gloves (Nitrile)	Meditrade
Parafilm 'M'	Pechiney Plastic Packaging
pH indicator strips	Merck Millipore
Pipette Tips, Ultrafine™	VWR
scalpel	Braun
serological pipettes (2 mL, 5 mL, 10 mL, 25 mL)	Sarstedt
Tubes (1.5 mL, 2 mL)	Sarstedt
Tubes (15 mL, 50 mL)	Sarstedt
LoBind Tubes (1.5 mL)	Eppendorf

3.4.2. Cell culture

equipment	supplier
cell counting chambers Countess II	Life Technologies
cell culture dish (3.5 cm, 6 cm, 10 cm)	Nunc
cell culture plate (6 well, 12 well, 96 well)	Nunc
microscope cover glasses (20 mm)	VWR
PES membrane filter, 0.45 μm	VWR
syringe (50 mL)	VWR

3.4.3. Molecular biology

equipment	supplier
FrameStar 384	4titude
MicroAmp Optical 8-Tube strip	Applied Biosystems
Microseal® 'B' Adhesive Seal	Bio Rad
PCR Strip tubes	VWR

3.4.4. Protein biochemistry

equipment	supplier
0.2 µm cellulose acetate membrane	GE Healthcare
Blotting Paper	Macherey-Nagel
Immobilon-P membrane, PVDF, 0.45 µM	Merck Millipore
Novex™ 10-20% Tricine Protein Gels	Thermo Fisher
MaxiSorb 96-well plate	Thermo Fisher

3.5. Chemicals and reagents

3.5.1. General consumables

equipment	supplier
2-propanol	Merck Millipore
Boric acid	Merck Millipore
Brij® 35	Sigma-Aldrich
citric acid	Sigma-Aldrich
dimethyl sulfoxide (DMSO)	Roth
ethanol	Merck Millipore
ethylenediaminetetraacetic acid (EDTA)	USB
fetal calf serum (FCS)	Life Technologies
fish gelatin	Sigma-Aldrich
formic acid	Sigma-Aldrich
gelatin	Sigma-Aldrich
Glycerole	Biomol
glycine	Biomol
Hepes	BioMol
KCl	USB
KH_2PO_4	Merck Millipore

methanol	Merck Millipore
MgCl$_2$	Roth
Na$_2$[B$_4$O$_5$(OH)$_4$] (Borax)	Sigma-Aldrich
Na$_2$HPO$_4$	Merck Millipore
H$_2$SO$_4$	Merck Millipore
Na$_2$HPO$_4$	Merck Millipore
NaCl	Merck Millipore
paraformaldehyde (PFA)	SERVA
sodium citrate	Sigma-Aldrich
sodium dodecyl sulfate (SDS)	Roth
sucrose	Sigma-Aldrich
Sudan Black B	Sigma-Aldrich
Tris	AppliChem
Triton X-100	Merck Millipore
Tryptone	BD Bioscience
Tween 20	Sigma-Aldrich
Xylol	Merck Millipore

3.5.2. Cell culture

equipment	supplier
Bovine serum albumin (BSA)	Sigma-Aldrich
DMEM Glutamax	Life Technologies
L-Glutamate	Sigma-Aldrich
L-Glutamine	Sigma-Aldrich
Lipofectamine2000	Life Technologies
Neurobasal	Life Technologies
Non-essential amino acids (NEAA)	Life Technologies
OptiMEM	Life Technologies
Penicillin/Streptomycin	Life Technologies
Poly-D-Lysine (PDL)	Sigma-Aldrich
Seahorse XF Assay-Medium	agilent technologies
Seahorse XF Calibrant	agilent technologies
tetracycline	Sigma-Aldrich
Trypsin (2.5%)	Life Technologies

3.5.3. Molecular biology

equipment	supplier
1 kb Plus DNA Ladder	Invitrogen
4',6-Diamidin-2-phenylindol (DAPI)	Roche Applied Science
Ampiciline	Boehringer Ingelheim
Antimycin	Sigma-Aldrich
Bromphenol blue	Merck Millipore
calf intestine alkaline phosphatase (CIP)	NEB
dNTP Mix, 10 mM	Thermo Scientific
FCCP	Sigma-Aldrich
GelRed^{TM}	Biotium
Oligomycin	Sigma-Aldrich
Q5 DNA polymerase	NEB
Random Hexamer Primer	Sigma-Aldrich
restriction enzymes	NEB
RiboLock RNase Inhibitor	Thermo Scientific
Rotenone	Sigma-Aldrich
SsoFast^{TM} Eva Green® Supermix	Bio Rad
T4 Ligase	NEB
Taq DNA polymerase	Promega
TO-PRO-3	Life Technologies
UltraPure^{TM} Agarose	Life Technologies
Proteinase K	Sigma-Aldrich

3.5.4. Protein biochemistry

equipment	supplier
ammonium persulfate	Sigma-Aldrich
Benzonase	Sigma-Aldrich
dithiothreitol (DTT)	Sigma-Aldrich
DNase	Sigma-Aldrich
Dynabeads™ Protein G	invitrogen
ECL plus	Thermo Scientific
enhanced chemiluminescence (ECL)	Thermo Scientific
i-Block	Tropix

NaN$_3$	Merck Millipore
protease inhibitor cocktail	Sigma-Aldrich
SeeBlue Prestained Protein Ladder Plus 2	Life Technologies
puromycin	Merck Millipore
tetramethylethylendiamin (TEMED)	USB
tricine	Sigma-Aldrich
β-mercaptoethanol	Merck Millipore
Acrylamid (37.5:1/40% (w/v))	BioRad
3,3',5,5'-Tetramethylbenzidine (TMB)	Sigma-Aldrich
GFP magnetic beads	chromotek

3.6. Antibodies

3.6.1. Primary antibodies

antigen	supplier	usage
mouse α GFP	Clonetech	WB
mouse α HA	Sigma-Aldrich	IF
mouse α HA, clone R001	Elisabeth Kremmer	WB, immunoassay
mouse α MTCO1	abcam	WB, IF
mouse α MTCO2	abcam	IF
mouse α PR, clone 32B3	Elisabeth Kremmer	WB, IF
mouse α puromycin	Merck Millipore	WB
mouse α RPL19	Santa Cruz Biotechnology	WB, IF
mouse α RPS25	Santa Cruz Biotechnology	WB, IF
mouse α RPS36A	Santa Cruz Biotechnology	WB, IF
mouse α RPS6	Santa Cruz Biotechnology	WB, IF
mouse α TIAR	Santa Cruz Biotechnology	IF
rabbit α BOP1	abcam	WB
rabbit α Calnexin	Proteintech	WB
rabbit α Fibrillarin	abcam	IF
rabbit α FMRP	abcam	IF
rabbit α G3BP	abcam	IF

rabbit α G3BP2	abcam	IF
rabbit α GFP, clone N38/8	Neuromab	WB
rabbit α GFP, clone N86/8	Neuromab	IF, IP
rabbit α GTPBP4	abcam	IF
rabbit α H4R3me2A	abcam	WB
rabbit α MAGOHB	abcam	IF
rabbit α mono methylated arginine	Cell Signaling	WB
rabbit α MRPL19	abcam	IF
rabbit α MRPS9	abcam	IF
rabbit α NOP56	Atlas Antibodies	IF
rabbit α PES1	Thermo Fisher	WB
rabbit α PRMT1	abcam	IF
rabbit α STAU2	abcam	IF
rabbit α symmetric di-methyl arginine	Cell Signaling	WB
rabbit α TRA2A	abcam	IF
rabbit α WDR77	Atlas Antibodies	IF
rabbit α YBX1	abcam	IF
rat α GR, clone 7H1	Elisabeth Kremmer	IF
rat α GST, clone 6G9	Elisabeth Kremmer	immunoassay

3.6.2. Secondary antibodies

antigen	supplier	label	usage
goat α mouse IgG	Life Technologies	Alexa488, 555 or 647	IF
goat α rabbit IgG	Life Technologies	Alexa488, 555 or 647	IF
goat α rat IgG	Life Technologies	Alexa488, 555 or 647	IF
goat α mouse IgG	Promega	horse radish peroxidase (HRP)	WB
goat α rabbit IgG	Promega	HRP	WB
goat α rat IgG	Merck Millipore	HRP	WB, ELISA

3.7. Kits

(a) Applied Biosystems TaqMan MicroRNA Reverse Transcription Kit; (b) DCS SuperVision 2 Kit (c) Macherey-Nagel Extract II Kit; (d) Macherey-Nagel NucleoBond®Xtra Midi; (e) Macherey-Nagel NucleoBond® Plasmid; (f) Macherey-Nagel NucleoSpin® Gel and PCR Cleanup; (g) Qiagen RNeasy Mini Kit; (h) Roche Cell Proliferation Kit II (XTT); (i) Promega CytoTox 96® Non-Radioactive Cytotoxicity (LDH);

3.8. Buffers

Components of buffers were dissolved in MilliQ water unless stated otherwise.

3.8.1. Buffers for cell culture experiments

equipment	supplier
borate buffer	40 mM boric acid 10 mM sodium tetra borate adjusted to pH 8.5
Coating solution for glass cover slips	1.5% PDL dissolved in borate buffer
HEK293 and HeLa medium	1% Penicillin/Streptomycin 1% NEAA 10% FCS in DMEM Glutamax
phosphate-buffered saline (PBS)	0.14 M NaCl 10 mM Na_2HPO_4 2.8 mM KH_2PO_4 2.7 mM KCl adjusted to pH 7.4

3.8.2. Buffers for molecular biology experiments

equipment	supplier
5x DNA loading buffer	50% Glycerol 50 mM Na_2EDTA 0.05% Bromophenol blue adjusted to pH 8.0
LB agar	1.5% agar 1% Tryptone 0.5% Yeast extract

	86 mM NaCl
lysogeny broth (LB) medium	1% Tryptone
	0.5% Yeast extract
	86 mM NaCl
sodium borate buffer (SB)	5 mM $Na_2[B_4O_5(OH)_4]$
	adjusted to pH 8.0 with H_3BO_3
immunoprecipitation lysis buffer	2% Triton X-100
	0.75 M NaCl
	1 mM KH_2PO_4
	3 mM Na_2HPO_4
immunoprecipitation basic buffer	50 mM Tris-HCl pH 7.5
	150 mM NaCl
	5% glycerol

3.8.3. **Buffers for biochemical experiments**

equipment	supplier
4x Lämmli sample buffer	4% SDS
	20% glycerol
	5% β-mercaptoethanol
	200 mM Na_2HPO_4
blocking buffer	0.2% i-Block in TBSTx
tricine gel running buffer	0.1 M Tris-HCl
	0.1 M Tricine
	0.1% SDS
RIPA buffer	50 mM Tris-HCl
	150 mM NaCl
	2 mM EDTA
	1% NP-40
	0.1% SDS
TBSTx	20 mM Tris
	0.14 M NaCl
	0.2% Triton X-100
	adjusted to pH 7.6
tricine buffer	0.1 M Tris-HCl
	0.1 M Tricine

	0.1% SDS
transfer buffer	25 mM Tris
	0.2 M Glycine
ribosome assay buffer	20 mM Hepes pH 7.4
	100 mM KOAc
	20 mM $MgCl_2$
	2 mM DTT (add freshly)

3.8.4. **Buffers for immunofluorescence and immunohistochemistry**

equipment	supplier
citrate buffer A	0.1 M citric acid
citrate buffer B	0.1 M sodium citrate
fixing solution	4% PFA
	0.15 mM NaOH
	0.13 mM NaH_2PO_4
	0.12 mM sucrose
	adjusted to pH 7.5
immunohistochemistry blocking buffer	2% FCS dissolved in PBS
immunohistochemistry wash buffer	0.05% Brij dissolved in PBS
immunofluorescence blocking buffer	2% fetal bovine serum
	2% bovine serum albumin
	0.2% fish gelatin
	dissolve in PBS
permeabilisation buffer	0.2% Triton-X-100
	50 mM NH4Cl
	dissolve in PBS

3.9. Bacteria strains and cell lines

equipment	supplier
DH5α and Stbl3 *E.coli* competent cells	Life Technologies
HEK293-FT	Life Technologies
HeLa	Life Technologies

3.10. DNA oligonucleotides and plasmids

3.10.1. Primers for cloning

name		sequence
GFP-GR$_{15}$/GR$_{53}$	sense	tcgagaggatccgccaccATGGTGAGCAAGGGC
	antisense	atactcgagttaTCTGCCTCGCCCCCGTCCCCGTCC,
		atactcgagttaCCTGCCTCGTCCGCGTCCCCTTCC, and
		atactcgagttaTCTGCCTCTGCCCCTGCCCCTGCC
RFP-hTRA2A	sense	ATAggcgcgccTATGAGTGATGTGGAGGAAAACAACTTCGAGGGC
	antisense	tatgcggccgcTCAATAGCGTCTTGGGCTGTAGGAACGAGATC
RFP-hTRA2B	sense	ATAggcgcgccTATGAGCGACAGCGGCGAGCAGAA
	antisense	tatgcggccgcTTAATAGCGACGAGGTGAGTATGATCGAGATCTGGAAC
RFP-hSRSF1 iso1	sense	ataggcgcgcctATGTCGGGAGGTGGTGTGAT
	antisense	gatcctgcaggTTATGTACGAGAGCGAGATCTGCT
RFP-hSRSF10	sense	ATAggcgcgccTATGTCCCGCTACCTGCGTCCC
	antisense	tatgcggccgcTCAGATCTTTCTTGAAGTGTAGTAAGCAGAACTGTAC
RFP-hNPM1	sense	ATAggcgcgccTATGGAAGATTCGATGGACATGGACATGAGCC
	antisense	tatgcggccgcTTAAAGAGACTTCCTCCACTGCCAGAGATCTTGAATA
RFP-hNOP56	sense	ATAggcgcgccTATGGTGCTGTTGCACGTGCTGTTTG
	antisense	tatgcggccgcCTAATCTTCCTGGGATGCTTTATGGAACTTTTTCTTC
RFP-hSTAU1	sense	ATAggcgcgccTATGAAACTTGGAAAAAAACCAATGTATAAGCCTGTTGA
	antisense	tatgcggccgcTCAGCACCTCCCACACACAGACATT
RFP-hYBX1	sense	ATAggcgcgccTATGAGCAGCGAGGCCGAGACCCAGC
	antisense	tatgcggccgcTTACTCAGCCCCGCCCTGCTCAGCC
RFP-hBRIX1	sense	ATAggcgcgccTATGGCGGCAACCAAGAGGAAACGG
	antisense	tatgcggccgcTTATTTTGTTTTCCCACTGTCCATCCTCTGTTTCATT
RFP-hGTPBP4	sense	ATAggcgcgccTATGGCACATTACAACTTCAAGAAAATTACGGTGGTGCC
	antisense	tatgcggccgcCTATCTCCTGTCCTTTTTACCAGCTTTCCTCTTCC

3.10.2. qPCR primers

target	sense sequence	antisense sequence
18S rRNA	GATGGTAGTCGCCGTGCC	GCCTGCTGCCTTCCTTGG
5.8S rRNA	ACTCGGCTCGTGCGTC	GCGACGCTCAGACAGG
BOP1	AGAGAAGACCTCTGAGGAGCA	TCATCTCTGGTCAGAGCACCTG
PES1	CCTCCATGAACCCATCGTCAA	ACTCGCTCTTCCCATAGGCT

3.10.3. Plasmids

construct	cloning strategy
FhSynW GFP-GA$_{50}$-GR$_{50}$-myc	Dieter Edbauer
FhSynW GFP-GA$_{50}$-PR$_{50}$-myc	Dieter Edbauer
FhSynW GFP	Dieter Edbauer
FhSynW PR$_{175}$-GFP NES	Dieter Edbauer
FhSynW-175xPR-GFP	Dieter Edbauer
FhSynW2 GFP-GR$_{149}$	Dieter Edbauer
FhSynW2 GFP-GR$_{149}$ NES	Dieter Edbauer
FhSynW2 GFP-GR$_{53}$	PCR from FhSynW2 GFP-GR149c BamHI/XhoI cloning into FhSynW2 GFP-GR149c
FU2 HA-hMEK1 constitutive active	Dieter Edbauer
FU3a tagRFP-hBRIX1	PCR from ORF clone (Daniel Hornburg) AscI/NotI cloning into FU3a-tagRFP-T2 2b
FU3a tagRFP-hEIF4A3	Dieter Edbauer
FU3a tagRFP-hGTPBP4	PCR from ORF clone (Daniel Hornburg) AscI/NotI cloning into FU3a-tagRFP-T2 2b
FU3a tagRFP-hNOP56	PCR from ORF clone (Daniel Hornburg) AscI/NotI cloning into FU3a-tagRFP-T2 2b
FU3a tagRFP-hNPM1	PCR from ORF clone (Daniel Hornburg) AscI/NotI cloning into FU3a-tagRFP-T2 2b
FU3a tagRFP-hSTAU1	PCR from ORF clone (Daniel Hornburg) AscI/NotI cloning into FU3a-tagRFP-T2 2b
FU3a tagRFP-rStau2-LL	Dieter Edbauer
FU3a tagRFP-hYBX1	PCR from ORF clone (Daniel Hornburg) AscI/NotI cloning into FU3a-tagRFP-T2 2b

FU3a tagRFP-hSRSF1 iso1	PCR from cDNA AscI/SfbI cloning into FU3a-tagRFP-T2 2b
FU3a tagRFP-hSRSF10	PCR from cDNA AscI/NotI cloning into FU3a-tagRFP-T2 2b
FU3a tagRFP-hTRA2A	PCR from ORF clone (Daniel Hornburg) AscI/NotI cloning into FU3a-tagRFP-T2 2b
FU3a tagRFP-hTRA2B	PCR from ORF clone (Daniel Hornburg) AscI/NotI cloning into FU3a-tagRFP-T2 2b
FU3a tagRFP-hYBX1	PCR from ORF clone (Daniel Hornburg) AscI/NotI cloning into FU3a-tagRFP-T2 2b
FU3a-H2B-mEGFP	Dieter Edbauer
FU3a-tagRFP-T2 2b	Dieter Edbauer
FU3a-tagRFP-T2 n1	Dieter Edbauer
pEF6 GFP	Dieter Edbauer
pEF6 GFP-GR$_{149}$	Dieter Edbauer
pEF6 GFP-GR$_{53}$	BamHI/EcoV cloning into pEF6 triple-tag control
pEF6 triple-tag control	Dieter Edbauer
pEF6-175xPR-GFP	Dieter Edbauer

4. METHODS

4.1. Molecular biology

4.1.1. Molecular cloning

4.1.1.1. *Cloning strategy*

Complementary DNA (cDNA) sequences of interest were either excised with restriction enzymes or polymerase chain reaction (PCR) amplified from a plasmid template or prepared cDNA. In order to insert cDNA sequences into a desired vector, restriction sites were chosen according to available restriction sequences in the multiple cloning site of the acceptor vector. Therefore, PCR primers were designed with restriction sites attached to the original primer sequences.

4.1.1.2. *Polymerase chain reaction*

For standard PCR reactions Taq, Pwo or the high fidelity Q5 polymerase were used according to the standard conditions given in the tables below. For optimization these protocols were modified with regard to annealing temperature.

Table 1:*Taq/Pwo* polymerase PCR standard components and temperature profile

components	volume
~150 ng template DNA	~ 2 µL
primer forward (10 µM)	0.2 µL
primer reverse (10 µM)	0.2 µL
dNTPs (10 mM each)	1 µL
10x Taq Buffer	5 µL
DNA Polymerase (5U/µL)	0.2 µL
MilliQ water	**ad 50 µL**

	temperature	time
initial denaturation	94°C	2 min
denaturation	94°C	30 sec
annealing	$T_{m(primer)}$-5°C	30 sec
elongation	73°C	1 min/1kb
final elongation	73°C	10 min
36 cycles		

Table 2: *Q5* polymerase PCR standard components and temperature profile

components	volume		temperature	time
~50 ng template DNA	~ 2 µL	initial denaturation	98°C	30 sec
primer forward (10 µM)	0.25 µL	denaturation	98°C	30 sec
primer reverse (10 µM)	0.25 µL	annealing	$T_{m(primer)}$-5°C	30 sec
dNTPs (10 mM each)	1 µL	elongation	72°C	30 sec/1kb
10x Taq Buffer	10 µL	final elongation	72°C	2 min
DNA Polymerase (5U/µL)	0.5 µL	**36 cycles**		
MilliQ water	**ad 50 µL**			

4.1.1.3. *Gel electrophoresis and isolation of DNA fragments*

In order to analyze and separate DNA fragments one dimensional agarose gel electrophoresis was performed. Gels containing 0.7% to 2% agarose in Sodium Borate (SB) buffer dependent on the expected DNA length were supplemented with GelRed (1:50,000) and subsequently loaded with DNA samples premixed with the respective amount of 5x DNA loading buffer. Gels were run at constant 300 V. DNA fragments were visualized by transillumination with ultraviolet light and analyzed by comparison of fragments to the DNA ladder. Finally, the DNA of interest was purified with the NucleoSpin® Gel and PCR Cleanup Kit (Macherey-Nagel) according to the manufacturer's instructions.

4.1.1.4. *Digest of DNA by restriction endonucleases and dephosphorylation*

Typically, plasmids or PCR products were digested at 37°C for 1 h or overnight, respectively, in a 50 µL reaction with the respective endonucleases. The amount of enzyme, the buffer system and the conditions required for a complete digest were chosen according to the information provided by the manufacturer (NEB). To prevent self-ligation of plasmid backbones 5' phosphoryl termini were removed by calf intestine phosphatase (CIP). In a typical reaction 1 unit phosphatase was used for 3 µg of vector DNA at 37°C for 1 h. Subsequently, processed plasmids or PCR fragments were purified by gel electrophoresis or on column (see 4.1.1.3).

4.1.1.5. *Ligation*

A typical 20 µL ligation reaction comprised 3 µL vector backbone, 9 µL PCR product or plasmid fragment, 2 µL T4 DNA Ligase catalyzing the formation of a phosphodiester bond between 5' phosphorylated and 3' hydroxylated termini, 2 µL reaction buffer and water. The reaction was incubated for 1 h at room temperature (RT).

4.1.1.6.   *Transformation*

The complete volume of the ligation reaction was used for transformation into chemically competent DH5α cells. First, 100 µL bacteria cells were thawed on ice and DNA was added gently. Afterwards, cells were incubated on ice for 20 min, heat shocked for 30 sec at 42°C and again incubated on ice for 3 min. 400 µL antibiotic free LB medium was added prior to horizontal shaking (300 rpm) at 37°C for 1 hour. Thereafter, each transformation reaction was plated on a prewarmed antibiotic selective agar plate and incubated overnight at 37°C. For all repeat containing and therefore recombination prone inserts the temperature was set to 30°C.

4.1.1.7.   *Plasmid preparation and determination of DNA concentration*

In order to inoculate a 4 mL culture (mini preparation) or 100 mL culture (midi preparation) single colonies were picked from agar plates using a sterile pipette tip and transferred to LB (antibiotic selective) medium. For further amplification the cultures were incubated overnight at 37°C (or 30°C for repeat containing DNA). The next day, cells were pelleted by centrifugation at 3000 *g* for 10 min at 4°C and plasmid DNA was extracted using the NucleoSpin® Plasmid kit (Macherey-Nagel) for mini preparation or the NucleoBond®Xtra Midi kit (Macherey-Nagel) for midi preparation according to the manufacturer's instructions. Finally, the DNA was eluted in MilliQ water and stored at -20°C. Concentrations were determined by measurement of absorbance at 260 nm (NanoPhotometer™, Implen).

4.1.1.8.   *Sequencing*

In order to verify successful cloning, purified plasmids were sent to GATC Biotech for sequencing. Standard primers binding in the backbone were provided by the company.

4.1.2.   **Quantitative real time PCR (qRT-PCR)**

4.1.2.1.   *RNA isolation*

Total RNA isolation including DNase treatment was performed using the RNeasy Mini Kit (Qiagen) according to the protocol provided by the manufacturer. Purified RNA was eluted in 40 µL RNase-free water. Also, RNase-free consumables and solutions were used during all isolation steps. Concentrations were measured on the NanoPhotometer at 260 nm. RNA samples were stored at -80°C.

4.1.2.2.   *cDNA synthesis*

In order to transcribe RNA into cDNA the protocol provided with the TaqMan MicroRNA Reverse Transcription Kit was followed. cDNA was typically synthesized from 50 ng RNA using random hexamer primers (N6) according to Table 3. For generation of a standard curve equal amounts of each RNA

sample were pooled and diluted to a 1:10, 1:100, 1:1000 and 1:10,000 ratio. Freshly prepared cDNA was subsequently used as template in the qRT-PCR reaction.

Table 3: cDNA synthesis standard components and temperature profile

components	volume
dNTPs (100 mM)	0.3 µL
RNA (50 ng)	10 µL
N6 primer (50 ng/µL)	0.2 µL
RNase inhibitor	0.38 µL
10x RT Buffer	3 µL
MultiScribe™ Reverse Transcriptase (50 U/µL)	2 µL
RNse-free water	**ad 30 µL**

temperature	time
4°C	5 min
25°C	10 min
48°C	30 min
95°C	5 min

4.1.2.3.   *Quantitative PCR primer design*

Primers for the qRT-PCR reaction were designed to bind in exon-intron border regions, span an intron larger than 1000 bases and show no to little off target effects. Furthermore, the optimal product size was set to be 80 to 100 base pairs with a primer melting temperature of optimally 60°C and a primer size of 20 bases. Therefore, mRNA sequences were taken from the NCBI database and analyzed for suitable primers using the Primer3 web tool (http://bioinfo.ut.ee/primer3/).

4.1.2.4.   *qRT-PCR*

For a single qRT-PCR reaction 2 µl of 1:5 diluted cDNA were used as a template. For each primer pair a SsoFast™ EvaGreen (Bio Rad) containing reaction mix according to Table 4 was prepared. The reaction was performed using the CFX384 Real-Time System (Bio Rad) with the temperature profile depicted in Table 4. Primer pair specificity was verified by a single peak in melting curve analysis from 60°C to 95°C with increases of 0.5°C every 5 sec in advance. Each reaction was performed as triplicate. Mean relative mRNA expression values were calculated with the Δ-Δ-C_t using YWHAZ and GAPDH as housekeeping genes.

Table 4: qRT-PCR standard components and temperature profile

components	volume		temperature	time
SsoFast™ EvaGreen	2.5 µL	initial denaturation	95°C	30 sec
primer forward (20 µM)	0.125 µL	denaturation	95°C	5 sec
primer reverse (20 µM)	0.125 µL	annealing	60°C	5 sec
RNase-free water	0.25 µL	elongation	95°C	10 sec
DNA Polymerase (5U/µL)	0.2 µL	**50 cycles**		
reaction volume	**5 µL**			

4.2. Cell Biology

4.2.1. Maintenance of cells

4.2.1.1. *Cultivation of Human Embryonic Kidney (HEK293-FT) and HeLa cells*

HEK293-FT and HeLa cells were cultivated in DMEM Glutamax medium supplemented with 10% FCS, 1% Penicillin/Streptomycin (Pen/Strep) and 1% non-essential amino acids (NEAA) at 37°C and 5% CO_2. At a confluency of 80%, cells were split in a ratio of 1:10. For passaging, cells were washed once with PBS, detached with 1 mL 0.05% Trypsin/EDTA and replated in new medium.

4.2.1.2. *Cultivation of primary neurons*

Primary cortical and hippocampal neurons were cultured from embryonic day 19 Sprague-Dawley rats and cultivated in Neurobasal medium at 37°C and 5% CO_2. For cortical neurons the medium was supplemented with 2% B27, 1% Pen/Strep and 0.25% glutamine, for hippocampal neurons 0.125% glutamate was additionally added. Neurons were either plated in plastic dishes or on cover slips treated with 65% nitric acid and sterilized at 200°C for 6h. 85,000 and 400,000 cells were seeded for hippocampal and cortical neurons, respectively. Typically, primary neurons were transduced or transfected at 7 days *in vitro* (DIV7).

4.2.1.3. *PDL coating of cell culture dishes*

In order to avoid detachment of cells, both, plastic dishes and cover slip containing plastic dishes, were coated with 1.5% PDL in 0.1 M borate buffer for 4°h and washed with water three times before plating HEK293 or neuronal cells. For neurons a final equilibration step with Neurobasal medium followed. Dishes were kept in the cell culture incubator until cells were seeded.

4.2.2. **Transfection**

4.2.2.1. *Transfection of HEK293-FT and HeLa cells*

In order to introduce foreign DNA into HEK293-FT or HeLa cells, 200,000 cells per mL were seeded the day before transfection. The transfection mix for one well of a 12-well plate was set up as follows:

component	amount for 1 well in 12-well plate
DNA in total	1 µg
OptiMEM	125 µL
combine with:	
Lipofectamin 2000	2.5 µL
OptiMEM	125 µL

For other plate formats the volumes were adjusted accordingly. After 20 min incubation time at RT, the mix was gently added into the cell culture medium and incubated for 48 h before cells were harvested for analysis.

4.2.2.2. *Transfection of primary neurons*

Just as HEK293 cells, neurons were transfected with Lipofectamin 2000 according to the manufacturer's instruction. The following table shows the setup of the neuronal transfection mix:

component	amount for 1 well in 12-well plate
DNA in total	1.8 µg
OptiMEM	100 µL
combine with:	
Lipofectamin 2000	3.2 µL
OptiMEM	100 µL

During the 20 min incubation time of the transfection mix, hippocampal neurons on glass cover slips were removed from the original plate, dipped into warm Neurobasal medium and transferred into a new plastic dish containing prewarmed Neurobasal medium supplemented with 1% Pen/Strep and 0.25% glutamine. Then, the transfection mix was added drop-wise into the new dish. 45 min later, cover slips were again removed, dipped in warm Neurobasal medium twice and transferred back into the original plate. Analysis followed three to five days after transfection.

4.2.3. **Usage of lentivirus**

4.2.3.1. *Lentivirus production*

In order to produce lentiviruses with high virus titer, low passage HEK293-FT cells were used for packaging. Per LTR vector, three 10 cm were plated with 5.5 million cells 24 before transfection with Lipofectamin 2000. Three essential constructs were needed to set up the transfection mix: pVSVg as envelope protein and psPAX as Gag-Pol-Rev containing plasmid which allows for the formation of the virus as well as the LTR vector harboring the construct of interest. The transfection mix was set up as follows:

component	amount for three 10 cm dishes
LTR vector	18.6 µg
pSPAX2	11 µg
pVSVg	6.4 µg
OptiMEM	4.5 mL
combine with:	
Lipofectamin 2000	108 µL
OptiMEM	4.5 mL

Again, the mixture was incubated for 20 min. In the meantime, medium in the 10 cm dishes was changed to 5 mL OptiMEM supplemented with 10% FCS. Then, 3 mL of the transfection mix per dish were slowly added and incubated with the cells for 24 h. Thereafter, medium was exchanged to 10 mL DMEM Glutamax plus 10% FCS, 1% Pen/Strep, 1% NEAA and 1.3% BSA. 24 h later, the virus containing medium was collected, filtered through a sterile 0.45 µm PES membrane filter and centrifuged at 66,000 *g* for 2 h at 4°C. The pellet was resuspended in 120 µL Neurobasal medium, aliquoted and stored at -80°C until usage.

4.2.3.2. *Transduction*

In order to transduce neurons with lentivirus, 1 µL of virus preperation was added to one well of a 12-well plate. For other plate formats the volume was adjusted accordingly. Cells were incubated for at least 7 days in case of DPR proteins to allow proper aggregate formation.

4.2.4. Cell viability assays

4.2.4.1. *XTT assay*

To assess cell viability, the 2,3-bis-(2-methoxy-4-nitro-5-sulfophenyl)-2H-tetrazolium-5-carboxanilide (XTT) assay from Roche was used according to the manufacturer's instructions. For this purpose, cells were cultivated in 96-well plates and after 48 h 50 µL of the freshly thawed XTT labeling reagent mixed with the electron-coupling reagent were added. After 24 h absorption was measured spectrophotometrically at 480 nm with a plate reader.

4.2.4.2. *LDH activity assay*

Toxicity assays in transduced primary cortical neurons (DIV7+14) and HEK293FT cells were performed in 96-well plates using the lactate dehydrogenase (LDH) cytotoxicity assay from Promega following the manufacturer's protocol. Therefore, first, the whole cell supernatants were transferred into a new plate and the remaining cells were frozen for 30 min at -80°C in order to lyse them. Then, cells were thawed again and resuspended in 100 µL medium. In a new 96-well plate 50 µL of the cell supernatant as well as the cell suspension was added to 50 µL of the substrate mix. After 10 to 20 min incubation at RT in the dark, the enzymatic reaction was stopped and absorption was measured at 490 nm wavelength. To calculate relative toxicity, first the mean background value was subtracted. Then the experimental LDH release was divided by the maximum LDH release and further normalized to the respective control.

4.2.5. Cell respiration assay

Cellular respiration was measured on the Seahorse XF96 extracellular flux analyzer (Agilent). The day before the assay, primary neurons were plated in PDL-coated 96-well Seahorse assay plates. One hour before cell respiration measurements started, cells were washed and the growth medium was exchanged with pre-warmed XF assay medium supplemented with 10 mM pyruvate and 10 mM glucose using the Seahorse XF prep station. The cells were then incubated at 37°C without CO_2 for at least 45 min. Oxygen consumption rates (OCR) were recorded at baseline and after Oligomycin, FCCP and a mixture of antimycin A and rotenone addition through the injector ports. Oligomycin (1 µM diluted in assay medium) injection allowed for calculation of ATP-linked OCR and the OCR due to proton leak. The maximal respiration was determined after adding FCCP (0.75 µM). The OCR independent of complex IV could be measured after Rotenone and antimycin A (10 µM each) injection. The analyzer was set to obtain three data points per respiratory stadium including 4 min of mixing and 4 min of measurement.

4.3. Protein biochemistry

4.3.1. Immunoblotting

4.3.1.1. *Cell lysate sample preparation*

HEK293-FT cells growing in a 12-well plastic dish were harvested in 1x PBS and centrifuged at 800 *g* for 5 min. The cell pellet was resuspended in 300 µL RIPA buffer supplemented with protease inhibitor cocktail (1:500) and incubated for 20 min on ice. Afterwards, the lysate was centrifuged at 17,000 *g* for 15 min at 4°C. However, when cells were harboring DPR proteins the lysate was only centrifuged at 1,000 *g* for 10 min. Finally, 4x Laemmli sample buffer was added to the supernatant in a 1:4 ratio and samples were boiled at 95°C for 5 min.

In order to prepare lysate from neurons, cells were directly harvested in 180 µL 2x Laemmli sample buffer per well.

4.3.1.2. *SDS-polyacrylamide gel electrophoresis (SDS-PAGE)*

In order to separate proteins by their molecular masses, SDS-PAGE was performed. Therefore, lysate samples were run under denaturing conditions using discontinuous ready-to-use 10-20% Tris-Tricine polyacrylamide gels from Novex. Gels were loaded with 10 to 20 µL of lysate samples and electrophoresis was carried out in tricine buffer with a voltage of 80 V until the dye front reached the stacking gel. Afterwards, the gel was run at 120 V. For comparison of molecular weights, the SeeBlue Protein marker was run side by side to the samples.

4.3.1.3. *Immunoblotting and immunodetection*

Previously separated proteins were blotted on an isopropanol activated polyvinylidene difluoride (PVDF) membrane at a constant current of 400 mA for 75 min using a wet blotting chamber. Subsequently, the membrane was blocked in 0.2% i-Block in TBSTx for 1 h at RT in order to reduce non-specific binding sites and afterwards incubated in primary antibody solution at 200 rpm and 4°C overnight. The next day, five washing steps with TBSTx followed. Then, the membrane was incubated for 1 h at RT with an HRP coupled secondary antibody appropriate for the species of the first antibody used and washed another five times. For detection of the protein of interest, the membrane was incubated with the chemiluminescence substrate ECL for 2 min. Directly afterwards, an X-ray film was exposed to the membrane in complete darkness and developed on an X-ray film processor.

4.3.2. SUnSET assay

In order to monitor total protein synthesis a Surface sensing of translation (SUnSET) assay was performed. Therefore, primary cortical neurons were treated with 10 µg/mL puromycin for 10 min at

37°C and 5% CO_2 in order to allow puromycin, as structural analogue of aminoacyl-transfer RNA, to incorporate into the newly synthesized peptide chains. Afterwards, cells were lysed and immunoblotted as described above and protein synthesis was analyzed by detection with a puromycin specific antibody.

4.3.3. Immunoprecipitation of GFP-tagged poly-GR and poly-PR aggregates

In order to analyze the whole proteome as well as the interacting proteins of GFP-$(GR)_{149}$, $(PR)_{175}$-GFP or GFP in infected cortical neurons (DIV7+8) and transfected HEK293FT cells quadruplicates of immunoprecipitation samples were prepared. Cells were harvested in 1 mL IP lysis buffer substituted with Benzonase (67 U/mL) per 10 cm dish. Lysates were rotated for 45 min at 4°C. For whole proteome analysis 10% of the samples were kept while the remaining lysate was centrifuged at 1000 g for 5 min at 4°C. In the meantime, 10 µg of GFP antibody were incubated with 50 µL Protein-G Dynabeads. Afterwards, lysate supernatant was united with the beads and incubated for 3 h at 4°C. Three washing steps in 1 mL IP basic buffer followed. 80% of the sample was used for further sample preparation for mass spectrometry analysis. 20% of the beads was boiled in 4x Laemmli sample buffer at 95°C in order to release the protein from the antibody and the resulting samples were run on a gel followed by immunoblotting.

4.3.4. Ribosome binding assay

For investigation of the binding capacity of a protein of interest (antigen) to a specific other target protein, in this case the ribosome, immunoassays were carried out. Importantly, all assay steps including blocking and washing, were performed with ribosome assay buffer (RB) in order to keep the Mg^{2+} concentration at 20 mM thereby guaranteeing an intact ribosome. Also, if not indicated otherwise, each incubation step was carried out on a horizontal shaker at 220 rpm for 1 h at RT. First, MaxiSorb 96-well plates were coated with 100 µL of 80S yeast ribosome (5-500 ng/well) at 4°C overnight. The next day, plates were washed three times with RB, blocked with 300 µL 1% BSA in RB and washed again. Then, the antigen (0.1-10 µg/well) was added for 1 h at RT, plates were washed three times and incubation with a primary antibody detecting the antigen started. After three more washing steps the plates were incubated with an HRP coupled secondary antibody. Thereafter, plates were washed again and incubated with 100 µL 3,3',5,5'-Tetramethylbenzidine (TMB), a liquid substrate for HRP, for 5 min in the dark. Finally, the reaction was stopped with 2 M sulfuric acid and absorption was measured at 450 nm or 630 nm on a plate reader.

4.3.5. Chromatin immunoprecipitation (ChIP) from HEK293 cells

In order to elucidate the binding of proteins of interest to certain chromatin regions, ChIP experiments were performed with the MAGnify Chromatin Immunoprecipitation System kit (Life Technologies). For

all reaction steps Lo-bind tubes were used. 1 million HEK293-FT cells served as starting material. The chromatin binding protein Histone 2B (H2B) was used as positive control. In a final step the eluted DNA binding to the protein of interest was amplified by PCR with specific primers prior to analysis by gel electrophoresis.

4.3.5.1. *Crosslinking*

Cells were harvested from 6-well plates in 5 mL medium and centrifuged 5 min at 200 *g.* After resuspension of the pellet in PBS, cells were counted and diluted to 1 million cells in 500 µL PBS. 13.5 µL 37% Formaldehyde was added and incubated for 10 min prior to the addition of 57 µL 1.25 M glycine and 5 min incubation in order to stop the reaction. Afterwards, the solution was centrifuged at 2800 *g* for 10 min at 4°C. Then, the pellet was washed with cold PBS and centrifuged again.

4.3.5.2. *Cell lysis and chromatin shearing*

The pellet was taken up in 50 µL PI containing lysis buffer (1:200) per 1 million cells, vortexed and incubated on ice for 10 min. 300 µL dilution buffer was added prior to sonication. The following sonication protocol was chosen: 30% amplitude with 0.6 sec duty cycle and 4 cycles of 30 sec pulse with 1 min pause. Thereafter, a centrifugation step of 20,000 *g* for 5 min at 4°C followed. In order to verify chromatin shearing into 200 base pair long fragments, 10 µL of the supernatant was incubated with 1 µL proteinase K at 55°C for 20 min and run on a 1.5% agarose gel. The rest of the supernatant was split into three aliquots with 100 µL each, 10% of the samples were kept as input.

4.3.5.3. *Immunoprecipitation*

To each sample 10 µL antibody precoupled Dynabeads were added and incubated on a rotator for 2 h at 4°C. For GFP-tagged proteins GFP-Trap®_M beads (chromotek) were used. Afterwards, beads were separated from the solution by a magnet, the supernatant was removed, and the beads were washed three times with 100 µL IP Buffer 1 and two times with IP Buffer 2.

4.3.5.4. *Reverse crosslinking and DNA isolation*

In order to separate proteins from DNA, 53 µL or 43 µL Reverse Crosslinking Buffer supplemented with Proteinase K (1 µL per sample) were added to IP or input samples, respectively, and incubated for 15 min at 55°C. Thereafter IP sample supernatants were harvested. Finally, all samples were incubated for 15 min at 65°C. DNA was isolated using DNA-binding magnetic beads. Therefore, 20 µL beads together with 50 µL DNA purification buffer were added to each sample and incubated for 5 min at RT. Then, beads were washed two times with 150 µL DNA wash buffer prior to incubation for 5 min at 55°C with 150 µL DNA elution buffer. The eluted DNA was separated from the beads and transferred into a new tube and stored at -20°C.

4.4. Imaging

4.4.1. Immunofluorescent stainings in patient tissue

The tissue was first de-paraffinated and rehydrated by incubating the tissue slides in xylene for 20 min and subsequently rinsing them 10x in 100% ethanol twice, once in 96% ethanol and finally twice in 70% ethanol. To retrieve the antigen, slides were boiled four times 5 min in citrate buffer pH 6.0 using a microwave and cooled down for 20 min. Blocking in inhibiting endogenous peroxidase was performed with 5% H_2O_2 in methanol for 15 min prior to a brief rinse with deionized water. After sections were washed in PBS/0.05% Brij35, blocking with 2% fetal calf serum in PBS for 5 min followed. Thereafter, primary antibody solution was applied over night at 4°C. The next day, the tissue was washed twice in PBS/0.05% Brij35 prior to incubation with Alexa-coupled secondary antibodies (1:500 in blocking buffer) for 1 h at RT in the dark. Thereafter, the brain sections were washed again, stained with DAPI (1:5000 in blocking buffer) 15 min and washed twice in 0.05% Brij35 in PBS and twice in PBS only. The tissue was treated with Sudan Black B for 1 min at RT, rinsed in PBS and mounted with Fluoromount Aqueous mounting medium.

4.4.2. Immunofluorescent stainings in cell culture

For immunostainings in cell culture, hippocampal neurons, HEK293-FT or HeLa cells were grown on PDL coated glass cover slips. All incubation steps were performed in a wet chamber in the dark. First, cells were fixed with 4% paraformaldehyde for 15 min and the nuclei were subsequently permeabilized by incubation with permeabilization buffer for 5 min. After three washing steps using PBS, the cover slips were blocked in blocking solution for 30 min and then incubated in primary antibody solution (blocking buffer diluted 1:10 in water containing the primary antibody) at RT for 1 h. Next, they were again washed with PBS and incubated in Alexa-coupled secondary antibody solution (1:400 in blocking buffer diluted 1:10 in water) for 1 h. Finally, the cells on cover slips were treated with DAPI or TO-PRO-3 (1:5000 in PBS) for 15 min in order to stain the nuclei and mounted on a glass microscope slides using Vectashield mounting medium.

4.4.3. Image acquisition

Single plane images from immunofluorescent stainings were acquired with the laser scanning microscope LSM 710 system from Carl Zeiss together with the ZEN 2010 software. Plan-Apochromat 40x and 63x oil objectives were used. For colocalization experiments the pinhole was set to 1 Airy Unit for the longest wavelength and adjusted for the others accordingly. The scanning speed was chosen according to the quality of the staining. In general, the scanning speed was much lower for patient tissue stainings and additionally, it was averaged over 2 or 4 images allowing for better quality. Images

were acquired at 1024 x 1024 pixels. In order to allow meaningful comparison between groups, all samples of one experiment were imaged with the same settings.

4.4.4.   Image analysis

All images were processed with the ImageJ software. When required, brightness and contrast were adapted by lower fixed grey value for thresholding the signal. For retaining comparability, same thresholds were applied for images of one channel. Whenever possible, images were analyzed blinded to the experimental conditions. Counting of aggregates and cells was done without software image analysis programs.

4.5. Statistical analysis

Statistical analysis was conducted with the GraphPad Prism software. Depending on the experimental setting and distribution of the data points the appropriate test including post-test was performed. Initially, it was tested for normal distribution. Mostly, multiple data groups should be compared to a control group. Here, the one-way ANOVA was used for normally distributed data points, whereas for non-normal distributed data, the Kruskal Wallis test was used. These tests are specified in the figure legends. Statistical significance was indicated as p-value as follows: * $p<0.05$, ** $p<0.01$, *** $p<0.001$.

5. RESULTS

Since the discovery that the $(GGGGCC)_n$ repeat expansion within the first intron of *C9orf72* in ALS/FTD patients is translated, DPR proteins have come into the focus of researchers. At the beginning of my PhD, the relative contribution of the two arginine-rich DPR species poly-GR and poly-PR to neurodegeneration was just starting to emerge. Besides impairment of splicing and disruption of rRNA processing only little was known. In order to address the role of poly-GR and poly-PR in ALS/FTD disease pathogenesis, my aim was to elucidate the mechanisms underlying DPR toxicity by analysis of an extensive interactome study in different cell culture systems. Importantly, the validation of poly-GR/PR interactors was aimed to be extended to patient tissue.

In order to express the two DPR species in different cell types, I used ATG-initiated synthetic poly-GR and poly-PR constructs during the whole study. The repeat sequences were harboring alternative codons preventing RNA based toxicity and reducing genomic repeat instability. The poly-GR sequence was C-terminally tagged with GFP containing 149 repeats resulting in GFP-$(GR)_{149}$, while poly-PR was tagged on the N-terminus and comprised 175 repeats resulting in $(PR)_{175}$-GFP. A GFP-only construct served as negative control in all experiments.

5.1. Subcellular localization and toxicity of poly-GR and poly-PR

I first analyzed general characteristics of poly-GR as well as poly-PR in two cell culture systems. For this purpose, I expressed GFP-$(GR)_{149}$ and $(PR)_{175}$-GFP in HEK293 cells and primary rat neurons and studied localization as well as toxicity.

5.1.1. Poly-GR and poly-PR localization differs between cell types

Consistent with previous results (Schludi et al., 2015b), in transfected HEK293 cells, GFP-$(GR)_{149}$ was found in both nucleolus and cytoplasm while $(PR)_{175}$-GFP mainly localized to the nucleolus. Surprisingly, in contrast to previous studies, lentiviral expression of GFP-$(GR)_{149}$ in primary neurons resulted in predominantly diffuse cytoplasmic localization and only little nucleolar expression suggesting different poly-GR interacting proteins in neurons and HEK293 cells may affect its subcellular localization. $(PR)_{175}$-GFP was mostly localized to the nucleolus as in HEK293 cells (Figure 5-1**A** and **B**).

Although the repeat length of poly-GR and poly-PR with 149 and 175 repeats, respectively, is considerably longer compared to previous studies, it is probably still shorter than in patients. Since poly-GR and poly-PR are found in the cytoplasm in patients and aberrant localization potentially alters the downstream toxic effects, I attempted to relocalize poly-GR and poly-PR to the cytoplasm in our cell culture system. Thus, I fused the constructs to a nuclear export signal (NES) from p53 (MFRELNEALELK) or $(GA)_{50}$, which by itself forms large cytoplasmic aggregates. Surprisingly, fusion with

(GA)$_{50}$ only led to even bigger nucleolar aggregates and also the NES failed to form poly-GR and poly-PR inclusions in the cytoplasm (Figure 5-1**C**).

5.1.2. Nucleolar poly-GR and poly-PR show significant toxicity *in vitro*

As reported in previous studies, poly-GR and poly-PR are toxic in various cell culture systems. Also in my hands, expression of both, (PR)$_{175}$-GFP and GFP-(GR)$_{149}$, showed growth impairment of HEK293 cells in an XTT proliferation assay. This test is measuring the activity of the succinate-tetrazolium reductase system which belongs to the respiratory chain of mitochondria and is only active in metabolically intact cells (Figure 5-2**A**). Next, active cell death was measured by an LDH colorimetric assay, detecting the presence of the LDH enzyme in the culture medium being released from cells where membrane integrity is compromised. However, (PR)$_{175}$-GFP and GFP-(GR)$_{149}$ expression in HEK293 cells did not lead to active cell death (Figure 5-2**B**). In neurons, surprisingly only nucleolar (PR)$_{175}$-GFP but not cytoplasmic GFP-(GR)$_{149}$ induced significant neuronal loss (Figure 5-2**C**) leading to the hypothesis that only nucleolar localization may be driving the poly-GR/PR toxicity observed *in vitro*. This would be in line with previous studies in which poly-GR was exclusively localized to the nucleolus and was notoriously toxic compared to the cytoplasmic GFP-(GR)$_{149}$ in this study. To further validate this hypothesis, I also performed a toxicity assay in GFP-(GA)$_{50}$-(GR)$_{50}$ and GFP-(GA)$_{50}$-(PR)$_{50}$ expressing

Figure 5-1: Poly-GR and poly-PR show nucleolar and cytoplasmic expression in HEK293 cells and neurons.

(**A, B**) GFP, GFP-(GR)$_{149}$ or (PR)$_{175}$-GFP were transduced or transfected in primary rat neurons and HEK293 cells, respectively. (**A**) Images show a single confocal plane depicting GFP fluorescence and anti-fibrillarin (red) staining to visualize nucleoli in cells stained with DAPI (blue). Scale bar denotes 20 µm. (**B**) Quantitative analysis of GFP-(GR)$_{149}$ or (PR)$_{175}$-GFP colocalization with fibrillarin-labeled nucleoli, n=17 for GFP-(GR)$_{149}$, n=13 for (PR)$_{175}$-GFP images in neurons and n=6 for GFP-(GR)$_{149}$, n=6 for (PR)$_{175}$-GFP images in HEK cells from two independent experiments, mean ± SEM is shown. (**C**) Images show GFP fluorescence of a single confocal plane of GFP-(GA)$_{50}$-(GR)$_{50}$, GFP-(GA)$_{50}$-(PR)$_{50}$, GFP-(GR)$_{149}$-NES or (PR)$_{175}$-GFP-NES expressing primary hippocampal neurons. Nuclei are visualized with DAPI. Scale bar denotes 20 µm.

neurons, which harbor big nucleolar inclusions with dense fluorescence signal. Here, GFP-(GA)$_{50}$-(GR)$_{50}$ and GFP-(GA)$_{50}$-(PR)$_{50}$ transduced neurons displayed even higher toxicity as measured by LDH release assay than (PR)$_{175}$-GFP transduction (Figure 5-2**D**).
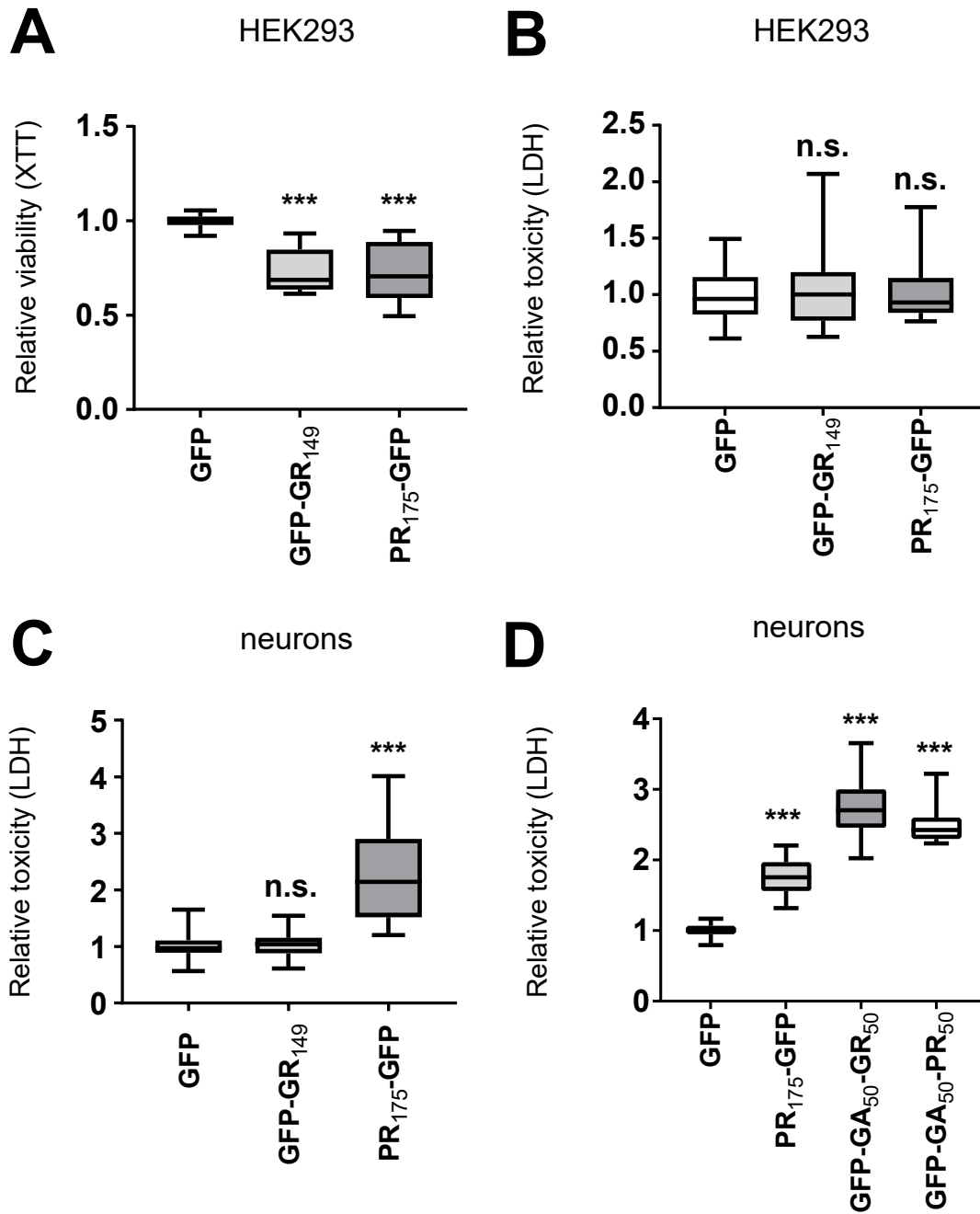
Figure 5-2: Nucleolar poly-GR and poly-PR show significant toxicity in HEK293 cells and neurons.

(A, B) GFP, GFP-(GR)$_{149}$ or (PR)$_{175}$-GFP were expressed in HEK293 cells. (A) 3 days after transfection cell viability was measured by XTT assay. GFP-(GR)$_{149}$ and (PR)$_{175}$-GFP showed significantly reduced cell growth compared to GFP control (12 replicates from 2 independent experiments, box plot is shown with 25th percentile, median and 75th percentile and whiskers representing minimum and maximum, *** denotes p<0.001 in one-way ANOVA with Dunnett's post-test). (B) LDH release assay detects no significant cell death upon expression of (PR)$_{175}$-GFP and GFP-(GR)$_{149}$ compared to GFP control (n=2 independent experiments with 6 replicates each, box plot is shown, n.s. denotes not significant in one-way ANOVA with Dunnett's post-test). (C, D) Primary cortical rat neurons were infected with indicated constructs. (C) LDH release assay detects significant toxic effect upon (PR)$_{175}$-GFP, but not GFP-(GR)$_{149}$ expression compared to GFP control. (18 replicates from 3 independent experiments, box plot is shown, *** denotes p<0.001 in one-way ANOVA with Dunnett's post-test). (D) LDH release assay reveals toxic effect comparable to (PR)$_{175}$-GFP upon expression of nucleolar GFP-(GA)$_{50}$-(GR)$_{50}$ and GFP-(GA)$_{50}$-(PR)$_{50}$ (12 replicates from 2 independent experiments, box plot is shown, *** denotes p<0.001 in one-way ANOVA with Dunnett's post-test).

5.1.3. GFP-(GR)$_{149}$ and (PR)$_{175}$-GFP bind DNA

Besides localization and toxicity, I also investigated the capacity of GFP-(GR)$_{149}$ and (PR)$_{175}$-GFP to bind negatively charged DNA as it is known that the positively charged arginine residues within the two DPR protein species have the ability to bind negatively charged RNA (Lipfert et al., 2014). Therefore, I isolated crosslinked DNA from HEK293 cells expressing poly-GR/-PR, and GFP as negative control and performed chromatin immunoprecipitation (ChIP) experiments with three replicates each. Histone 2B as DNA-binding protein served as positive control. After the last purification step, the DNA was amplified with primers specific for Presenilin 2 exon 7 and visualized on an agarose gel. The intensity of the PCR products shows that in comparison to the GFP control, GFP-(GR)$_{149}$ and (PR)$_{175}$-GFP have a higher binding capacity to DNA suggesting that the positively charged residues of arginine bind to the negatively charged phosphate group of the DNA (

Figure 5-3). As expected, the positive control H2B had the highest binding capacity.
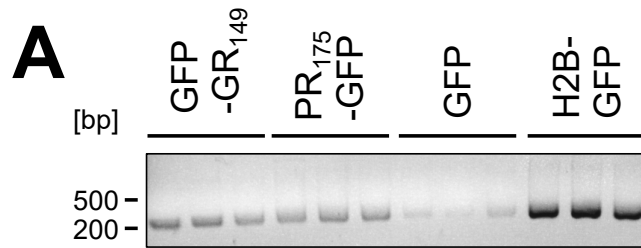
Figure 5-3: Poly-GR and poly-PR bind DNA in HEK293 cells.

ChIP assay performed with DNA extracted from cell lysates of GFP-(GR)$_{149}$, (PR)$_{175}$-GFP, GFP or H2B-GFP expressing HEK293 cells 3 days after transfection. Histone 2B served as positive control and GFP as negative control. DNA was amplified with primers specific for Presenilin 2 exon 7 and visualized on an agarose gel. Note that in comparison to the GFP control, GFP-(GR)$_{149}$ and (PR)$_{175}$-GFP have a higher DNA binding capacity.

Overall, the two DPR species analyzed in this study show both cytoplasmic and nucleolar localization upon expression in HEK293 cells and primary rat neurons. In HEK293 cells, both bind to DNA. Importantly, expression of nucleolar GFP-(GR)$_{149}$ and (PR)$_{175}$-GFP is accompanied by cellular toxicity *in vitro*, while cytoplasmic poly-GR is not.

5.2. Poly-GR/PR preferentially interact with RNA-binding proteins

The main focus of this work was to identify the mechanisms driving poly-GR/PR toxicity in cellular models and ultimately in *C9orf72*-ALS/FTD. In order to understand the physiological and functional consequences of poly-GR/PR expression in ALS/FTD patients, my first approach was to set up a proteome study in cell culture. Therefore, I first conducted an immunoprecipitation (IP) experiment using a GFP antibody in order to pull down GFP-(GR)$_{149}$, (PR)$_{175}$-GFP or GFP from transduced cortical neurons (DIV7+8) and transfected HEK293FT cells. To reduce indirect RNA-mediated interactions, the lysates were treated with benzonase before IP. Immunoblotting validated the enrichment of poly-GR and poly-PR as well as the GFP control in the IP samples (Figure 5-4**A** and **B**). In a second step, label-free quantitative liquid chromatography-tandem mass spectrometry (LC-MS/MS) was performed in collaboration with Daniel Hornburg and Jakob Bader from the Max-Planck Institute for Neurobiology. That way it was possible to identify a plethora of poly-GR/PR interacting proteins. In order to analyze differences in global protein expression between poly-GR/PR and GFP expressing cells, additionally, whole proteome analysis was performed from the neuronal extracts.
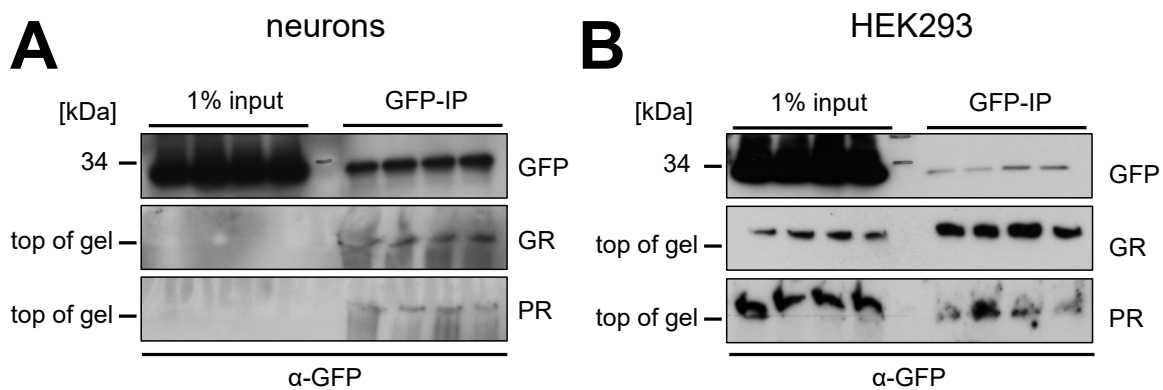
Figure 5-4: Poly-GR and poly-PR can be immunoprecipitated from neuron and HEK293 cell lysates.

Primary cortical rat neurons (DIV7+8) **(A)** and HEK293 cells **(B)** expressing GFP, GFP-(GR)$_{149}$ or (PR)$_{175}$-GFP were subjected to anti-GFP immunoprecipitation. Immunoblotting with a GFP specific antibody confirms pull-down of GFP, GFP-(GR)$_{149}$ as well as (PR)$_{175}$-GFP in the GFP-IP lanes.

5.2.1.   **Poly-GR/PR predominantly interact with ribosomes in primary neurons**

In primary cortical neurons, we discovered in total close to 600 proteins binding to GFP-$(GR)_{149}$ and $(PR)_{175}$-GFP, but not the GFP control. In detail, we found 89 proteins significantly enriched in poly-GR expressing neurons and 104 in poly-PR expressing neurons, of which 39 were shared interactors mostly associated with stress granules and the ribosome (Figure 5-5**A** and Table S1/

Table S2). Among the poly-GR and poly-PR interacting proteins CCDC40, a dynein regulator, as well as C1QBP, a multifunctional protein involved in protein synthesis, splicing and apoptosis, were found to show the highest enrichment (Figure 5-5**B**). Moreover, analysis of interactors showed significant enrichment in proteins containing low complexity domains (LCD) (Figure 5-5**C**) in poly-GR and poly-PR expressing neurons, which is consistent with previous observations (Lee et al., 2016a; Lin et al., 2016). In line with the role of LCD containing proteins in assembly of membrane-less organelles, ~60% of the enriched proteins were annotated as RNA-binding (Gerstberger et al., 2014). They can be clustered into components of the nucleolus and stress granules, with interactors such as NPM1, STAU2, and YBX1, as well as proteins involved in splicing and methylation, like PRMT1/5, WDR77, and SRSF proteins. Furthermore, functional classification analysis revealed that the most abundant class of interacting proteins were ribosomal subunits. About 30% of them were identified as mitochondrial ribosomal proteins that are required for translation of the 13 subunits of respiratory chain complexes.
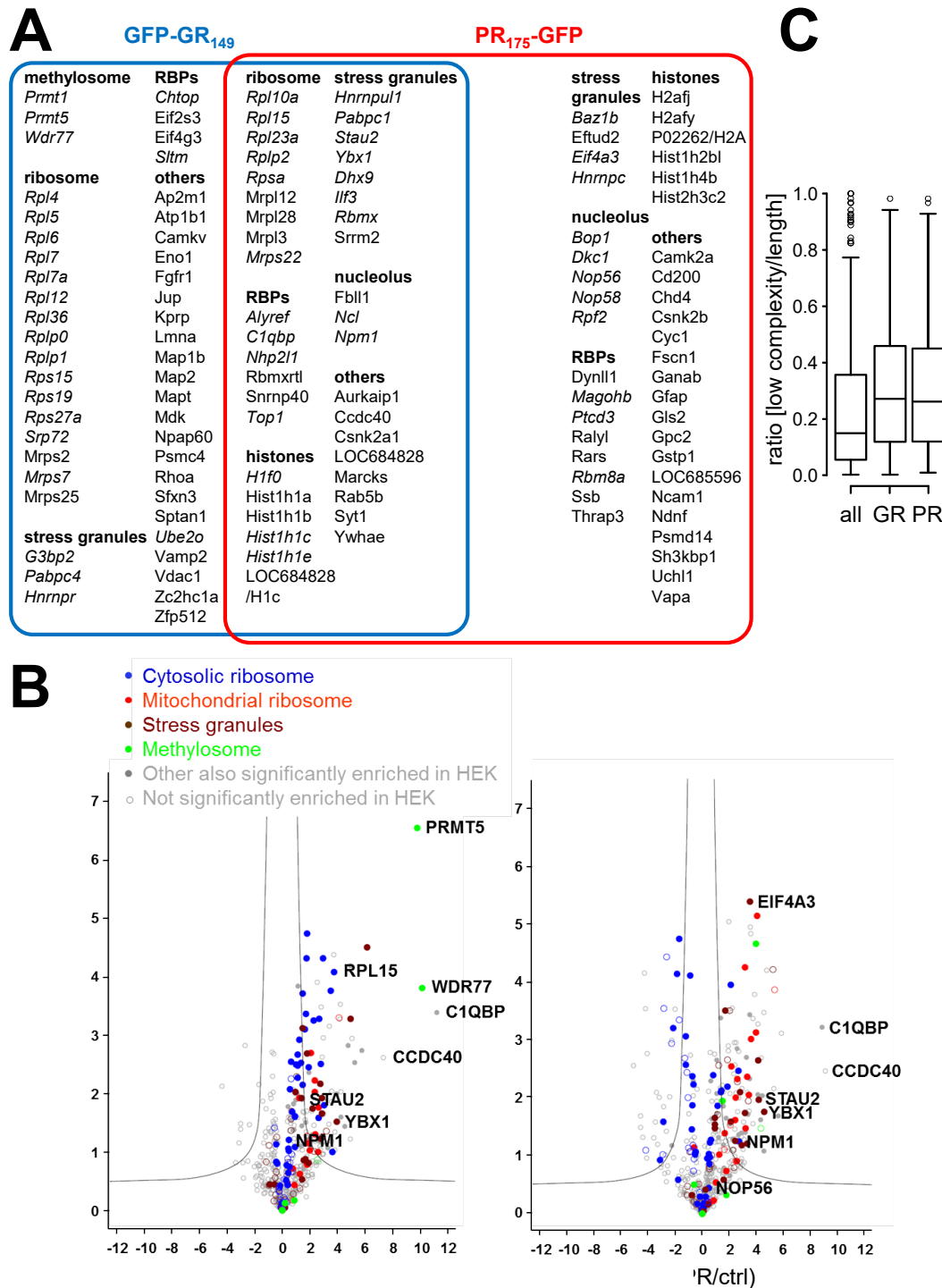
Figure 5-5: Poly-GR/PR predominantly interact with ribosomes in primary neurons.

(A, B, C) Quantitative proteomic analysis of GFP immunoprecipitations from cortical neurons expressing GFP, GFP-(GR)$_{149}$ or (PR)$_{175}$-GFP (DIV7+8). **(A)** Graph showing proteins with significant enrichment in poly-GR and pol-PR interactomes compared to GFP control. Interactors were manually grouped into functional categories. Note that the ribosome is the class with most interactors. Orthologs of proteins in italics were also found in the poly-GR/PR interactomes from HEK293 cells. **(B)** Proportion of low complexity regions (IUPred-L) of all proteins identified in the neuronal interactome analysis, the poly-GR interactome and the poly-GR interactome, ** denotes p < 0.01 in Mann-Whitney-Wilcoxon test. **(C)** Volcano plots show interacting proteins plotted as log$_2$ fold change versus the −log$_{10}$ of the *P*-value. Grey line indicates significance cut-off. Enriched protein families are color coded: cytoplasmic ribosome (blue), mitochondrial ribosome (red), stress granules (brown) (Jain et al., 2016) and methylosome (green). The top enriched proteins (sorted by fold-change) and the proteins analyzed in this study are labeled with gene names. Filled circles indicate proteins significantly altered in HEK293 cells.

5.2.2. Mitochondrial ribosomal proteins are the most abundant interactors in the poly-GR/PR interactome of HEK293 cells

In order to compare the neuronal interactome of GFP-(GR)$_{149}$ and (PR)$_{175}$-GFP with an additional cellular system, I analyzed the poly-GR/PR interactome in HEK293 cells. Here, 394 proteins were associated with poly-GR and 50 were identified being enriched in poly-PR (Figure 5-6 and Table S3/Table S4). The two DPR species had 49 interactors in common while CD2AP was the only protein exclusively interacting with poly-PR (Figure 5-7**A**). Classification revealed that poly-GR associates with methyltransferases, such as PRMT1 and PRMT5, and numerous proteins from the 80S ribosome. In addition, both, poly-GR and poly-PR interactors were related to splicing with DDX/DHX and SRSF proteins being examples for RNA helicases and RNA splicing factors. Also stress granule associated proteins were enriched in both DPR interactomes with STAU1 being among them (Figure 5-5**A** proteins marked in italics). With ~15% of poly-GR interactors and ~67% of poly-PR interactors, mitochondrial ribosomal proteins were the most represented interactors. Moreover, about 80% of the interacting proteins were annotated as RNA-binding proteins, similar to the interactors of the neuronal interactome.
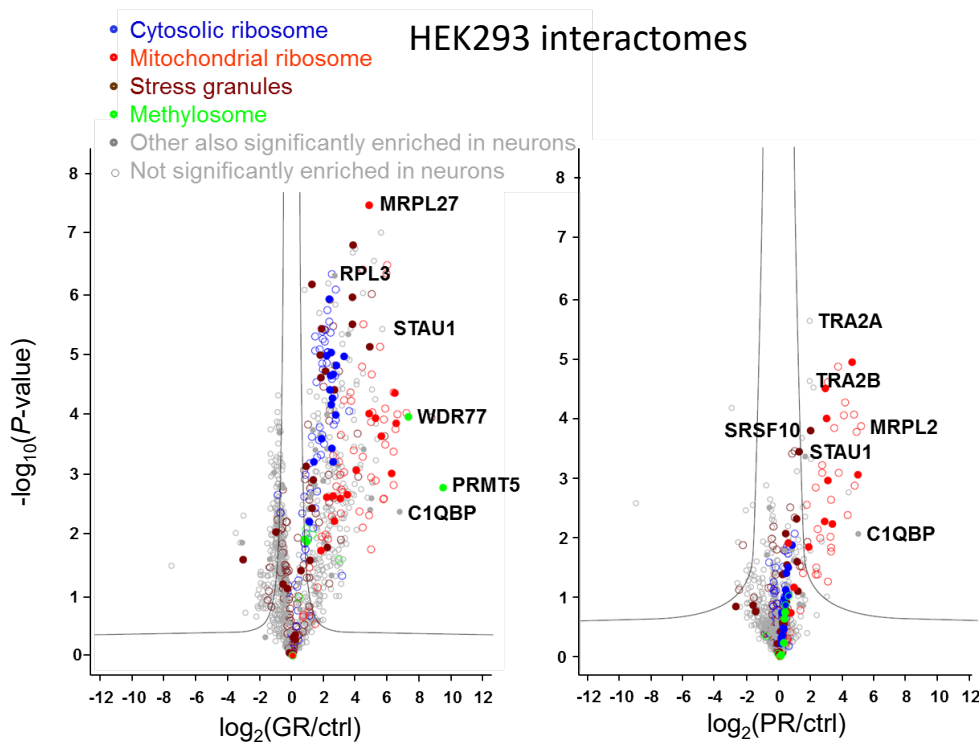
Figure 5-6: Mitochondrial ribosomal proteins are the most abundant interactors in the poly-GR/PR interactome of HEK293 cells.

Quantitative proteomic analysis of GFP immunoprecipitations from HEK293 cells transduced with GFP, GFP-(GR)$_{149}$ or (PR)$_{175}$-GFP. Volcano plots show all significantly enriched interactors. The data for all proteins are plotted as log$_2$ fold change versus the −log$_{10}$ of the *P*-value. Grey line indicates significance cut-off. Enriched protein families are color coded: cytoplasmic ribosome (blue), mitochondrial ribosome (red), stress granules (brown) (Jain et al., 2016) and methylosome (green). The top enriched proteins (sorted by fold-change) and the proteins analyzed in this study are labeled with gene names. Filled circles indicate proteins significantly altered also in neurons.

5.2.3. The interactomes of poly-GR/PR identify overlapping interactors in the two cell culture systems
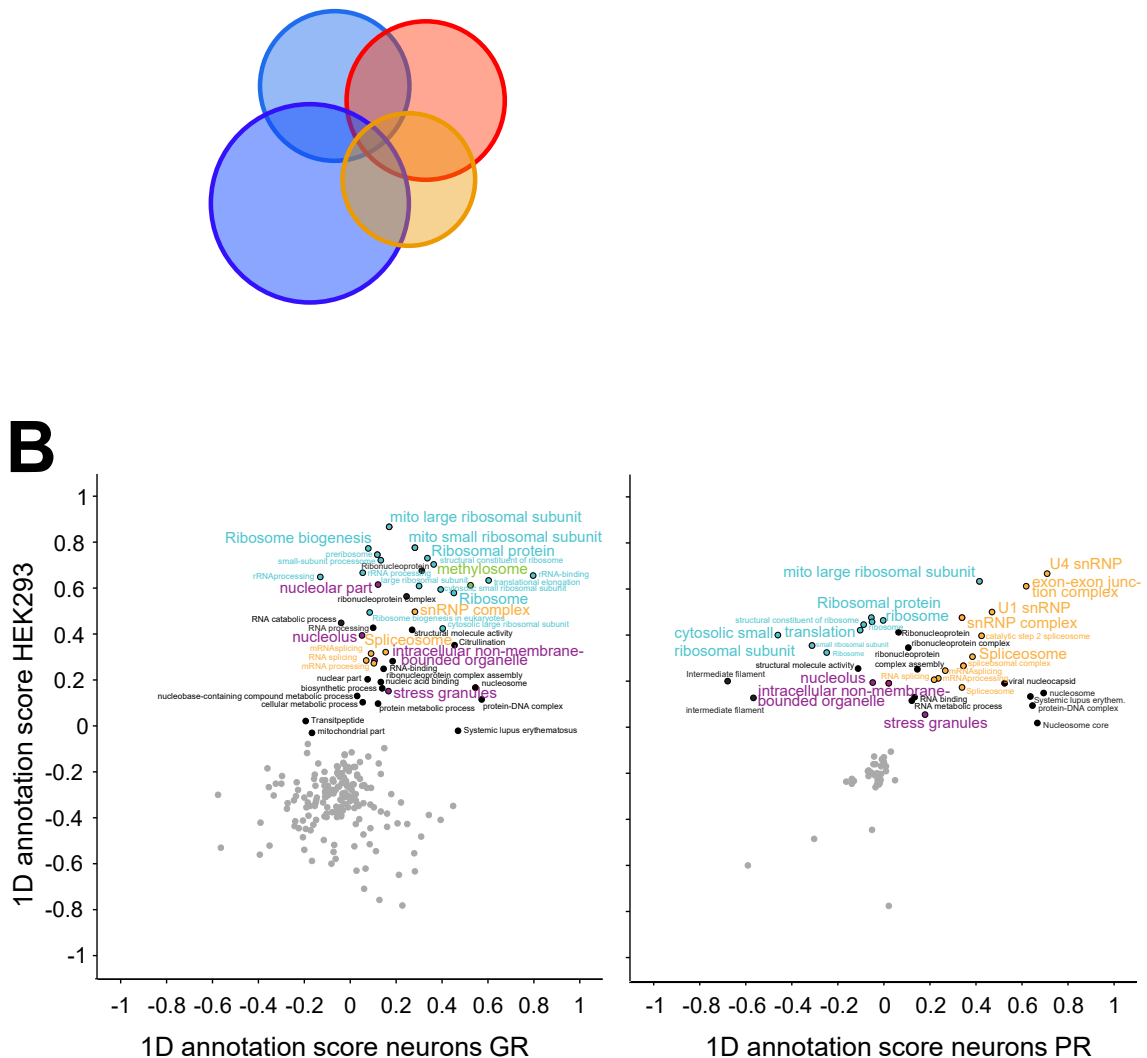
Figure 5-7: Poly-GR and poly-PR interact with similar RNA-binding proteins in neurons and HEK293 cells.

(A, B) Comparison of poly-GR/PR interactomes of HEK293 cells and neurons expressing GFP, GFP-(GR)$_{149}$ or (PR)$_{175}$-GFP. (A) Venn diagram directly comparing individual interactors of poly-GR and poly-PR between cell types. (B) 2D analysis of gene ontology terms (GOMF, GOCC, GOCC, GOPB, KEGG, Uniprot Keywords) and stress granule proteins (Jain et al., 2016) for proteins identified in the poly-GR and poly-PR interactome in primary neurons and HEK293 cells (Fig. 5.5B and 5.6). Dots with nearly identical position and annotation were removed for clarity. Related terms from the main enriched protein families are color coded: ribosome (blue), nucleolus and stress granules (purple)(Jain et al., 2016), methylosome (green), splicing (yellow) and others (black). Annotation terms with a Benjamini-Hochberg FDR (q-value) smaller than 0.1 and comprising at least six proteins quantified by mass spectrometry are shown. 1D annotation scores close to 1 indicate strongest enrichment over the GFP control, scores close to 0 depict no enrichment and scores close to -1 strongest depletion. The analysis was performed in the Perseus software (Tyanova et al., 2016).

To elucidate whether primary rat neurons and human HEK293 cells show similar interactors which can be grouped into parallel pathways, I compared their interactomes directly. Detailed analysis revealed that neurons and HEK293 cells have 33 proteins in common in GFP-$(GR)_{149}$ immunoprecipitates, such as NCL, C1QBP, and PRMT5. The poly-PR interactomes from both cell types on the other hand only share 11 identical proteins mostly being ribosomal subunits from mitochondria (C1QBP, MRPL3, MRPL17, MRPL22, MRPL27, MRPL28, MRPL41, MRPS30, MRPS9, SRSF10, YBX1) (compare Figure 5-5**B** with Figure 5-6 and Figure 5-7**A**). All four interactomes share C1QBP, MRPL3, MRPL28, and YBX1. When comparing gene ontology (GO) terms enriched in poly-GR interactors of the two cell types it becomes clear that there is a high selectivity for proteins associated with the nucleolus, ribosomes, the spliceosome, stress granules, and the methylosome. On the other hand, poly-PR interactors were mostly enriched in proteins connected to the U1 and U4 snRNP, the exon junction complex and the large ribosomal subunit from mitochondria (Figure 5-7**B**).

Taken together, the poly-GR and poly-PR interactomes of primary rat neurons and human HEK293 cells revealed RNA-binding proteins as the most abundant interactors. In line with this finding, functional classification analysis showed that these interactors were associated with the cytosolic and mitochondrial ribosome, the nucleolus, the spliceosome and stress granules.

5.3. Whole proteome analysis of poly-PR expressing cells shows reduction of ribosomal proteins

Although the analysis of the GFP-$(GR)_{149}$ and $(PR)_{175}$-GFP interactomes could already give new insights into the variety of interactors associated with poly-GR/PR, I was also interested in the changes on global protein levels in poly-GR/PR expressing cells. Therefore, we additionally analyzed global protein expression using quantitative LC-MS/MS in primary cortical neurons transduced with GFP-$(GR)_{149}$, $(PR)_{175}$-GFP and GFP. In poly-GR transduced neurons the expression of individual proteins was not obviously affected. After correction for multiple comparison only CSPG4 and NIFK were statistically different. In contrast, $(PR)_{175}$-GFP expression significantly altered expression of numerous proteins compared to the GFP control (Figure 5-8**A**). Here, reduction of protein expression was very prominent and enrichment analysis revealed that especially cytosolic ribosome protein levels were reduced which was accompanied by a strong downregulation of synaptic and axonal proteins (Figure 5-8**B**). Interestingly, at the same time, expression of proteins associated with ribosomal biogenesis, such as BOP1 and PES1 were upregulated suggesting a compensatory effect. Also, proteins of the nucleolus and mitochondria were found to be slightly increased. Expression of stress granule components was

neither altered in (PR)$_{175}$-GFP expressing nor in GFP-(GR)$_{149}$ expressing neurons. Finally, GO annotation analysis showed a slight decrease in ribosomal proteins also in poly-GR transduced neurons (Figure 5-8**B**).

Overall, these observations suggest that poly-PR expression leads to the loss of ribosomal proteins which might directly affect global protein expression in neurons. Furthermore, the striking effect of nucleolar poly-PR, but not cytoplasmic poly-GR, on the whole neuronal proteome strongly supports the toxic effect of only (PR)$_{175}$-GFP in neurons.
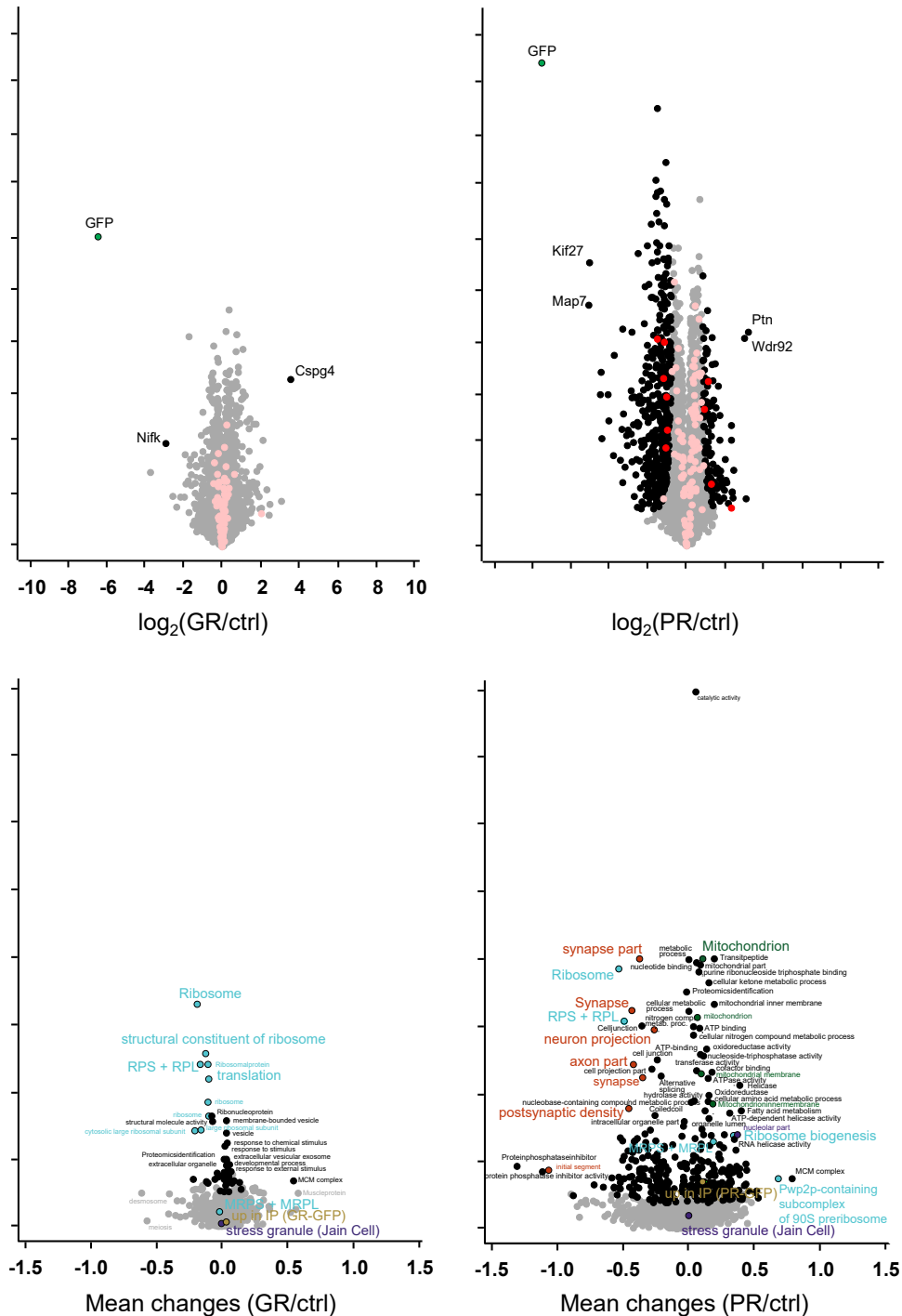
Figure 5-8: Poly-PR expression alters the whole proteome in neurons.

(A) Volcano plot showing individual proteins quantified in whole proteome of GFP-(GR)$_{149}$ and (PR)$_{175}$-GFP transduced primary cortical neurons from the same mass spectrometry samples used for the interactome studies in Figures 5.5 to 5.7. The data for all proteins identified in whole cell lysates are plotted as log$_2$ fold change versus the −log$_{10}$ of the P-value. Significantly altered proteins (q-value <5%) are highlighted as black dots. Interactors significantly enriched (q-value <5%) are shown in red. Transparent black and red dots denote proteins that are not significantly changed. **(B)** 1D annotation enrichment analysis for comparison of gene ontology terms of respective proteome. GOMF, GOCC, GOCC, GOPB, KEGG, Uniprot Keywords, stress granule proteins (Jain et al., 2016) and proteins enriched in the neuronal poly-GR/PR interactome are shown. Annotations indicated in color or black are Benjamini-Hochberg FDR significant (q-value <5%). The analysis was performed in the Perseus software.

5.4. Functional analysis of poly-GR/PR interactors reveals multiple pathways to be involved in *C9orf72*-associated toxicity

Even though the analysis of the GFP-(GR)$_{149}$ and (PR)$_{175}$-GFP interactomes in primary neurons and HEK293 cells already revealed possible mechanisms involved in DPR toxicity, my aim was to further elucidate the connection of poly-GR/PR with the underlying pathways and validate interacting proteins involved. Thus, the following functional analysis focuses on the proteins associated with methylation, splicing, mitochondria, the nucleolus, stress granules and ribosomes as suggested by enrichment analysis of the interactome of both poly-GR and poly-PR. In order to functionally confirm putative poly-GR/PR interacting proteins and their connection to *C9orf72* pathogenesis, the major method was to co-express RFP-tagged interactors together with GFP-(GR)$_{149}$, (PR)$_{175}$-GFP or control GFP in neurons and HEK293 cells and study their effect on the localization of the DPR proteins and *vice versa*. Additionally, various other methods such as qRT-PCR, toxicity assays, immunoblotting and immunofluorescent stainings in cell culture and patient tissue were used.

5.4.1. Effects of poly-GR and poly-PR on methylation and splicing

5.4.1.1. *Expression of various splicing factors leads to diffused nuclear poly-PR*

First, I tested the splicing factors SRSF1, SRSF10, TRA2A and TRA2B which we identified as interactors in both GFP-(GR)$_{149}$ and (PR)$_{175}$-GFP expressing HEK293 cells, but not in neurons. As expected, in HEK293 cells, all RFP-tagged interacting proteins involved in splicing localized to the nucleus. Compared to the GFP control, co-expression of GFP-(GR)$_{149}$ did not lead to obvious changes in poly-GR or in RFP-SRSF1/SRFS10/TRA2A/TRA2B expression or localization. In contrast, all four interactors recruited otherwise nucleolar poly-PR into the remaining parts of the nucleus thereby leading to a diffuse expression pattern and colocalization with the respective splicing factor (Figure 5-9**A**). An explanation for changed (PR)$_{175}$-GFP localization might be the spatial proximity of the DPR protein with the splicing factors within the nucleus compared to more cytoplasmic poly-GR. Thus, SRSF1, SRSF10, TRA2A and TRA2B, which are representing the group of proteins involved in splicing, could be validated as interacting proteins in poly-PR expressing HEK293 cells.

A

B

Figure 5-9: Expression of splicing factors alter poly-PR distribution while poly-PR expression alters arginine methylation patterns.

(A) HEK293 cells co-expressing GFP, GFP-(GR)$_{149}$ or (PR)$_{175}$-GFP and RFP tagged splicing factors. Single plane images were obtained on a confocal microscope. Left columns show GFP fluorescence and right columns show merge of GFP, RFP-tagged proteins and nuclear DAPI staining (blue). Scale bar denotes 20 μm. Note that poly-PR shows diffuse nuclear localization upon expression of splicing factors. (B) Primary rat cortical neurons (DIV6+7) were transduced with GFP, GFP-(GR)$_{149}$ or (PR)$_{175}$-GFP. Immunoblots show reduced methylation in poly-PR expressing neurons detected with antibodies specific for histone methylation as well as general single and di-methylation. Calnexin was used as loading control.

5.4.1.2. *Poly-GR does not affect methylation in neurons*

To assess the role of the methylosome, which was suggested to be potentially altered in GFP-(GR)$_{149}$ expressing cells, I had a closer look at methylation in primary neurons. Therefore, I conducted western blot analysis using antibodies detecting Histone H4 asymmetric di-methylation, general mono-methylation and symmetric di-methylation of arginines. In cortical neurons transduced with GFP-(GR)$_{149}$, the methylation pattern and methylation intensity were indistinguishable from the one in the GFP control. Thus, interaction of poly-GR with PRMT5/WDR77 may reflect arginine-methylation of poly-GR itself. In contrast, (PR)$_{175}$-GFP expressing cells showed a general reduction of methylated

proteins (Figure 5-9**B**) which is probably a secondary effect of overall reduction of protein expression already revealed by whole proteome analysis.

5.4.2. **Mitochondria are stressed upon poly-GR/PR expression**

5.4.2.1. *Poly-GR and poly-PR do not alter the mitochondrial ribosome*

Given the wide-spread interaction of the mitochondrial ribosome with both poly-GR and poly-PR, I next analyzed if expression of GFP-(GR)$_{149}$ or (PR)$_{175}$-GFP alters localization or distribution of subunits of the mitochondrial ribosome in HEK293 cells as well as in neurons. Immunofluorescence stainings showed that, as expected, MRPL19 and MRPS9 localize to the cytoplasm in a dot-like manner in cells expressing the GFP control. Also upon transfection or transduction of GFP-(GR)$_{149}$ or (PR)$_{175}$-GFP, the

Figure 5-10: The mitochondrial ribosome is not altered upon poly-GR or poly-PR expression in neurons.

(A, B) Hippocampal and cortical rat neurons transduced with GFP, GFP-(GR)$_{149}$ or (PR)$_{175}$-GFP lentivirus (DIV6+7). **(A)** Immunofluorescent stainings of components of the small (MRPS9) and large (MRPL19) ribosomal subunits of mitochondria. Single confocal planes are shown. Left columns visualize mitochondrial ribosomal proteins and right columns show merge of GFP, MRP (red) and nuclear DAPI staining (blue). Scale bar denotes 20 µm. **(B)** Immunoblots show no changes in MRPS9 expression in poly-GR or poly-PR expressing neurons. Calnexin was used as loading control.

distribution pattern, as well as the expression levels of the endogenous proteins of the small ribosomal subunits of mitochondria, remained unchanged (Figure 5-10**A**). In addition, immunoblotting analysis showed that MRPS9 protein levels were not significantly altered in cortical neurons upon poly-GR and poly-PR transduction (Figure 5-10**B**) confirming the observations from immunofluorescence.

5.4.2.2.   *Poly-PR transduced neurons show respiratory deficits*

Although poly-GR and poly-PR did not seem to have an effect on localization and expression levels of the mitochondrial ribosome, I was curious whether the extensive interaction of the two DPR proteins with MRPS/L proteins identified in the MS analysis is affecting mitochondria directly. As previous studies only reported oxidative stress without showing effects on mitochondrial morphology or respiration, I assessed subcellular localization and checked for mitochondrial integrity. I first stained HeLa cells and hippocampal neurons using antibodies specific for the mitochondrial proteins MTCO2 and MTCO1, two cytochrome c oxidase components of the respiratory chain, respectively. GFP expressing HeLa cells maintained healthy mitochondria membranes and showed mitochondria-specific tubular, cytoplasmic MTCO2 staining. Interestingly, upon transfection with GFP-(GR)$_{149}$ and also (PR)$_{175}$-GFP, mitochondrial morphology was changed to a string-like, hyper-fused distribution (Figure 5-11**A**) indicating mitochondrial stress. In hippocampal neurons transduced with GFP or GFP-(GR)$_{149}$, MTCO1 showed a dot-like mitochondrial pattern. This pattern remained unchanged upon expression of (PR)$_{175}$-GFP, but overall MTCO1 signal was reduced (Figure 5-11**A**) suggesting that poly-PR toxicity may be associated with loss of mitochondria.

This strong downregulation of the mitochondria related MTCO1 protein detected in immunofluorescence stainings was also validated by immunoblotting experiments. Here, MTCO1 expression levels were significantly reduced in poly-PR transduced cortical neurons, while poly-GR expressing neurons showed similar MTCO1 levels as the GFP control (Figure 5-11**B**).

In order to elucidate whether this downregulation of the cytochrome c subunit, which catalyzes the reduction of oxygen to water, has a direct effect on mitochondrial respiration, I measured oxygen consumption rates (OCR) using the Seahorse analyzer. Quantification of cellular respiration in GFP-$(GR)_{149}$ and GFP expressing neurons showed the typical OCR pattern. $(PR)_{175}$-GFP expressing neurons, however, displayed reduced basal respiration accompanied by reduced maximal respiration upon uncoupling with FCCP, resulting in an overall significant lower respiratory capacity (Figure 5-11**C**).

Figure 5-11: Mitochondria are stressed especially in poly-PR expressing cells.

(A, B, C) HeLa cells, hippocampal and cortical rat neurons (DIV6+7) were transfected or transduced with GFP, GFP-$(GR)_{149}$ or $(PR)_{175}$-GFP. **(A)** Immunofluorescent stainings of subunits 1 and 2 of the mitochondrial cytochrome c complex of the inner mitochondrial membrane in HeLa cells and hippocampal neurons. Left columns show single confocal planes of MTCO2 or MTCO1 stainings and right columns show merge of GFP, the cytochrome c complex (red) and DAPI marking nuclei (blue). Scale bar denotes 20 µm. **(B)** Immunoblot shows reduction of MTCO1 levels in cortical neurons expressing $(PR)_{175}$-GFP. Calnexin was used as loading control. **(C)** Mitochondrial respiration was quantified in hippocampal and cortical neurons in real-time using the Seahorse analyzer. The oxygen consumption rate (OCR) was normalized to total protein concentration. After recording basal respiration, oligomycin (final concentration 1 µM) was added to inhibit ATP synthase (proton leak). Thereafter injection of FCCP followed to measure maximal respiration and antimycin A/rotenone was added to calculate non-mitochondrial oxygen consumption. Mean ± SEM is shown. (6 replicates from 1 experiment, * denotes $p<0.05$, ** denotes $p<0.01$ and *** denotes $p<0.001$ in two-way ANOVA, only shown for significant data points in poly-PR expressing neurons.) **(D)** Immunofluorescent staining of MTCO1 in *C9orf72* patient cortex and control. DAPI stains nuclei in blue. Single confocal planes are shown. Scale bar depicts 20 µm.

Lastly, I wanted to assess the role of mitochondria in *C9orf72* patients. Therefore, I probed brain slices from patients with an MTCO1 specific antibody. Immunofluorescence stainings showed that MTCO1 distribution was unchanged in *C9orf72* patient compared to healthy control. Furthermore, MTCO1 did not co-aggregate with poly-GR (Figure 5-11**D**).

Although the interactome of poly-GR and poly-PR shows extensive interaction of the two DPR species with mitochondrial ribosomal subunits, the analysis *in vitro* reveals no clear role of the mitochondrial ribosome in disease pathogenesis so far. However, mitochondria themselves seem to be stressed upon poly-GR and poly-PR expression showing changed morphology in HeLa cells and respiratory deficits in primary neurons. In *C9orf72* patients, there is no evidence for altered mitochondrial morphology. In accordance to the stress phenotype of the mitochondria observed in these experiments, also Lopez-Gonzalez and colleagues found increased mitochondrial reactive oxygen species (ROS) in patient derived iPSC neurons (Lopez-Gonzalez et al., 2016). Nevertheless, together with the findings in this work, that study is the only one making involvement of mitochondria a subject of discussion in poly-GR/PR mediated toxicity although mitochondrial ribosomal proteins were associated with the two arginine-rich DPR proteins in previous proteome and interactome studies (Lopez-Gonzalez et al., 2016; Yin et al., 2017; Zhang et al., 2018b). Thus, it remains to be elucidated whether stress in this cellular compartment is indeed involved in a pathogenic mechanism.

5.4.3.   Poly-PR expression alters nucleolar structure

Next, I examined the nucleolar proteins NOP56 and NPM1, which we identified as poly-PR/GR interacting proteins in both HEK293 cells and neurons, respectively. In HEK293 cells, expression of RFP-NOP56 and RFP-NPM1 resulted in colocalization with GFP-(GR)$_{149}$ and (PR)$_{175}$-GFP in the nucleolus as expected, but had no effect on localization or expression of either DPR protein (Figure 5-12**A**). In hippocampal neurons, however, expression of RFP-NPM1 surprisingly shifted otherwise cytoplasmic GFP-(GR)$_{149}$ into the nucleolus showing colocalization in nearly every cell (Figure 5-12**B** and **D**). In contrast, in RFP-NOP56 transduced neurons, poly-GR was not affected and remained in the cytosol similar to cells with RFP expression (Figure 5-12**B** and **D**). Furthermore, RFP-NOP56 co-expression did not change (PR)$_{175}$-GFP localization in neurons. Interestingly, *vice versa*, (PR)$_{175}$-GFP expression altered the distribution of RFP-NOP56 within the nucleolus compared to GFP or GFP-(GR)$_{149}$ co-transfected cells (Figure 5-12**C** close-up). While RFP-NOP56 would typically be evenly distributed in the nucleolus, expression of poly-PR led to the formation of a granular pattern with granules surrounding the PR aggregate. This result is in line with the specific interaction of poly-PR with NOP56 in neurons (Figure 5-5**A**).

A
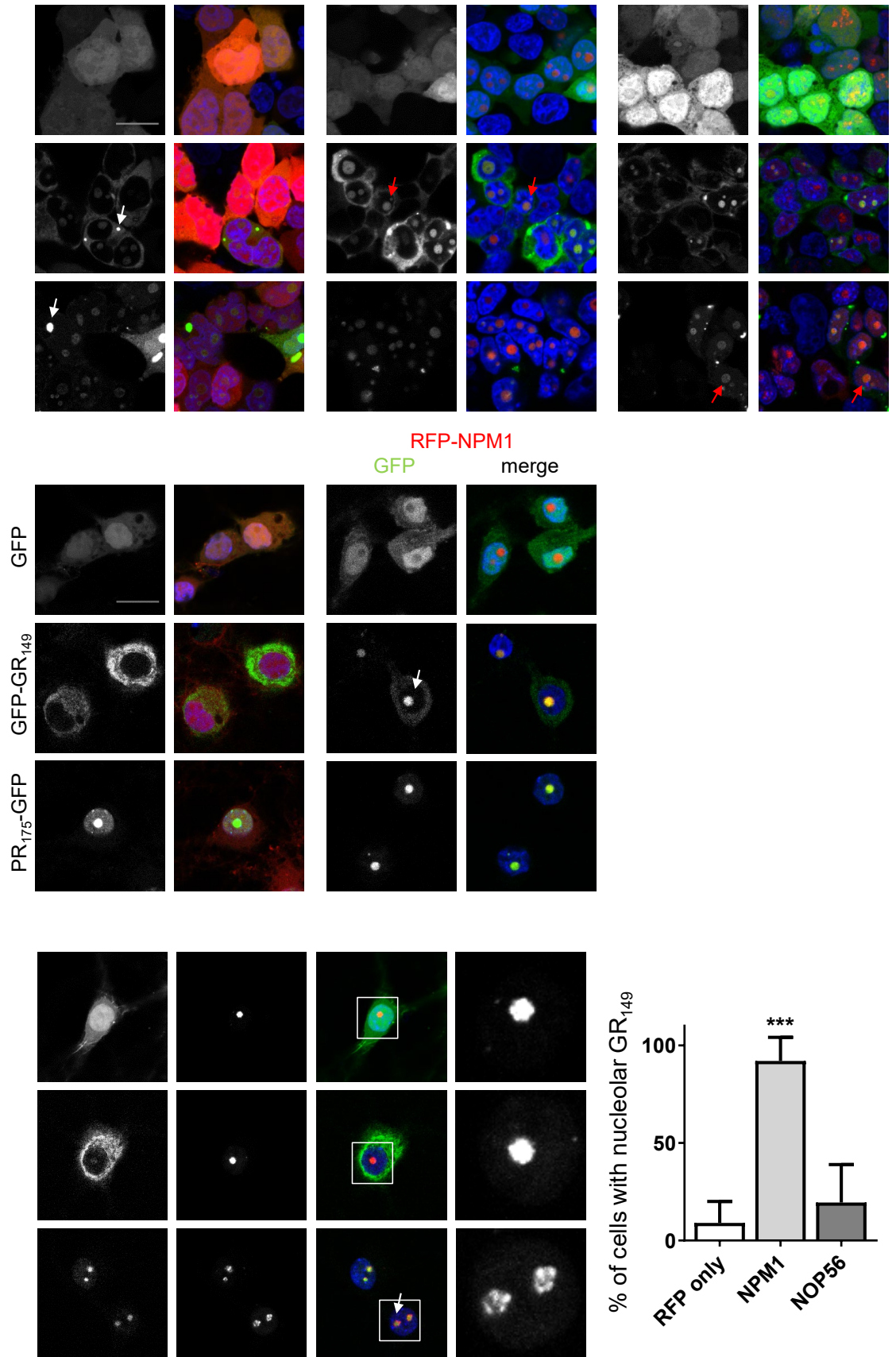
Figure 5-12: Nucleolar interactors colocalize with poly-GR/PR in HEK293 cells and neurons.

(A-D) HEK293 cells and hippocampal neurons (DIV6+7) co-expressing GFP, GFP-(GR)$_{149}$ or (PR)$_{175}$-GFP and the RFP-tagged nucleolar interacting proteins NPM1 and NOP56. Single focal planes were analyzed. RFP was used as negative control. Scale bars denote 20 μm. **(A, B, C)** Left columns show GFP fluorescence and columns labeled with 'merge' show merge of GFP, RFP-tagged proteins and nuclear DAPI staining (blue). **(A)** Poly-GR and poly-PR colocalize with RFP-NPM1 and RFP-NOP56 in nucleoli in HEK293 cells (red arrows). White arrows indicate poly-GR/PR granules occasionally seen the cytoplasm. **(B)** RFP-NPM1 is localizing to nucleolar poly-PR in hippocampal neurons. Note that NPM1 expression recruits poly-GR into the nucleolus (white arrow). **(C)** Poly-PR expression in neurons results in altered RFP-NOP56 distribution (RFP-NOP56 channel and close-up). **(D)** Percentage of neurons with poly-GR localized to the nucleolus in NPM1- and NOP56-expressing neurons compared to the RFP control (RFP: n=9; RFP-NPM1: n=11; RFP-NOP56: n=10 images (40x objective) from 3 independent experiments, mean ± SEM, *** denotes p<0.001 in one-way ANOVA with Dunnett's post-test).

To further validate that poly-PR expression has an influence on nucleolar structure, I analyzed the nucleolar markers proteins fibrillarin and GTPBP4 in hippocampal neurons by immunofluorescence. Also here, the nucleolar disorganization was clearly visible in (PR)$_{175}$-GFP expressing neurons. Cells transduced with GFP-(GR)$_{149}$ and GFP showed a ring-like or even distribution of fibrillarin as well as GTPBP4, whereas poly-PR expression resulted in granule-like dots within the nucleolus (Figure 5-13).

Overall, these findings suggest that the nucleolus, which emerged from the enrichment analysis of both interactomes, is indeed a cellular compartment affected by DPR protein expression *in vitro*. This is underlined by the observations that the interaction of poly-GR/PR with co-expressed nucleolar proteins has sufficient affinity to alter the subcellular distribution of either binding partner and that especially poly-PR has direct effect on nucleolar structure also on an endogenous level *in vitro*.
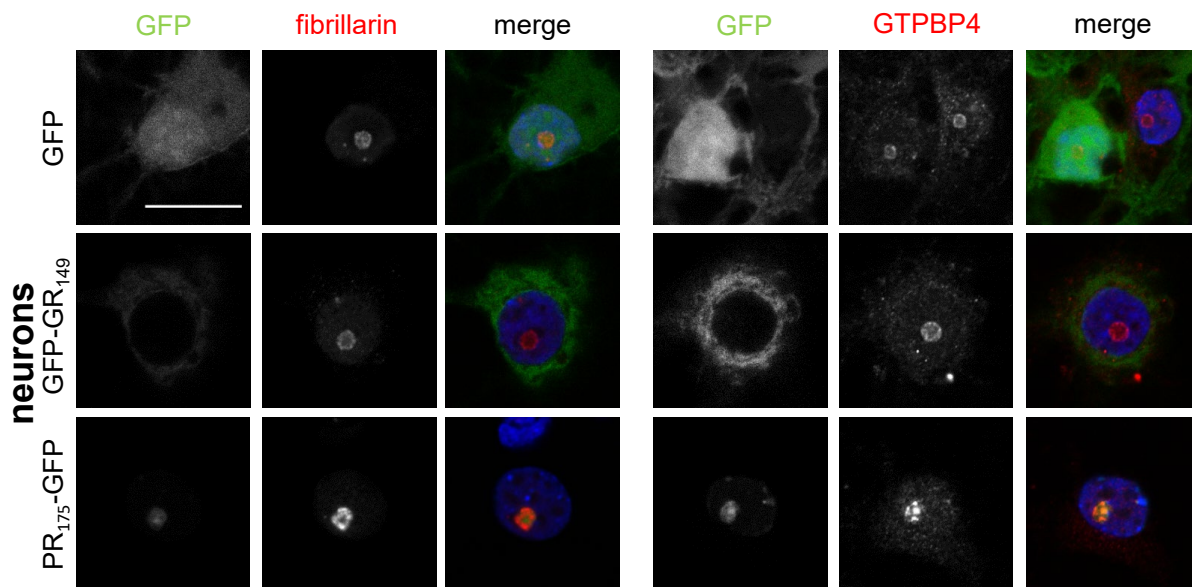

Figure 5-13: Poly-PR expressing neurons show altered nucleolar distribution in hippocampal neurons.

Hippocampal rat neurons (DIV6+7) were infected with GFP, GFP-(GR)$_{149}$ or (PR)$_{175}$-GFP. Single confocal planes of immunofluorescent stainings of the nucleolar marker proteins fibrillarin and GTPBP4 were analyzed. Left columns show GFP fluorescence, middle columns visualize stainings of fibrillarin/GTPBP4 and right columns show merge of GFP, nucleoli (red) and DAPI marks nuclei (blue). Scale bar denotes 20 μm. Note that poly-PR expression results in disruption of the nucleolus.

5.4.4. **Cytoplasmic poly-GR/PR clusters resemble stress granules**

5.4.4.1. *Poly-GR/PR forms large granule-like structures in the cytoplasm*

As various proteins linked to stress granules were found to interact with poly-GR/PR in both HEK293 cells and neurons, I again conducted co-expression experiments to elucidate their role in DPR protein toxicity. Therefore, I expressed the interactors RFP-STAU1, RFP-STAU2, RFP-YBX1, and RFP-EIF4A3 together with GFP-(GR)$_{149}$, (PR)$_{175}$-GFP or a GFP control in HEK293 cells and neurons. Under RFP control conditions, transfection of both poly-GR and -PR occasionally resulted not only in nucleolar aggregation, but also formation of small cytoplasmic granules in HEK293 cells (white arrows in Figure 5-12**A**). Interestingly, upon co-expression of RFP-STAU1/STAU2 and RFP-YBX1, these cytoplasmic granules were significantly increased in number, size, and intensity. Of note, not only poly-GR/PR were rerouted to the cytoplasm, but also the stress granule associated proteins themselves clustered into the large cytoplasmic inclusions leading to colocalization of the two DPR species and STAU1/STAU2/YBX1 (white arrows in Figure 5-14**A**). Among the tested stress granule components only EIF4A3, identified in the poly-PR interactome, did not alter cytoplasmic poly-GR/PR proteins. Quantitative analysis confirmed that the GFP-(GR)$_{149}$ and (PR)$_{175}$-GFP inclusions in the cytoplasm are increased in number and also the average size upon expression of RFP-STAU1, RFP-STAU2 and RFP-YBX1, but not RFP-EIF4A3 (Figure 5-14**B**).

Next, I repeated this experiment in primary hippocampal neurons to elucidate whether dense cytoplasmic poly-GR or -PR granules can also be detected in this cellular system. To allow higher expression levels I co-transfected GFP-(GR)$_{149}$, (PR)$_{175}$-GFP or a GFP control with RFP-STAU1/STAU2 and RFP-YBX1. While transfection of (PR)$_{175}$-GFP resulted in high toxicity (compared to the lower expression in transduced neurons) and probably killed all poly-PR expressing neurons, poly-GR transfected neurons showed similar colocalization with the stress granule associated proteins in the cytoplasm as seen in HEK293 cells. Also here, the even cytoplasmic distribution was disrupted and resulted in granule like inclusions (Figure 5-14**C**). In transduced neurons, expression levels were presumably too low to affect poly-GR/PR distribution (data not shown).
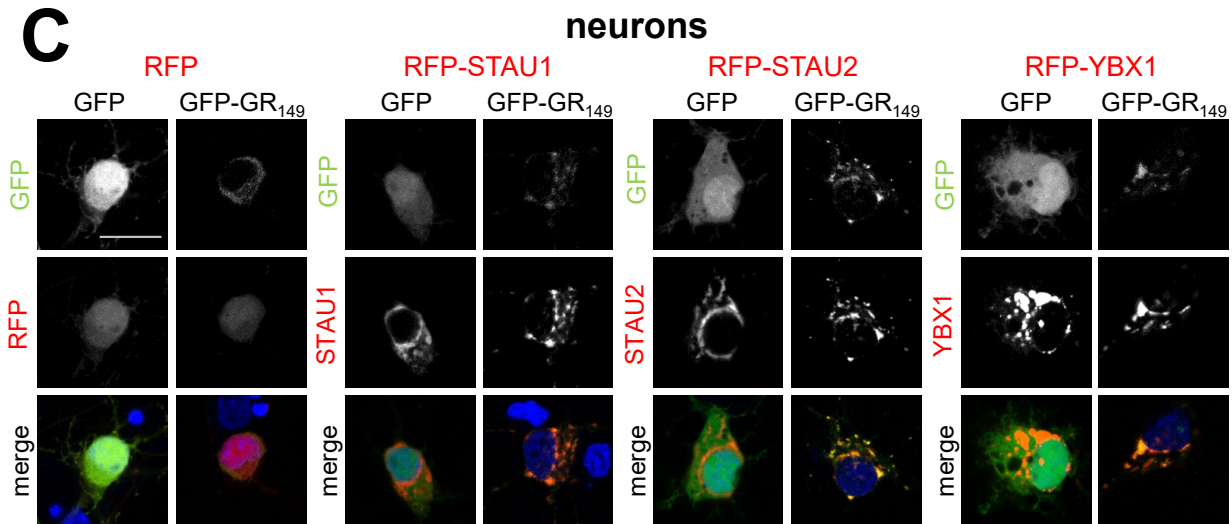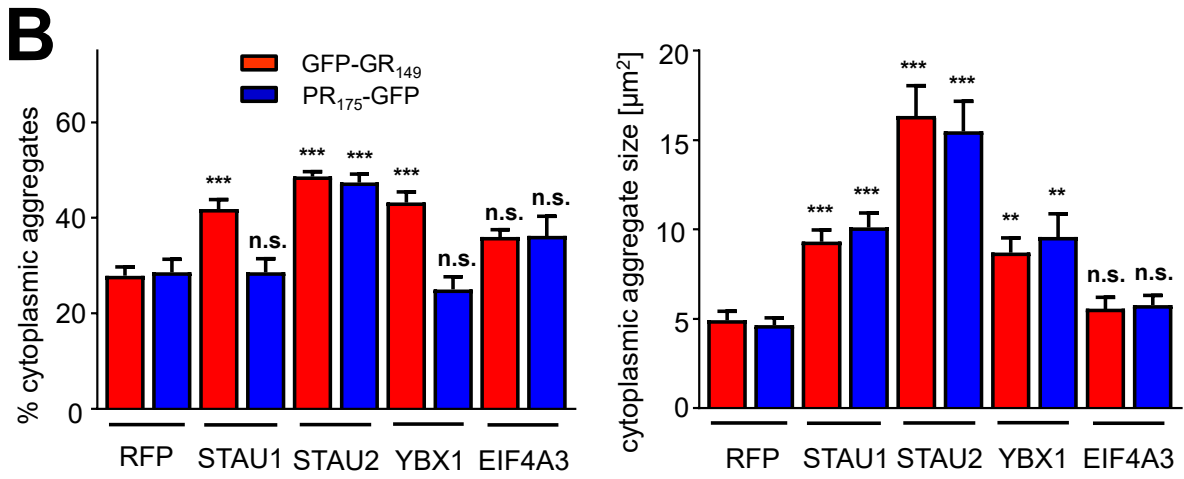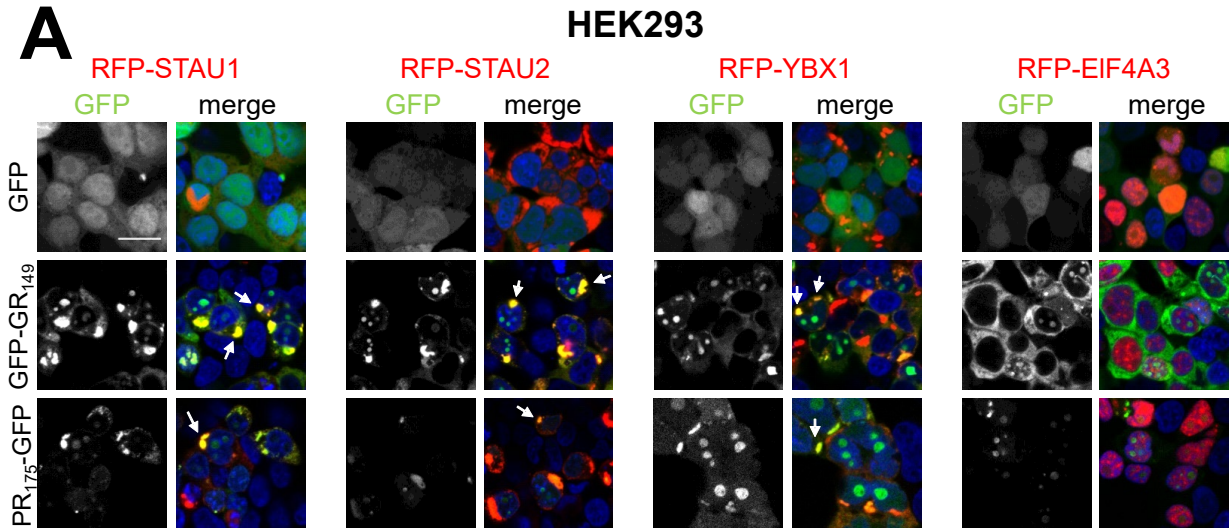
Figure 5-14: STAU1/2 and YBX1 recruit poly-GR/PR into large cytoplasmic granules.

HEK293 cells and primary cortical neurons co-expressing GFP, GFP-(GR)$_{149}$ or (PR)$_{175}$-GFP and RFP-tagged interactors related to stress granules. **(A)** Single confocal planes of immunofluorescence images of HEK293 cells showing co-expression of RFP-STAU1/2, RFP-YBX1 or RFP-EIF4A3 together with the two DPR proteins or GFP are shown. Left columns visualize GFP fluorescence, right columns show merge of GFP, RFP-tagged proteins and nuclear DAPI staining (blue). Scale bar denotes 20 µm. Note that STAU1/2 and YBX1 reroute poly-GR and -PR into large cytoplasmic granules (white arrows). **(B)** Quantifications of cytoplasmic poly-GR/PR structures seen in (A). Left bar graph represents percentage of cytoplasmic granules out of all analyzed granules in both, nucleolus and cytoplasm in poly-GR (red bars) and poly-PR (blue bars). RFP served as control (GR/RFP: n=16; PR/RFP: n=14; GR/RFP-STAU1: n=19; PR/RFP-STAU1: n=20; GR/RFP-STAU2: n=10; PR/RFP-STAU2: n=8; GR/RFP-YBX1: n=14; PR/RFP-YBX1: n=14; GR/RFP-EIF4A3: n=6; PR/RFP-EIF4A3: n=6 images (40x) from two independent experiments). Cytoplasmic granule size is visualized by the right bar graph (GR/RFP: n=130; PR/RFP: n=132; GR/RFP-STAU1: n=104; PR/RFP-STAU1: n=132; GR/RFP-STAU2: n=123; PR/RFP-STAU2: n=65; GR/RFP-YBX1: n=119; PR/RFP-YBX1: n=53; GR/RFP-EIF4A3: n=93; PR/RFP-EIF4A3: n=71 aggregates from two independent experiments). Mean ± SEM is shown, *** denotes $p<0.001$ and ** denotes $p<0.01$ in one-way ANOVA with Dunnett's post-test. **(C)** Immunofluorescence images of neurons (DIV7+3) co-transfected with RFP-STAU1, RFP-STAU2 or RFP-YBX1 and GFP-(GR)149 or GFP. Single focal planes are shown. Top rows show GFP signal, middle rows visualize RFP fluorescence of stress granule proteins or RFP control and bottom rows show merged signals including DAPI marking nuclei (blue). Note that the largely homogenous poly-GR pattern in the RFP control is largely

5.4.4.2.   *The large cytoplasmic poly-GR/PR granules are G3BP1 positive*

To assess the nature of these cytoplasmic poly-GR/PR clusters detected in both HEK293 cells and neurons, I analyzed classical stress granule markers G3BP1, TIAR and FMRP in HEK293 cells co-transfected with GFP-(GR)$_{149}$, (PR)$_{175}$-GFP or a GFP control and RFP-STAU1 or RFP-YBX1 by immunofluorescence. Strikingly, all three markers colocalized with the poly-GR/PR granules in RFP-STAU1 and RFP-YBX1 transfected HEK293 cells indicating that the large cytoplasmic inclusions represent bona fide stress granules (white arrows in Figure 5-15**A** and **B,** FMRP not shown, YBX1 transfected cells not shown). In addition, also an antibody against YBX1 itself nicely detected the granules (data not shown). However, the less frequent small cytoplasmic poly-GR/PR inclusions formed in RFP control conditions were also predominantly G3BP1, TIAR and FMRP-positive suggesting that expression of the RFP-tagged stress granule associated proteins enhances the formation of stress granules by boosting the process existing under basal conditions.

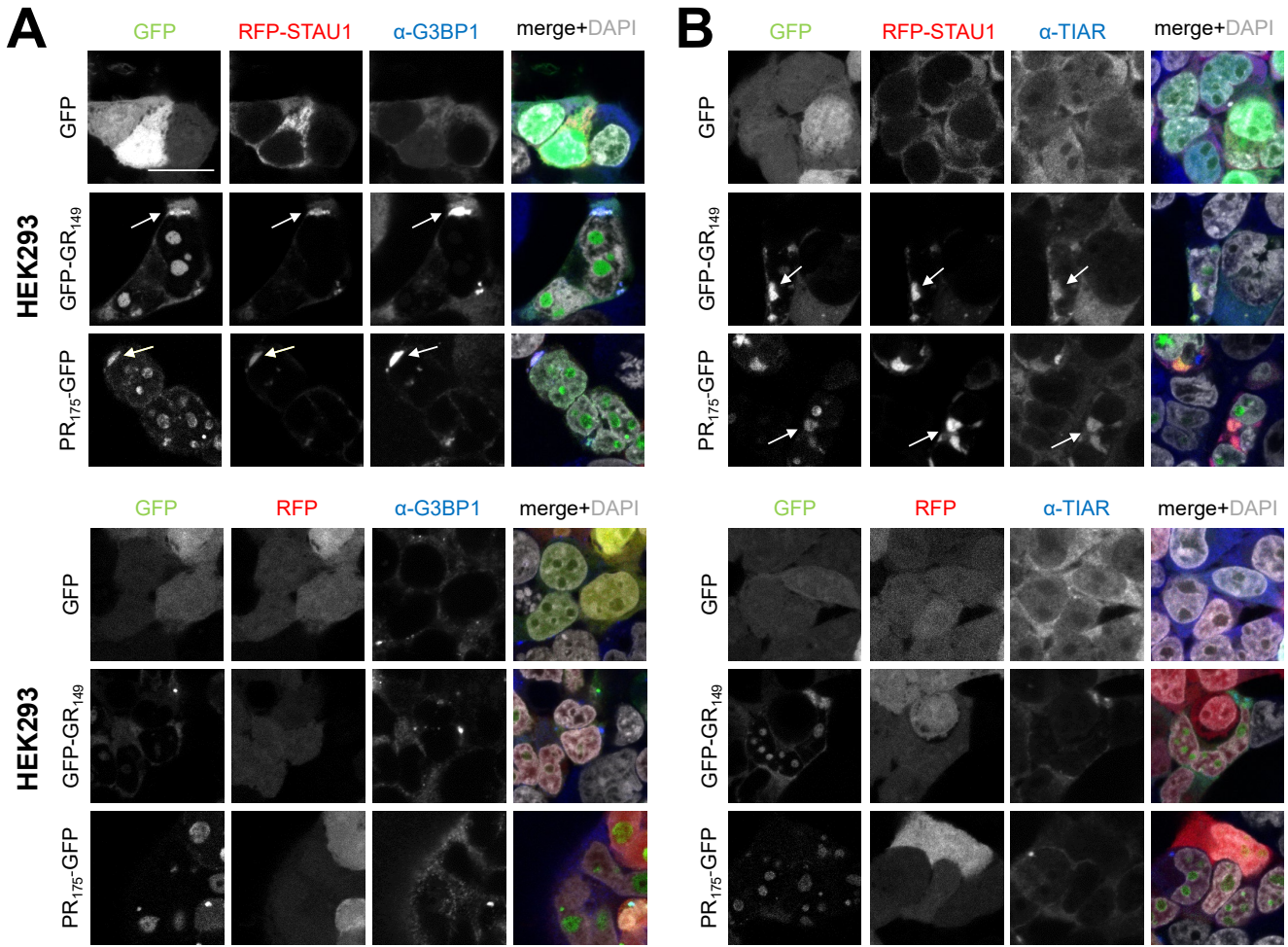**Figure 5-15:** Cytoplasmic poly-GR/PR granules are identified as stress granules in HEK293.

HEK293 cells were co-transfected with GFP, GFP-(GR)$_{149}$ or (PR)$_{175}$-GFP and RFP-STAU1. Immunofluorescence images show colocalization of cytoplasmic poly-GR/PR with the stress granule markers **(A)** G3BP1 and **(B)** TIAR in HEK293 cells co-transfected with RFP-STAU1. Left three columns show individual channels as indicated. Right columns visualize merge with additional nuclear DAPI staining in white. Arrows indicate cytoplasmic inclusions co-labeled with G3BP1 or TIAR. Single confocal planes were taken. Scale bar depicts 20 µm.

5.4.4.3.   *STAU2 but no other SG proteins are found in poly-GR aggregates in* C9orf72 *patient brain*

In order to elucidate whether stress granules also play a role in FTD/ALS patients, I additionally probed FTD patient brains with *C9orf72* repeat expansion and healthy control brains with two different stress granule markers and antibodies detecting the poly-GR/PR interacting proteins YBX1 and STAU2. As expected, the *C9orf72* FTD case showed widespread poly-GR and sparse poly-PR cytoplasmic inclusions in the frontal cortex. Cytoplasmic G3BP2 and nuclear TIAR did not show convincing colocalization with aggregates stained with a poly-GR antibody. Also, the interactor YBX1 could not be discovered in cytoplasmic poly-GR inclusions. Only STAU2 colocalized with approximately 25% of the poly-GR aggregates in the frontal cortex of two *C9orf72* patients (Figure 5-16**A**).
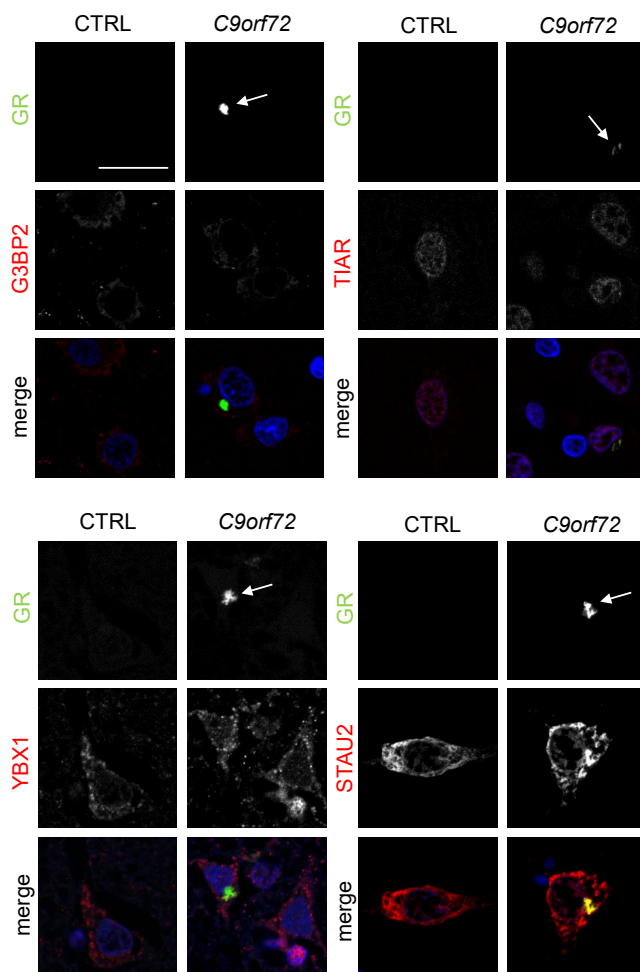

Figure 5-16: STAU2 colocalizes with poly-GR aggregates in C9orf72 patient brain.

C9orf72 patients and a healthy controls were analyzed in immunofluorescence images of frontal cortex. Stress granule components TIAR, G3BP2, YBX1 and STAU2 were stained in red while poly-GR was labeled in green. Merge shows additional DAPI staining (blue) marking nuclei. Arrows point to poly-GR aggregates. Single confocal planes were taken. Scale bar depicts 20 µm.

In conclusion, although poly-GR and poly-PR interact with various stress granule related proteins and are recruited into stress granules upon expression of STAU1/2 and YBX1, classical stress granule markers are not labeling the poly-GR inclusions in patient brains. Here, only STAU2 was convincingly co-aggregating with poly-GR. These findings indicate that a more transient interaction exists between stress granule proteins and the two DPR proteins in *C9orf72* patients.

5.4.5. Poly-GR and poly-PR bind the cytosolic ribosome and inhibit translation

5.4.5.1. *Ribosomal proteins are absent from cytoplasmic stress granule-like inclusions*

Next, I wondered whether the poly-GR/PR cytoplasmic stress granule-like inclusions found upon STAU1/2 and YBX1 expression are also recruiting parts of the ribosome, as ribosomal proteins were the most prominent interactors of poly-GR and poly-PR in both primary neurons and HEK293 cells. Therefore, I stained HEK293 cells co-expressing poly-GR/PR and RFP-STAU1, as representative example, with an antibody directed against the 40S ribosomal protein RPS6. As expected, the small ribosomal subunit was diffusely distributed throughout the cytoplasm in control RFP cells independent of GFP or poly-GR/PR expression (Figure 5-17 lower image). Co-expression of the stress granule component RFP-STAU1 with poly-GR/PR did not change the localization of RPS6 and only modest amounts of RPS6 were detected in cytoplasmic poly-GR/PR inclusions (Figure 5-17 upper image).
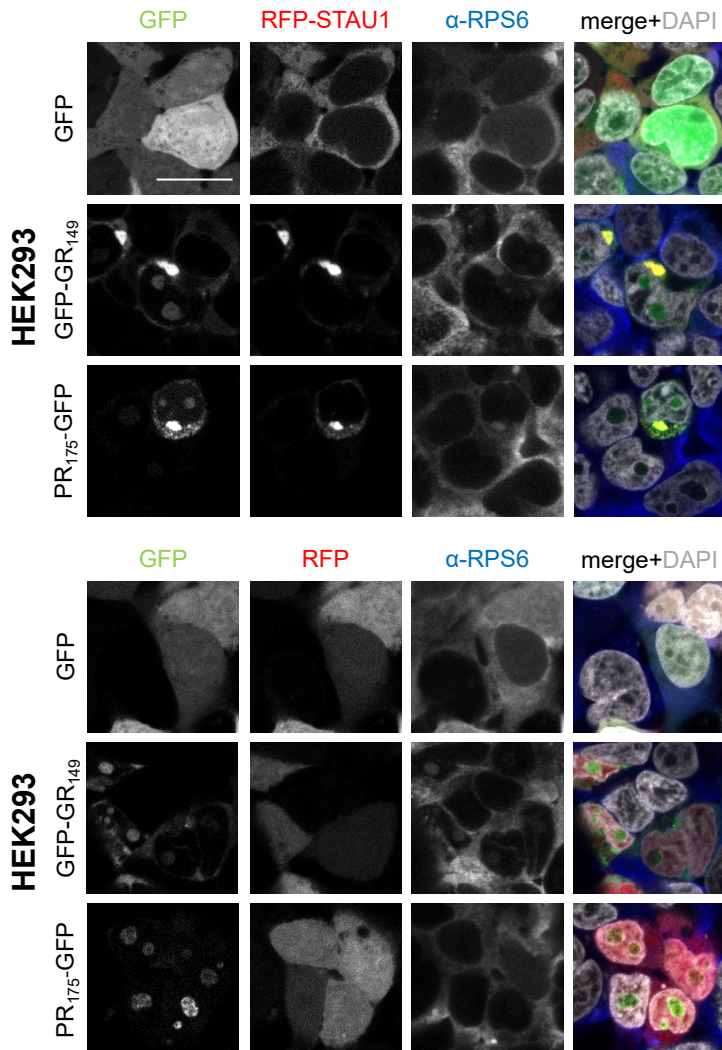

Figure 5-17: RPS6 does not label large cytoplasmic poly-GR/PR inclusions *in vitro*.

HEK293 co-expressing GFP, GFP-(GR)$_{149}$ or (PR)$_{175}$-GFP and RFP-STAU1 were imaged on a confocal microscope. Endogenous staining of the ribosomal subunit RPS6 was analyzed. Left three columns show individual channels as indicated. Right columns visualize merge with additional nuclear DAPI staining in white. Scale bar depicts 20 µm. Note that the large cytoplasmic poly-GR/PR granules induced by STAU1 expression are not clearly stained with RPS6 when comparing intensities to the cytoplasm.

5.4.5.2. *Poly-PR expression reduces ribosomal proteins in neurons*

In order to validate and investigate individual poly-GR/PR interactors I so far mainly used co-expression of RFP-tagged proteins, but tagging of ribosomal proteins without affecting their function is difficult. Therefore, I first analyzed expression of endogenous ribosomal proteins in immunoblotting experiments. Strikingly, primary cortical neurons transduced with $(PR)_{175}$-GFP showed significant reduction of RPS6, RPL19, and RPL36A levels compared to the GFP control, while GFP-$(GR)_{149}$ expression had no overt effect (Figure 5-18**A**). This finding was confirmed by quantification of the respective immunoblots (Figure 5-18**B**).
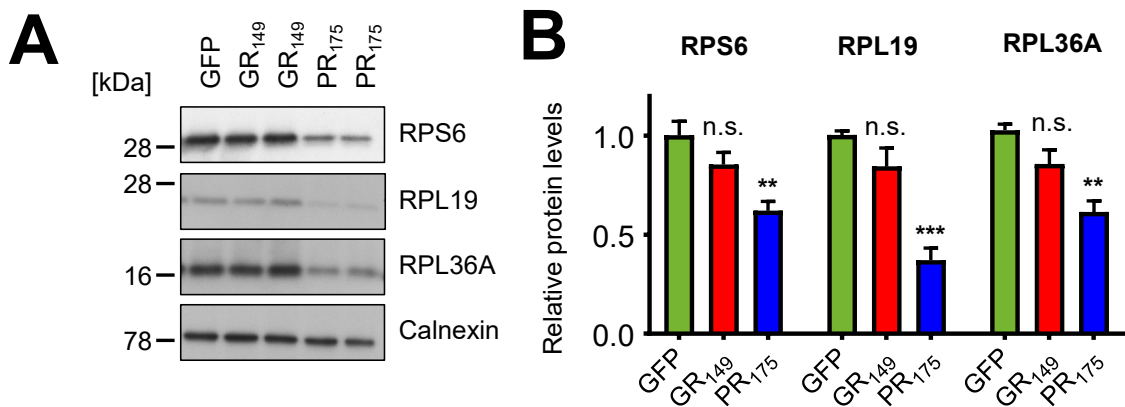

Figure 5-18: Subunits of the cytoplasmic ribosome are reduced upon poly-PR expression in neurons.

(**A**) Cortical rat neurons were transduced with GFP, GFP-$(GR)_{149}$ or $(PR)_{175}$-GFP lentiviral constructs (DIV6+7) and analyzed on immunoblots. Poly-PR expressing neurons show reduction of several ribosomal subunits compared to GFP and poly-GR. Calnexin was used as loading control. (**B**) Quantification of RPS6 signal normalized to Calnexin (n=6 from 3 independent experiments, mean ± SEM, ** denotes p<0.01 in one-way ANOVA with Dunnett's post-test), RPL19 signal normalized to Calnexin (n=6 from 3 independent experiments, mean ± SEM, *** denotes p<0.001 in Kruskal-Wallis test with Dunn's post-test) and RPL36A signal normalized to Calnexin (n=6 from 3 independent experiments, mean ± SEM, ** denotes p<0.01 in Kruskal-Wallis test with Dunn's post-test).

To further study the effects of the two DPR proteins on the cytosolic ribosome, I additionally examined the localization of ribosomal subunits in neurons expressing GFP-$(GR)_{149}$ and $(PR)_{175}$-GFP using immunofluorescence stainings. As expected, RPS6 as well as RPL19 diffusely localized to the cytoplasm in control GFP conditions. While expression of GFP-$(GR)_{149}$ had no effect on the localization or the expression level of the two ribosomal subunits, expression of poly-PR was causing a more disordered and granular pattern of RPS6. In line with the findings from the immunoblotting experiments, poly-PR strongly reduced RPL19 staining intensity (Figure 5-19**A**).

To examine the role of cytosolic ribosomes *in vivo*, I performed immunofluorescence stainings of ribosomal proteins in FTD patient brains harboring the *C9orf72* repeat and controls. In contrast to the results from neuronal cell culture, immunofluorescence analysis of RPS6 and RPL19 in *C9orf72* patients did not reveal differences in protein levels compared to healthy controls (Figure 5-19**B**).
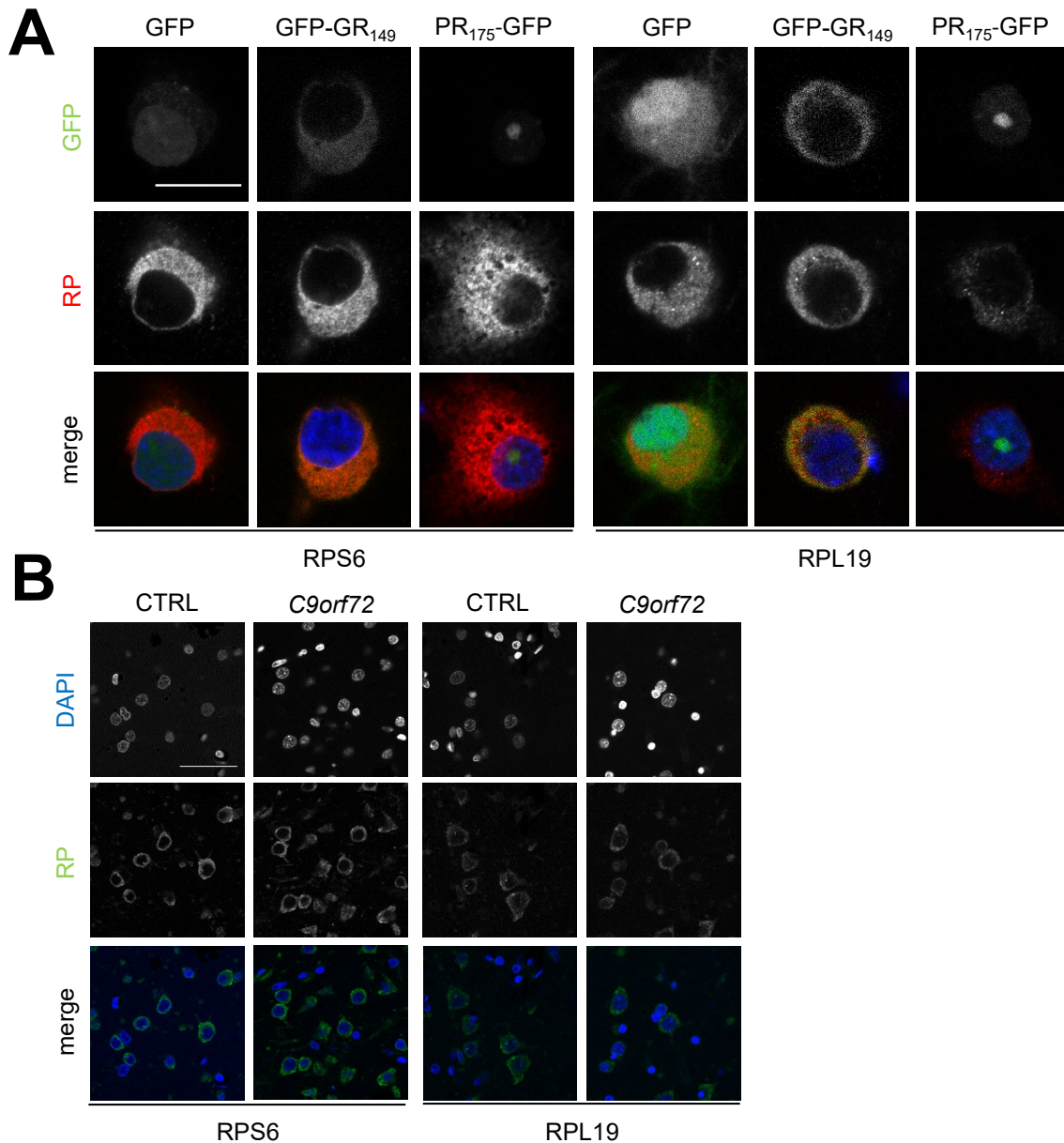
Figure 5-19: The cytosolic ribosome is not reduced in *C9orf72* patient brain.

(A) Hippocampal primary neurons (DIV6+7) were infected with GFP, GFP-(GR)$_{149}$ or (PR)$_{175}$-GFP lentiviral constructs. Single focal images of immunofluorescence stainings of the ribosomal subunits S6 and L19 were analyzed. Upper rows show GFP fluorescence, middle rows visualize ribosomal proteins (RP) in red and in merge DAPI marks nuclei (blue) additionally. Compare ordered RPS6 staining in GFP and poly-GR with unstructured RPS signal in poly-PR. Also, note that RPL19 signal is reduced in poly-PR expressing neurons. Scale bar denotes 20 μm. (B) Immunofluorescence stainings of RPS6 and RPL19 in *C9orf72* patient cortex and healthy control. DAPI stains nuclei in blue. Single confocal planes are shown. Scale bar depicts 50 μm.

Thus, especially poly-PR expression results in an overall reduction of the cytosolic ribosome which could be validated on protein level by immunoblotting and immunofluorescence stainings in primary neurons, but not in neurons bearing poly-GR/PR inclusions in *C9orf72* patient brains.

5.4.5.3. *Ribosomal subunits are found in poly-GR/PR inclusions in patients*

Although the reduction of ribosomal proteins could not be validated in patient tissue, interestingly, I noticed that RPS6, RPL19 as well as RPS25 and RPL36A showed condensed spots within the cytoplasm which colocalized with poly-GR inclusions in double immunofluorescent stainings. In contrast, ribosomal subunits were evenly distributed in healthy controls (Figure 5-20**A** and **B**). Quantification revealed that strikingly about one-third of cytoplasmic poly-GR inclusions in the cortex were positive for ribosomal proteins (Figure 5-20**C** and **D**). This enrichment of ribosomal proteins was less in poly-PR aggregates (Figure 5-20**A**) and the low number of aggregates did not allow reliable quantification. Overall, this observation suggests that the ribosome is not only affected by poly-GR/PR *in vitro*, but also plays a significant role in *C9orf72* patients.
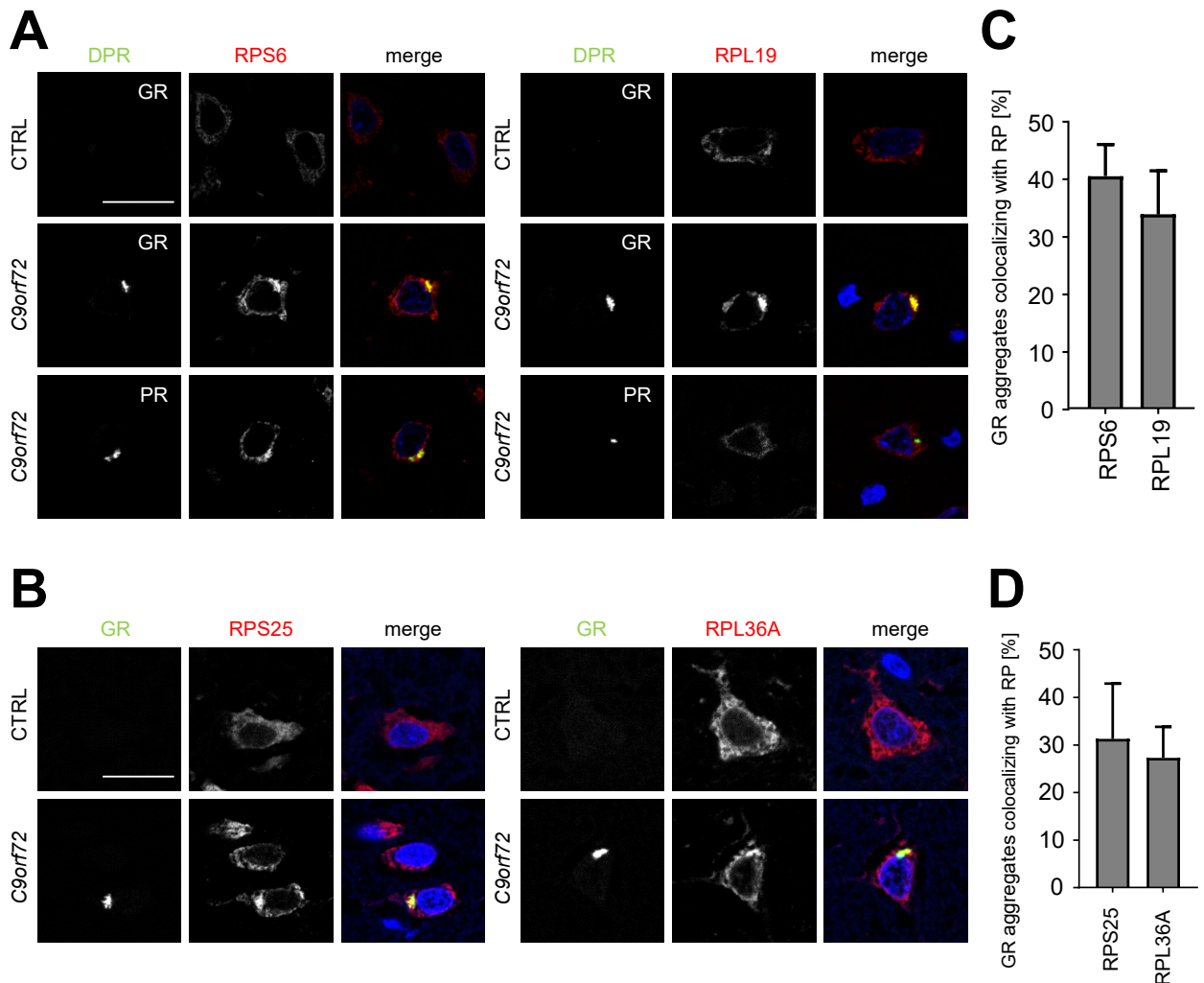

Figure 5-20: Ribosomal proteins co-aggregate with poly-GR and -PR in C9orf72 patient brain.

Confocal images of immunofluorescent stainings of **(A)** RPS6, RPL19, **(B)** RPS25 and RPL36 in *C9orf72* patient cortex and healthy control. Note that ribosomal proteins are sequestered into poly-GR/PR inclusions. DAPI marks nuclei in blue. Single confocal planes are shown. Scale bar depicts 20 μm. **(C, D)** Quantitative analysis of colocalization of ribosomal proteins with poly-GR aggregates (n=3 sections with 100 poly-GR aggregates counted each from *C9orf72* cortex, mean ± SEM is shown).

5.4.5.4.   *Translation is impaired by poly-PR in primary neurons*

Next, I was curious whether the reduction of ribosomal proteins detected *in vitro* would also affect translation. This would be in line with the proteomics finding that in poly-PR expressing neurons hundreds of proteins, including the ribosome itself, were downregulated. To verify this hypothesis, I performed a so-called 'surface sensing of translation' (SUnSET) assay, which measures puromycin incorporation into newly synthesized proteins using a puromycin specific antibody. Immunoblotting showed that translation was substantially reduced in neurons expressing $(PR)_{175}$-GFP after 10 min and 20 min of puromycin incubation compared to the GFP control and poly-GR (Figure 5-21**A**). This significant reduction in protein expression was quantified in Figure 5-21**B**. Hence, the loss of ribosomal subunits led to an overall translational repression suggesting that poly-PR expression leads to a reduction of functional/assembled ribosomes.
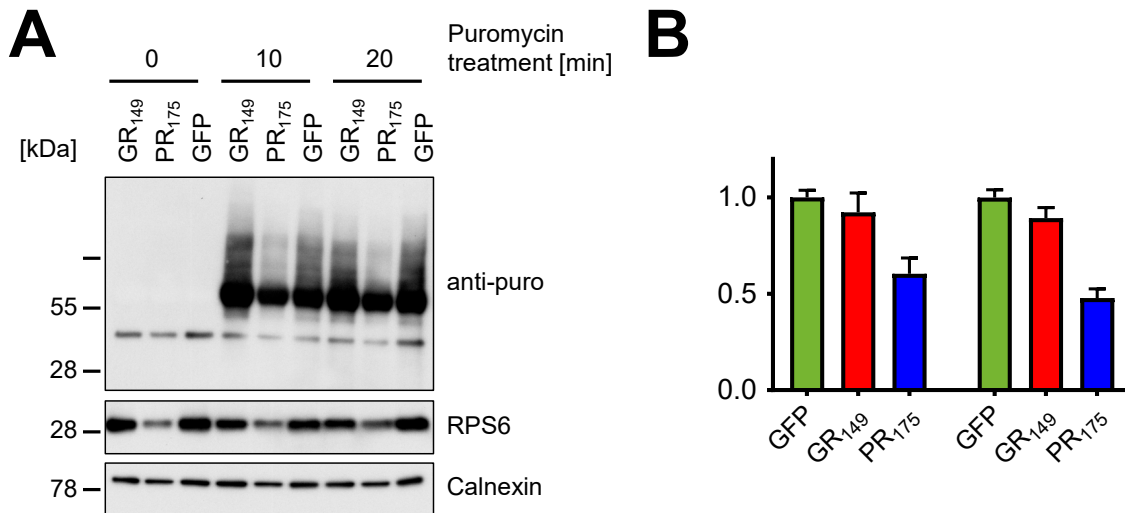

Figure 5-21: Poly-PR expression in neurons inhibits translation.

(A) Cortical rat neurons were transduced with GFP, GFP-$(GR)_{149}$ or $(PR)_{175}$-GFP lentiviral constructs (DIV6+7) and incubated with 1 µM puromycin (puro) for 0, 10 and 20 min prior to sample preparation in order to quantify global translation. Immunoblot of SUnSET assay shows that poly-PR expressing neurons have less puromycin incorporated in newly synthesized proteins compared to poly-GR and GFP control. **(B)** Quantification of RPS6 signal normalized to Calnexin (n=3, mean ± SEM, Kruskal-Wallis test with Dunn's post-test, not significant) and puromycin signal normalized to Calnexin (n=6, mean ± SEM, one-way ANOVA with Dunnett's post-test, *** denotes p<0.001).

5.4.5.5.   *rRNA processing is not changed in DPR expressing cells*

The observations that poly-PR expression disrupts nucleolar structure and reduces translation in neurons imply that rRNA processing might also be impaired. To test this, I performed quantitative PCR on RNA extracted from GFP-$(GR)_{149}$, $(PR)_{175}$-GFP and GFP transduced neurons. The primers I used covered the 18S and 5.8S rRNA. Primers specific for the whole unprocessed 45S rRNA and the 28S part only resulted in melting curves with multiple maxima or irregular standard curves making them

impracticable for analysis (Figure 5-22**A**). Relative expression levels of 18S and 5.8S rRNA revealed that none of the tested rRNA fragments was significantly altered upon poly-GR or poly-PR expression in primary neurons (Figure 5-22**B**) suggesting that aberrant rRNA processing is not the major pathway driving impaired translation under physiological conditions.
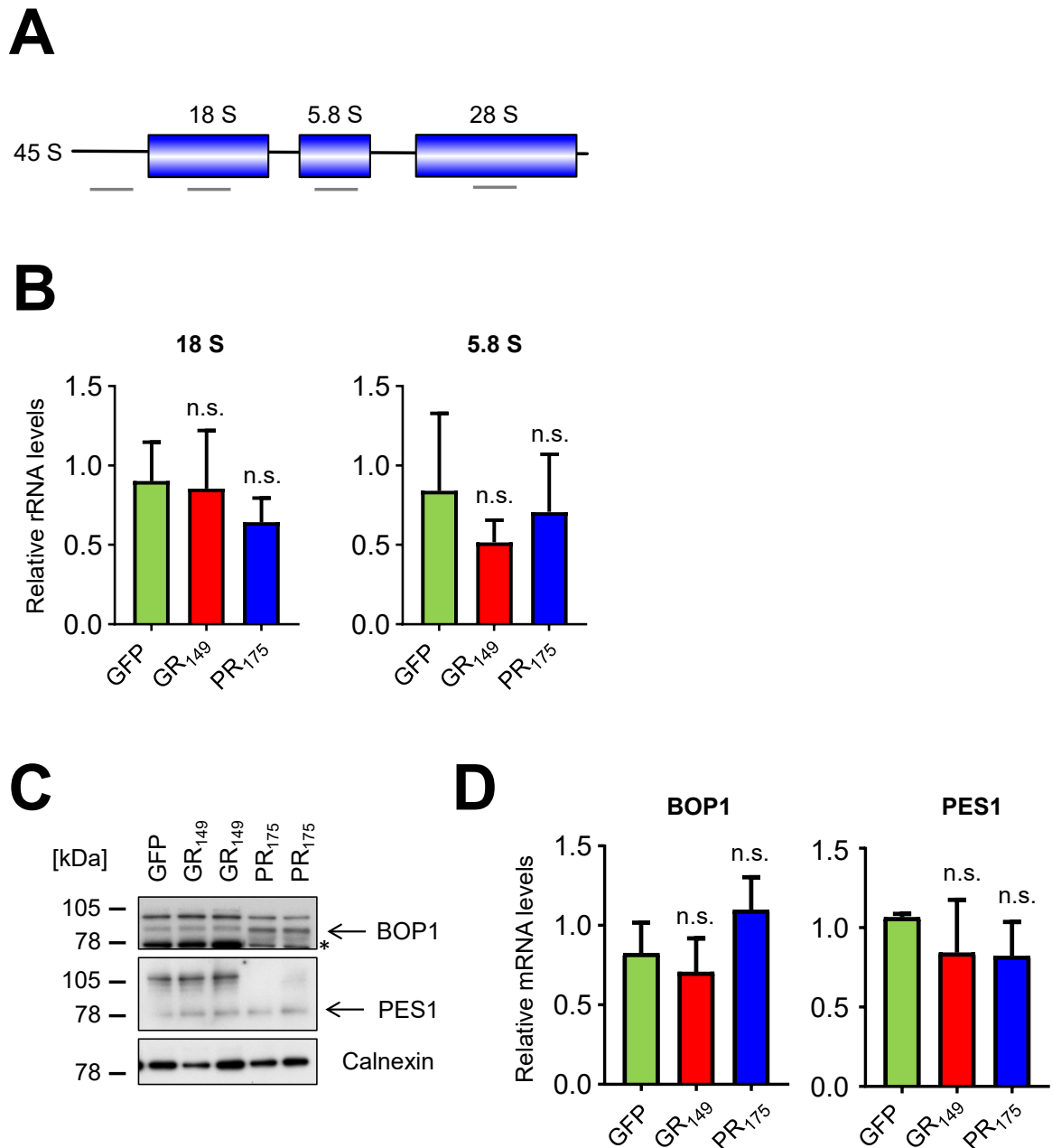

Figure 5-22: Reduction in ribosomal proteins is independent of rRNA maturation, but may trigger ribosomal biogenesis.

(A) Schematic of rRNA primer binding sites depicted in grey. (B-D) Cortical rat neurons were transduced with GFP, GFP-(GR)$_{149}$ or (PR)$_{175}$-GFP lentiviral constructs (DIV6+7). (B) Analysis of quantitative RT-PCR showing rRNA levels of the 18S and 5.8S fragments relative to PGK (n=4 from 2 individual experiments, mean ± SEM, one-way ANOVA with Dunnett's post-test). (C) Immunoblots of neuronal lysates were exposed to antibodies specific for BOP1 and PES1. Calnexin was used as a control. Note that the 83 kDa BOP1 protein is increased upon poly-PR expression. The 71 kDa large isoform 2 of BOP1 is marked with asterisks. All other bands are unspecific. (D) qRT-PCR analysis visualizing mRNA levels of the ribosome biogenensis proteins BOP1 and PES1 relative to PGK (n=4 from 2 individual experiments, mean ± SEM, one-way ANOVA with Dunnett's post-test).

GO term analysis of differentially expressed proteins in the whole proteome of poly-PR transduced primary cortical neurons showed upregulation of proteins involved in ribosome biogenesis, including NSA2, RRP1, BRIX1, NOC2L, WDR75 and TSR1 suggesting neurons may trigger a compensatory response to evade cell death (Figure 5-8**C**). BOP1 and PES1, two of the three proteins of the PeBoW complex involved in processing the 28S and 5.8S rRNA and subsequent maturation of the large 60S ribosomal subunit were significantly upregulated in the proteome analysis. WDR12 was not altered in the proteome. To validate this finding, I analyzed expression levels by immunoblotting experiment and qPCR in GFP-(GR)$_{149}$, (PR)$_{175}$-GFP and GFP transduced neurons. Here, the 83 kDa large BOP1 protein was indeed upregulated in poly-PR expressing cells, but the small increase in mRNA levels did not reach significance (Figure 5-22**C** and **D**). This modest effect, however, is in line with 1.66-fold enrichment of BOP1 in neurons expressing poly-PR. Although PES1 was also enriched at the same level in the mass spectrometry analysis of poly-PR expressing neurons, it did not show elevated protein or mRNA levels (Figure 5-22**C** and **D**).

5.4.5.6. *NPM1 has no rescue effect, but MEK1 does*

The next step was to determine whether boosting translation would prevent neuronal death in poly-PR expressing neurons. Thus, I first tested whether expression of poly-GR or poly-PR interactors is able to reverse the translational impairment seen in (PR)$_{175}$-GFP transduced neurons. As the nucleolus is the major compartment associated with ribosome biogenesis, I first tested interactors which are nucleolar and linked to ribosomes, namely NOP56, NPM1, GTPBP4 and BRIX1. NOP56 and GTPBP are involved in the assembly of the 60S ribosomal subunit, NPM1 is chaperoning ribosomal proteins, and BRIX1 also functions in biogenesis of the 60S ribosomal subunit. However, co-expression of poly-PR with the four nucleolar proteins did not restore translation efficiency in the SUnSET assay compared to the poly-PR/RFP control (Figure 5-23**A**).

The next step was to test whether expression of proteins other than poly-GR/PR interactors could rescue impaired ribosome biogenesis. Therefore, I chose MEK1, the main activator of the MAPK/ERK/S6K pathway which boosts translation by phosphorylation of RPS6. The effect on translation of the constitutive active form (S218D and S222D mutations) of MEK1 in GFP-(GR)$_{149}$, (PR)$_{175}$-GFP and GFP transduced neurons was again analyzed by the SUnSET assay as before. Here, expression of MEK1 resulted in increased puromycin signal in poly-GR as well as in poly-PR and GFP expressing neurons compared to the empty vector control. Notably, in poly-PR expressing neurons the puromycin signal was restored to control levels (Figure 5-23**B**) and similarly, also RPS6 levels were almost restored suggesting that poly-PR toxicity induced by impaired protein synthesis could be rescued by overexpression of MEK1. To substantiate this hypothesis, I performed an LDH toxicity assay in neurons (DIV7+14) in the same experimental settings. Here, MEK1 expression slightly inhibited basal

cell death in GFP and (non-significantly) also in poly-GR expressing neurons. This is not surprising as MEK1 positively regulates ERK1/2 which activate anti-apoptotic proteins (Lu and Xu, 2006). Strikingly, MEK1 overexpression reduced cell death induced by poly-PR expression nearly to GFP control levels suggesting impaired translation contributes to cell death.

Taken together, MEK1, a key regulator of translation and cell growth, was able to reverse poly-PR induced translational impairment and toxicity in neurons, while overexpression of poly-GR/PR interacting proteins associated with ribosome biogenesis had no effect.
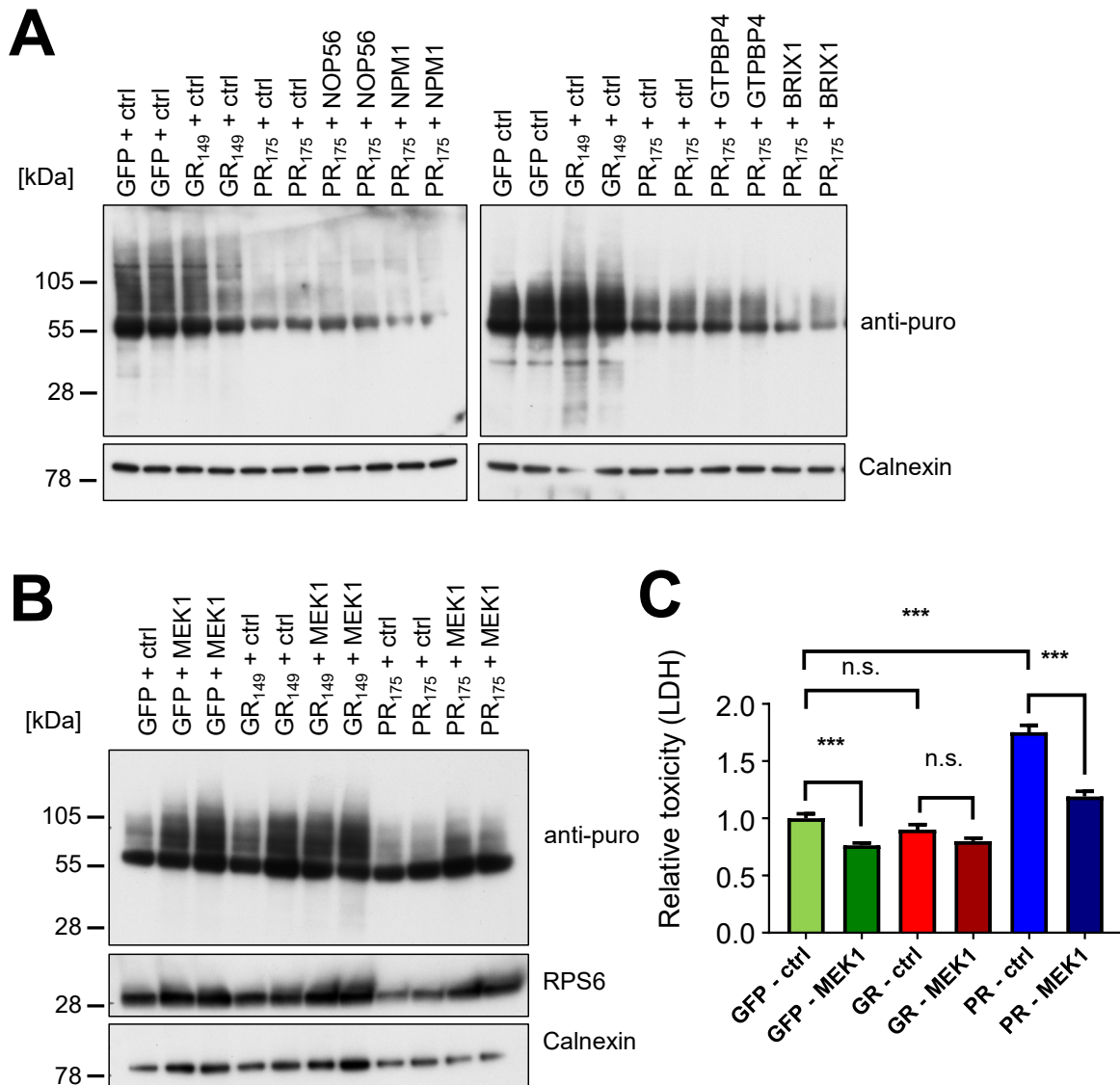

Figure 5-23: Reduction of ribosomal proteins can only be rescued by the constitutive active form of MEK1.

(A, B) Cortical rat neurons were co-transduced with GFP, GFP-(GR)$_{149}$ or (PR)$_{175}$-GFP lentiviral constructs and RFP tagged rescue constructs (DIV6+7). (A) Immunoblots of SUnSET assays in neurons expressing poly-GR/PR and ctrl or nucleolar RFP-NOP56/NPM1/GTPBP4/BRIX1 detecting newly synthesized proteins by puromycin incorporation. Calnexin was used as a control. (B) SUnSET assay in poly-GR/PR and ctrl/MEK1 transduced neurons. Purocmycin, RPS6 and Calnexin immunoblots are shown. Note elevated RPS6 and translation levels in MEK1 expressing neurons. (C) LDH release assay detects significant reduction in cell death upon expression of MEK1 in neurons (DIV7+14) transduced with (PR)$_{175}$-GFP compared to (PR)$_{175}$-GFP only control (n=2 independent experiments with 6 replicates each, mean ± SEM, *** denotes p<0.001 in one-way ANOVA with Dunnett's post-test).

5.4.5.7. *PR and GR proteins/peptides bind to the yeast ribosome*

To further elucidate the connection between the ribosome and poly-GR/poly-PR, I tested whether the two DPR species directly interact with ribosomes. In a first experiment, I coated 96-well plates with 500 ng of the purified 80S yeast ribosome and then added recombinant GR_{25}-GST, PR_{25}-GST or GST protein in a concentration series. Finally, I detected the interaction with an antibody specific for GST. A secondary antibody together with 3,3',5,5'-Tetramethylbenzidine (TMB) led to a reaction product that was read at 450 nm or 630 nm. At 100 ng, GR_{25}-GST bound the ribosome specifically compared to the GST control. The higher the amount of protein was, the more protein was binding (Figure 5-24**A**). I speculated this signal may be due to residual RNA co-purified with GST from *E. coli*. In order to obviate this, I repeated the ribosome binding assay with chemically synthesized DPR peptides harboring 20 repeats and an HA tag to exclude RNA contamination. Strikingly, the GR_{20}-HA peptide also significantly bound to the yeast ribosome in all three tested concentrations compared to the HA control peptide. At the highest concentration (10 µg) PR_{20}-HA binding did not reach significance, although there was a small trend towards elevated binding capacity (Figure 5-24**B**). This experiment suggests that poly-GR and possibly also poly-PR induce toxicity by effectively binding to the ribosome and thereby preventing it from performing its normal function.
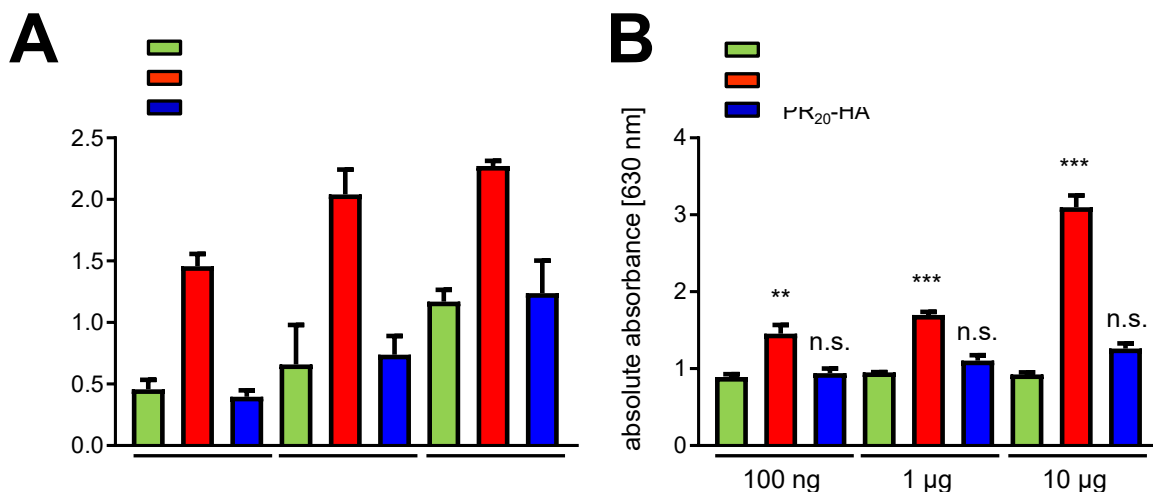

Figure 5-24: Purified poly-GR/PR bind to the yeast ribosome.

Increasing amounts of purified **(A)** GR_{25}-GST/PR_{25}-GST/GST or **(B)** GR_{20}-HA/PR_{20}-HA/HA protein were incubated with 500 ng purified 80S yeast ribosome in an immunoassay. Binding of proteins to the ribosome was detected by HRP-labeled secondary antibody which was bound by 3,3',5,5'-Tetramethylbenzidine (TMB) leading to a reaction product that was read at 450 nm or 630 nm. Bar graphs depict absolute absorbance signal. Note that especially poly-GR binds the yeast ribosome significantly compared to the GFP control. (n=4 replicates for GST assay and n=2 for HA assay, mean ± SEM, *** denotes p<0.001, ** denotes p<0.01, * denotes p<0.05 in one-way ANOVA with Dunnett's post-test).

5.4.6. **Most poly-GR and poly-PR interactors are not enriched in DPR inclusions in *C9orf72* patients**

After extensive testing of interesting interacting proteins identified in the poly-GR and poly-PR interactomes *in vitro*, it was particularly important to elucidate whether these poly-PR/GR interactors would also be altered in *C9orf72* patient brain.
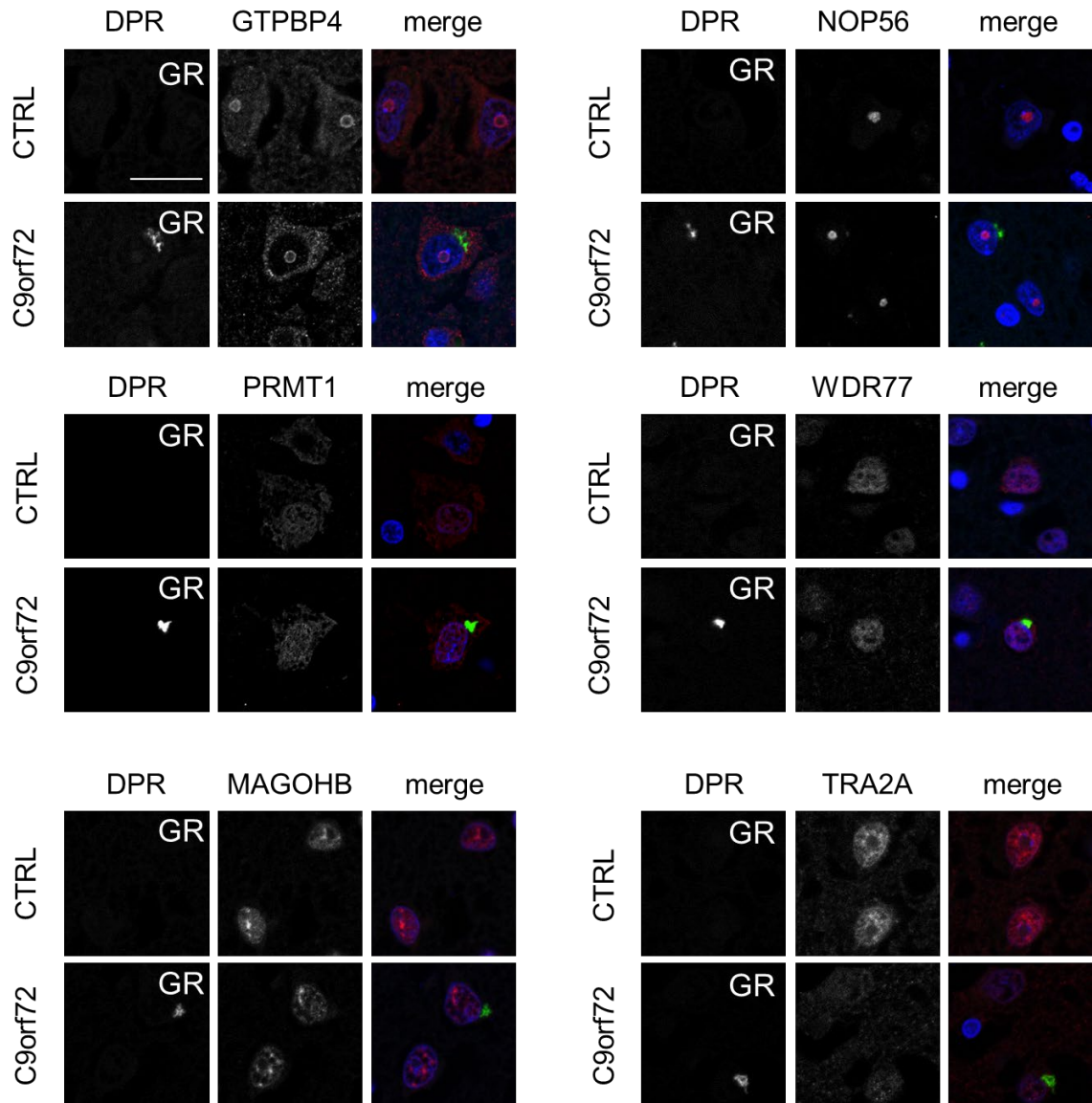
Figure 5-25: Several tested interactors do not colocalize with poly-GR in *C9Orf72* patient brain.

Immunofluorescence stainings of the frontal cortex of a *C9orf72* patient and a healthy control case to analyze colocalization of poly-GR with the interacting proteins GTPBP4, NOP56, PRMT1, WDR77, MAGOHB and TRA2A.

Therefore, I analyzed the distribution of several other poly-GR/PR interactors in *C9orf72* patients and controls by immunofluorescence. Apart from the experiments shown above, I tested antibodies for 22

additional proteins, among which 6 showed convincing staining of endogenous protein distribution. However, I could not detect co-aggregation of the nucleolar proteins GTPBP4 or NOP56, PRMT1 or WDR77, two proteins involved in methylation, or the splicing factors MAGOHB or TRA2A with poly-GR in the cortex of *C9orf72* patients (Figure 5-25**B** and 4.4.1).

Summing up, among the ~30 tested poly-GR/PR interacting proteins, STAU2 and subunits of the cytosolic ribosome are relevant co-aggregating proteins in *C9orf72* patients in this study.

5.5. Nucleolar poly-GR shows poly-PR characteristics in neurons

5.5.1.1.　　*Rerouting poly-GR into the nucleolus disrupts nucleolar architecture*

As described before, basic characterization of GFP-(GR)$_{149}$ and (PR)$_{175}$-GFP showed that both DPR species are impairing cell growth in HEK293 cells and that only (PR)$_{175}$-GFP is toxic in primary rat neurons (Figure 5-1**A** and **B**). In HEK293 cells, GFP-(GR)$_{149}$ and (PR)$_{175}$-GFP localize to the nucleolus, while in neurons only (PR)$_{175}$-GFP expression resulted in nucleolar localization (Figure 5-2**A** and **B**). Given these findings, I wondered whether the absence of GFP-(GR)$_{149}$ from the nucleolus in primary neurons, despite a significant overlap of interacting proteins with (PR)$_{175}$-GFP, might explain lack of toxicity. Therefore, my aim was to shift diffuse cytoplasmic localization of GFP-(GR)$_{149}$ into the nucleolus and investigate the outcome of this relocalization in neurons. Since other groups reported toxicity for shorter poly-GR repeat constructs, I truncated the GFP-(GR)$_{149}$ construct. A poly-GR version with 53 repeats showed diffuse cytoplasmic localization as well as strong localization to the nucleolus in 77.5% of GFP-(GR)$_{53}$ transduced neurons (Figure 5-26**A**). Additionally, I analyzed nucleolar organization itself using immunofluorescence stainings of fibrillarin. While in GFP-(GR)$_{149}$ and GFP expressing neurons most nucleoli showed homogeneous distribution of the nucleolar marker, interestingly, GFP-(GR)$_{53}$ expression resulted mostly in a ring-like fibrillarin staining and occasionally in a granular pattern. This disrupted nucleolar organization was even more pronounced in (PR)$_{175}$-GFP expressing neurons as described above (compare Figure 5-13**A** and Figure 5-26**A** and **B**). Moreover, acute toxicity was significantly induced upon GFP-(GR)$_{53}$ expression although not as strong as in neurons transduced with (PR)$_{175}$-GFP (Figure 5-26**C**).
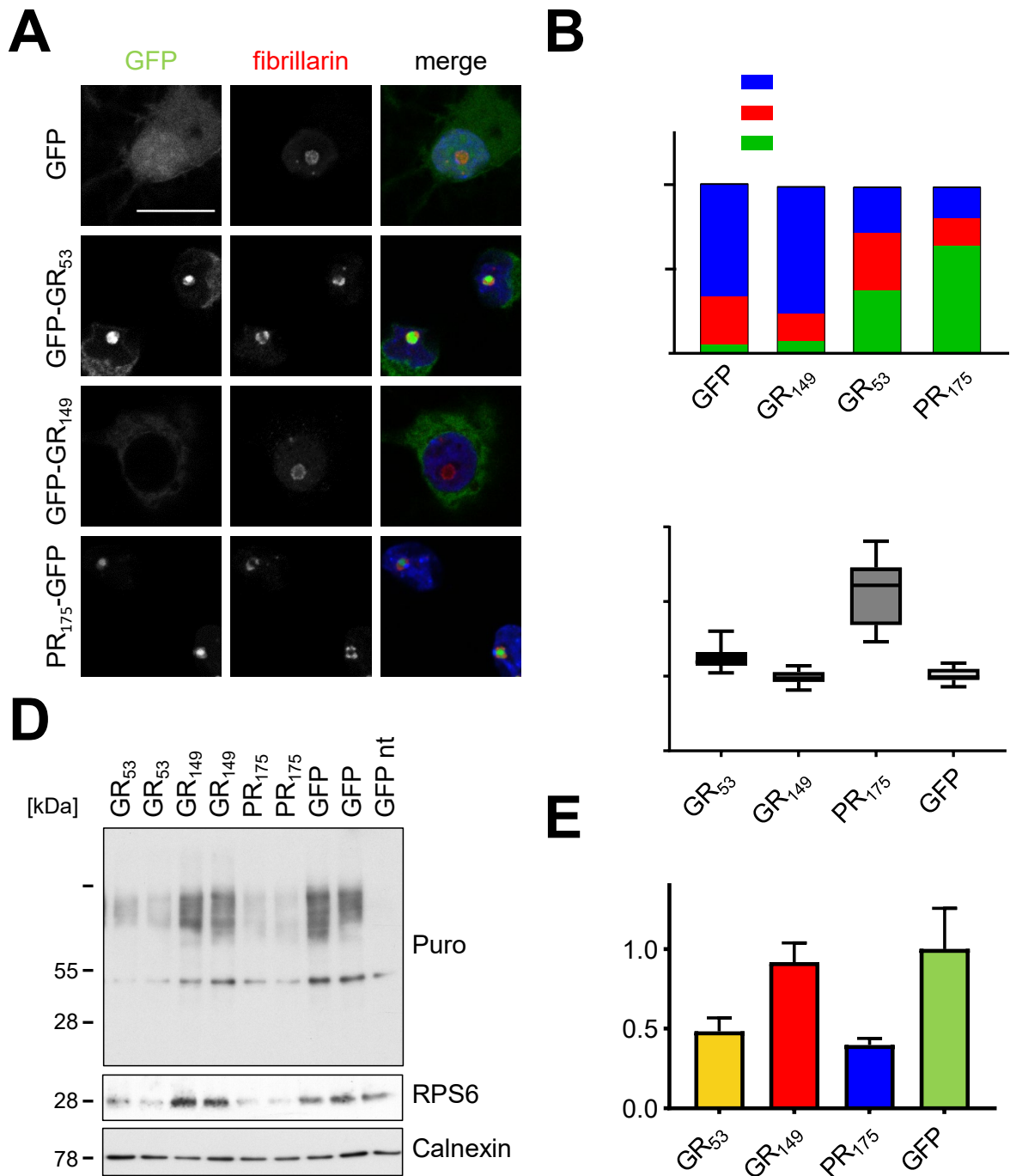
Figure 5-26: Nucleolar poly-GR$_{53}$ disrupts nucleolar structure and inhibits translation.

Primary rat neurons were transduced with GFP, GFP-(GR)$_{53}$, GFP-(GR)$_{149}$ or (PR)$_{175}$-GFP lentiviral constructs. **(A)** Confocal images show immunofluorescence staining of fibrillarin in hippocampal neurons. Left two columns visualize GFP signal and fibrillarin staining (red) in various DPR species as indicated. Right column shows merge depicting nuclei with DAPI staining in blue additionally. Scale bar denotes 20 µm. **(B)** Classification and quantification of fibrillarin distribution within the nucleolus from (A) n= 6 to 16 images were analyzed. **(C)** LDH release assay detects significant cell death upon lentiviral expression of (PR)$_{175}$-GFP and GFP-(GR)$_{53}$, but not GFP-(GR)$_{149}$ compared to GFP control in primary rat neurons (DIV7+14) (n=3 individual experiments with 6 replicates each, box plot is shown with 25th percentile, median and 75th percentile and whiskers representing minimum and maximum, *** denotes p<0.001 and ** denotes p<0.01 in one-way ANOVA with Dunnett's post-test). **(D)** Immunoblot showing SUnSET assay in GFP-(GR)$_{53}$, GFP-(GR)$_{149}$, (PR)$_{175}$-GFP or GFP-expressing primary cortical neurons (DIV6+7). Cortical neurons were exposed to 1 µM puromycin (puro) for 10 min or not treated (nt). Note the reduced synthesis of proteins indicated by puromycin signal in neurons expressing GFP-(GR)$_{53}$ and (PR)$_{175}$-GFP. **(E)** Quantification of puromycin signal normalized to Calnexin (n=6 from 3 independent experiments, mean ± SEM, *** denotes p<0.001 and ** denotes p<0.01 in one-way ANOVA with Dunnett's post-test).

5.5.1.2. *Nucleolar poly-GR impairs ribosome biogenesis*

The effects of nucleolar GFP-(GR)$_{53}$ on nucleolar structure and toxicity in primary neurons are comparable to the effects seen in (PR)$_{175}$-GFP neurons suggesting that other poly-PR specific deficiencies might also be found in poly-GR$_{53}$ expressing cells. To test this hypothesis, I conducted another SUnSET assay and analyzed expression levels of the small ribosomal subunit with an antibody specific to RPS6. Lentiviral expression of GFP-(GR)$_{53}$ indeed significantly reduced protein synthesis as well as RPS6 levels similar to (PR)$_{175}$-GFP, while GFP-(GR)$_{149}$ had no effect (Figure 5-26**D** and **E**).

Thus, nucleolar localization of poly-GR/PR may be required for the toxicity observed *in vitro*.

6. DISCUSSION AND OUTLOOK

In this study, I analyzed the interactomes of poly-GR and poly-PR in transduced rat cortical neurons and transfected HEK293 cells using GFP-(GR)$_{149}$ and (PR)$_{175}$-GFP immunoprecipitation. In both cell lines, poly-GR and poly-PR interact with RNA-binding proteins including numerous components of stress granules, the nucleolus, and the ribosome. Interestingly, overexpression of the interactors STAU1, STAU2, and YBX1 reroutes poly-GR and poly-PR into large stress granule-like structures. In addition, NPM1 overexpression leads to relocalization of poly-GR into the nucleolus. Strikingly, expression of poly-PR disrupts nucleolar organization, reduces levels of ribosomal subunits and impairs translation *in vitro*. The latter effects are dependent on nucleolar localization of poly-GR and poly-PR. Most importantly, ribosomal proteins are present in cytoplasmic DPR inclusions in *C9orf72*-ALS/FTD patient brains suggesting that sequestration of ribosomes may chronically affect protein synthesis even in absence of nucleolar localization.

Compared to several competing reports, my data most accurately reflects the patient situation for several reasons. First, the constructs I used in this work are significantly longer than in all other studies and thus, better replicate the situation in patients, which typically harbor hundreds of repeats. While I used poly-GR and poly-PR containing 149 and 175 repeats, respectively, previous groups report expression of only 80 repeats or less (Lee et al., 2016a; Lopez-Gonzalez et al., 2016). Second, as other studies also administered 20-mer or 30-mer poly-GR and poly-PR peptides at high concentrations, my experiments more precisely mirror the low abundance of poly-GR/PR expression in patients (Boeynaems et al., 2017; Kanekura et al., 2016; Lin et al., 2016; Yin et al., 2017). Third, GFP-(GR)$_{149}$ almost exclusively localized to the cytoplasm in neurons, as observed in patient brains, arguing that other groups with nucleolar poly-GR expression possibly study *in vitro* artifacts. The increased toxicity of truncated poly-GR constructs with nucleolar localization also in my hands strongly support this concern. Finally, I performed my experiments and validated the findings in primary cortical neurons, while most other groups studied poly-GR/poly-PR mainly in non-neuronal cell lines. Thus, the system I used in this work is the most physiologically accurate among all competing studies. On top of this, only I extended my validation efforts to patient brains, representing the most important validation step.

6.1. Poly-GR and poly-PR interactomes

The interactomes of GFP-(GR)$_{149}$ and (PR)$_{175}$-GFP identified numerous RNA-binding proteins enriched in splicing factors, stress granule, and nucleolar components as well as in the mitochondrial and cytoplasmic ribosome in neurons and HEK293 cells. These results are consistent with previous interactome studies which reveal similar poly-GR/PR associated cellular pathways and protein groups to be enriched independent of cell type (Boeynaems et al., 2017; Kanekura et al., 2016; Lee et al., 2016a; Lin et al., 2016; Lopez-Gonzalez et al., 2016). Thus, the poly-GR and poly-PR interactomes of my work, which were performed under physiological conditions, support previous interactome data and indicate that the cellular components and biological processes found might be indeed disease relevant.

Regarding the DPR proteins individually, enrichment analysis revealed that poly-GR expressing cells show a high selectivity for ribosomes, stress granules, and the methylosome. The poly-PR interactomes from HEK293 cells and neurons are most enriched in proteins connected to the U1 and U4 snRNP consistent with reported effects of poly-PR on splicing (Kwon et al., 2014). Nonetheless, poly-GR and poly-PR overall share a large set of interacting proteins. This interesting observation was made throughout all other interactome studies in which up to 40% of interactors were overlapping (Lee et al., 2016a). This may reflect the preferential binding of both poly-GR and poly-PR to LCD containing proteins.

In the following, especially the difference in poly-GR and poly-PR toxicity in my neuron model and possible toxic mechanism emerging from the interactomes and my validation experiments will be discussed.

6.1.1. Poly-GR and poly-PR toxicity depends on subcellular localization

In this study, (PR)$_{175}$-GFP localized to the nucleolus resulting in impairment of cell growth as well as toxicity in both HEK293 cells and neurons, respectively. Expression of nucleolar GFP-(GR)$_{175}$ led to less proliferation in HEK293 cells. In neurons, however, cytoplasmic GFP-(GR)$_{149}$ caused no cell death within 14 days. Thus, these data strongly indicate that mainly nucleolar localization is triggering the acute poly-GR/PR mediated toxicity observed in many *in vitro* systems. I designed several DPR protein constructs to enhance or reduce nucleolar localization of poly-GR/PR, but all variants either promoted nucleolar localization or had no effect. All DPR variants with enhanced nucleolar expression, like GFP-(GR)$_{53}$, GFP-(GA)$_{50}$-(GR)$_{50}$ and GFP-(GA)$_{50}$-(PR)$_{50}$, caused toxicity in an LDH assay. Strikingly, their expression additionally resulted in reduced RPS6 levels and impaired protein synthesis just as in (PR)$_{175}$-GFP transduced neurons (Figure 5-26 and data not shown) providing evidence that also toxic mechanisms are mediated by nucleolar localization alone.

Nearly every study analyzing individual DPR proteins reports poly-PR to be almost exclusively localized within the nucleolus independent of cell type or expression system, whereas poly-GR is typically found both in the nucleolus and the cytoplasm (Kramer et al., 2018; Kwon et al., 2014; Lee et al., 2016a; Tao et al., 2015; Wen et al., 2014; Yamakawa et al., 2015; Zhang et al., 2018b). However, *C9orf7*2-ALS/FTD *post mortem* brains do not display any evidence for nucleolar poly-PR or other DPR species. Most DPR inclusions are cytoplasmic and most nuclear DPR inclusions are para-nucleolar (Schludi et al., 2015a). Thus, I propose that acute poly-GR/PR toxicity seen in many model systems is mainly due to aberrant nucleolar localization. A reason for nucleolar localization in cellular models might be that unphysiologically high DPR amounts more likely lead to relocalization as the effect of poly-GR and poly-PR mimicking the nuclear localization signals (NLS) is more prominent. Therefore, the data deriving from *in vitro* experiments in which DPR proteins localize to the nucleolus likely exaggerate the patient situation or might even be artifacts. Nonetheless, it cannot be excluded that during the ALS/FTD time course, poly-GR and poly-PR temporarily localize to the nucleolus triggering some of the effects seen in cell culture models.

Regarding the interactome studies of this work, the overlap in poly-GR and poly-PR interactors in neurons is striking despite differential toxicity as measured by LDH release assays and evident from the whole proteome data (see below). A reason for this discrepancy might be that a small percentage of GFP-(GR)$_{175}$ transduced neurons additionally showed nucleolar localization - enough to detect interactors by mass spectrometry but too little to induce significant neuronal death. It would be interesting to compare the interactomes of purely nucleolar to purely cytoplasmic poly-GR, but we were not able to generate such constructs so far.

To understand the toxicity exclusive to poly-PR, I analyzed the proteins which selectively interact with poly-PR, e.g. CD2AP. However, the analysis did not lead to a clear mechanism of toxicity due to these interactors. My data is most consistent with nucleolar localization as the main driver of poly-PR mediated toxicity *in vitro.* Poly-PR expression results in dramatic down-regulation of numerous proteins in neurons. In fact, gene ontology analysis reveals that especially the expression of ribosomal subunits is significantly reduced. This finding suggests that poly-PR mediated reduction of ribosome numbers directly affects global protein translation leading to reduced expression of hundreds of proteins, including axonal and synaptic proteins, and finally cell death. Comparable calnexin levels and therefore total cell numbers between poly-PR and control expressing cells validate this. Poly-GR expressing neurons do not show alterations in global protein expression which is consistent with the observation that poly-GR expression does not lead to cellular toxicity in this system. In HEK293 cells, high-level expression of poly-GR and poly-PR through transient transfection inhibit cell growth to a similar extent. It would be interesting to see whether poly-PR has the ability to reduce global protein levels in this cell system although there is no active cell death detected. If so, nucleolar poly-GR

expression might result in comparable effects. Eventually, however, the strict distinction between poly-GR and poly-PR toxicity might not be relevant for *C9orf72* pathogenesis as poly-PR almost completely co-aggregates with poly-GR and the other DPR proteins in *C9orf72*-mediated ALS/FTD brains (Mori et al., 2013a).

6.1.2.　**No evidence for nucleocytoplasmic transport deficits in the interactomes of poly-GR/PR**

In recent studies, disruption of the nuclear pore complex and nucleocytoplasmic transport has emerged as a cellular mechanism underlying *C9orf72*-mediated toxicity. Not only have different genetic modifier screens identified numerous proteins linked to the nuclear pore to be enhancers or suppressors of *C9orf72*-associated toxicity, but also have interactome studies shown various NPC, import and export proteins to interact with poly-GR and -PR (Boeynaems et al., 2016; Freibaum et al., 2015; Jovicic et al., 2015; Lee et al., 2016a; Lin et al., 2016; Zhang et al., 2015). However, our mass spectrometry-based proteome studies in poly-GR/PR bearing cells could not detect components of the nuclear pore interacting with these two DPR protein species similar to other reports (Kanekura et al., 2016; Lopez-Gonzalez et al., 2016). Also, the transcriptome profile of poly-$(GR)_{100}$ expressing mice did not identify any NPC-associated transcript to be altered (Zhang et al., 2018a). Poly-GA expression, however, leads to a transport deficit particularly of TDP-43 leading to enhanced cytoplasmic localization. This effect was not significant in poly-GR and poly-PR expressing neurons (Khosravi et al., 2017). Thus, my data provide no evidence supporting dysfunctional nucleocytoplasmic transport due to poly-GR/PR and therefore I suggest that poly-PR/GR toxicity is mostly triggered by other mechanisms.

6.1.3.　**Poly-GR/PR and their link to nucleoli and stress granules**

My interactome study could convincingly show that a large set of nucleolar and stress granules components are binding partners of poly-GR and poly-PR which is consistent with other reports (Boeynaems et al., 2017; Lee et al., 2016a; Tao et al., 2015). Lee, Boeynaems, and colleagues support these physical interactions by reporting impaired NPM1, NCL and G3BP1 dynamics upon expression of poly-$(GR)_{50}$ and poly-$(PR)_{50}$ (Boeynaems et al., 2017; Lee et al., 2016a). In contrast, my validation efforts concentrated on the impact of interactors on poly-GR/PR expression, aggregation as well as localization and most importantly, their alterations in *C9orf72* patient brain.

Co-expression of nucleolar candidates and poly-GR/PR in primary neurons showed that NPM1 recruits otherwise predominantly cytosolic GFP-$(GR)_{149}$ into the nucleolus, whereas NOP56 had no such effect. Higher endogenous NPM1 levels in HEK293 cells compared to primary neurons may contribute to the differential localization of poly-GR in both cell types. The other way around, poly-PR strikingly altered the distribution of NOP56 and other nucleolar proteins. This observation was

confirmed in other reports in which NCL displayed disrupted distribution in patient-derived lymphoblasts as well as iPS motor neurons. Also in hippocampal neurons expressing poly-PR, the majority of nucleoli appeared fragmented (Haeusler et al., 2014; Schludi et al., 2015a). Disorganization of the nucleolus likely reflects functional impairment. And indeed, numerous proteins associated with the nucleolus were found to modulate poly-GR and poly-PR toxicity in a modifier screen in flies (Lee et al., 2016a). Since super-resolution microscopy revealed that poly-GR/PR localize to the outer subregions of the nucleolus where ribosome assembly takes place, specifically this step of ribosome biogenesis might be affected (Lee et al., 2016a). Also the interference of poly-GR/PR with NOP56 and NPM1, observed in this study, most likely leads to impaired biogenesis of ribosomes as the two nucleolar proteins play a role in assembly of the 60S subunit and chaperoning ribosomal subunits (Hayano et al., 2003; Maggi et al., 2008). Hence, my observations provide first evidence that poly-GR and poly-PR toxicity may ultimately emerge from impaired translation mediated by nucleolar dysfunction. To gain deeper insight into the role of the nucleolus in *C9orf72*-mediated ALS/FTD, detailed nucleolar organization would be worth investigating to find the connection between this compartment and translation inhibition. Importantly, in *C9orf72* patient *post mortem* brains, DPR protein inclusions do not localize to the nucleolus (Schludi et al., 2015a; Vatsavayai et al., 2016). However, larger nucleoli have been reported in poly-GR expressing neurons (Mizielinska et al., 2017) suggesting that the effects of poly-GR/PR on the nucleolus observed *in vitro* are of a more subtle nature in patients.

I showed that co-expression of the stress granule components STAU1, STAU2, and YBX1 leads to striking colocalization with poly-GR and poly-PR in large cytoplasmic granules. Since the two DPR proteins already form small cytoplasmic inclusions in control situations (Figure 5-14) in HEK293 cells, it is likely that expression of STAU1, STAU2, and YBX1 promotes expansion of these structures. I propose that these inclusions are stress granules since they are positive for G3BP1, YBX1 as well as STAU1 (Figure 5-15), all representing proteins found in this cellular compartment (Jain et al., 2016; Thomas et al., 2009). In line with my findings, several other groups made similar observations linking stress granules to poly-GR and poly-PR: In poly-$(PR)_{100}$ expressing HeLa cells, aggregated cytoplasmic poly-PR could be co-stained with the stress granule marker protein G3BP. Zhang *et al.* additionally show that both poly-GR and poly-PR significantly induce the formation of SGs compared to controls (Boeynaems et al., 2017; Zhang et al., 2018b). Also, poly-PR preferentially interacts with proteins localized to stress granules (Boeynaems et al., 2017; Lee et al., 2016a) and several SG associated proteins like YBX1 and Ataxin2 are altered upon poly-PR expression in cell culture (Boeynaems et al., 2017). Moreover, numerous proteins linked to stress granules were found to be enhancers or suppressors of poly-GR/PR_{50} toxicity in a *Drosophila in vivo* screen. Summarizing, my observations

together with other studies clearly suggest a significant role of stress granules in cellular and animal models.

There are many ways how co-expression of the DPR proteins with stress granule components might lead to enhanced stress granule formation. STAU1, for example, functions in dissolution of the latter by stabilization of polysomes (Thomas et al., 2009). It is possible that after recruitment to the stress granules, STAU1 is sequestered by poly-GR and poly-PR. The interaction with the two DPR species might prevent STAU1 from performing its normal function which ultimately leads to accumulation of STAU1 and expansion of the inclusions. However, it is not clear whether these stress granule proteins are recruited into the granule-like poly-GR/PR clusters or *vice versa*.

Overall, it is also possible that poly-GR and poly-PR disrupt stress granule protein function through liquid-liquid phase separation. Several groups could validate these relations by showing disturbed dynamics of nucleolar and stress granule components such as NPM1, NCL, and G3BP1. In addition, poly-GR and poly-PR changed phase transition of FUS, NPM1, TIA1, hnRNPA1 or intermediate filaments (Boeynaems et al., 2017; Lee et al., 2016a; Lin et al., 2016). Moreover, $(PR)_{30}$ increased β-sheet content in FUS droplets over time (Boeynaems et al., 2017). Consequently, poly-GR/PR may interfere with liquid-liquid phase separation by enhancing the formation of amyloid-like structures. Since poly-GR and poly-PR preferentially bind to intrinsically disordered proteins, disturbed phase transition might impair formation and function of membrane-less organelles as another toxic mechanism in *C9orf72*-ALS/FTD.

Interestingly, G3BP1 knockdown strongly enhanced poly-GR toxicity in an RNAi screen in flies (Lee et al., 2016a). Since G3BP1 is required for SG formation, this observation, in turn, indicates that the appearance of SGs upon poly-GR/PR expression might be protective. However, it is known that stress granules occur upon cellular stress and typically contain mRNA as well as 40S ribosomal subunits (Buchan and Parker, 2009) which are kept in an inactive state. Therefore, it is conceivable that DPR induced formation of SGs alone or the sequestration of key components of translation via DPR proteins lead to stalled protein synthesis. Thus, SG formation might still be harmful to the cell. This hypothesis is in line with a study from Zhang and colleagues showing colocalization of the small ribosomal subunit RPS6 and poly-GR_{100} in eIF3η-positive cytoplasmic inclusions (Zhang et al., 2018b). How arginine-rich DPR proteins are further connected to translational inhibition is discussed in the following chapter.

Although the data of my interactome study are consistent with other reports uncovering numerous stress granule constituents to bind to poly-GR and poly-PR (Lee et al., 2016a; Lin et al., 2016; Lopez-Gonzalez et al., 2016), I could not detect classical stress granule markers in poly-GR aggregates in *C9orf72* patient brains. Similarly, Zhang *et al.* observed cytoplasmic TIA-1 co-aggregation with poly-GR inclusions in *C9orf72* repeat expressing mice but failed to show such results in patients (Zhang et al., 2018b). Among the non-ribosomal interactors I tested, only STAU2 colocalized with poly-GR in the

frontal cortex of *C9orf72* patient brain, suggesting that STAU2 binding may be involved in poly-GR aggregation *in vivo*.

Taken together, the observations made in terms of both the nucleolus and stress granules upon poly-GR/PR expression raise the possibility that the two DPR proteins indirectly affect ribosomal biogenesis or function by interacting with proteins within the two compartments.

6.1.4.   Poly-PR toxicity is linked to impaired translation

Kwon and colleagues provided the first evidence that poly-GR and poly-PR interfere with ribosome biogenesis by showing that some of the 45S rRNA processing products were strongly reduced upon administration of 30 µM GR_{20} or PR_{20} peptide to U2OS cells. In particular, the 5.8S rRNA was decreased by 70% (Kwon et al., 2014). However, upon transduction of poly-GR or poly-PR in primary rat neurons, I could not observe such an effect. There might be two explanations why poly-GR/PR expressing neurons do not show impaired rRNA maturation. First, the conditions found in my cellular system are in contrast to the non-physiologically conditions in which poly-GR or poly-PR peptides are added in high molecular concentrations localize predominantly to the nucleolus- potentially leading to spurious effects. Second, in primary neurons transduced with poly-PR, two components of the PeBoW complex, BOP1 and PES1, are upregulated as shown by MS. These two proteins are known to be associated with rRNA splicing and the assembly of the large ribosomal subunit. In fact, it was shown that depletion of BOP1 or PES1 leads to inhibition of 36S pre-rRNA processing and therefore, the maturation of the downstream rRNA fragments (Rohrmoser et al., 2007). Thus, the upregulation of BOP1 and PES1 in neurons might boost rRNA processing preventing reduction of 5.8S rRNA as seen in U2OS cells in Kwon *et al.* Together, these data suggest that impairment of rRNA synthesis is not the main mechanism underlying poly-GR and poly-PR toxicity in neurons.

In this work, I show significantly decreased protein synthesis in a SUnSET assay in poly-PR transduced primary neurons. These findings are confirmed in *in vitro* translation assays monitoring incorporation of S^{35} as well as puromycin into newly synthesized proteins following expression of poly-PR and poly-GR in NSC-34 cells, astrocytes and HeLa cells (Kanekura et al., 2016; Lee et al., 2016a). As the poly-PR construct used in this study is highly toxic to neurons, in contrast to poly-GR, and its expression results in diminished protein translation, one can conclude that impaired protein synthesis is a major mechanism by which poly-PR drives toxicity. Kanekura and colleagues provide evidence that this effect is not caused by changed phosphorylation of the translation initiation factors, as cells treated with $(PR)_{20}$ did not show altered levels of phospho-eIF4B, phospho-eIF4E or phospho-eIF4G. Thus, distinct pathways need to be involved. Kanekura *et al.* further suggest that direct binding of $(PR)_{20}$ to mRNA might block access of translation factors (Kanekura et al., 2016). However, in my experiments, only nucleolar poly-$(GR)_{53}$ and poly-PR show strong reduction of protein synthesis

compared to the cytoplasmic poly-(GR)$_{149}$. Considering the cytoplasm being the compartment where mature mRNA is located, these observations argue against Kanekura *et al.*'s hypothesis.

Interestingly, I found that the cytosolic ribosome is the top hit in gene enrichment analysis of the interactomes, which is also true for all other interactome studies elucidating the binding partners of poly-GR and poly-PR (Tao et al. 2015; Lopez-Gonzalez et al. 2016; Kanekura et al. 2016; Lee et al. 2016; Boeynaems et al. 2017). Subsequently, I confirmed direct interaction between the ribosome and the two DPR species by a ribosome binding assay with purified (PR)$_{15}$/(GR)$_{15}$ and yeast ribosomes. Binding was also observed with synthetic peptides encoding poly-GR/PR, confirming that the interaction of DPR proteins with the ribosome is independent of poly-GR/PR bound RNA. However, I cannot exclude that the peptides bound yeast rRNA. Most importantly, I found that small and large subunits of the ribosome colocalize with 30% of poly-GR/PR in the cortex of *C9orf72*-FTD/ALS patient brains. This finding provides strong support for the *in vivo* relevance of poly-GR/PR impaired translation. It suggests that cytoplasmic poly-GR and poly-PR chronically impair protein synthesis even in absence of nucleolar localization. At the same time, Zhang and colleagues independently reported colocalization of cytoplasmic poly-GR to RPS6, RPL21 and the translation initiation factor eIF3η in transgenic mouse cortex and *C9orf72*-ALS/FTD brain (Zhang et al. 2018). Thus, in *C9orf72*-ALS/FTD, poly-GR/PR may lead to milder translational inhibition and slower neurodegeneration than in the acute cellular models.

I can only speculate whether poly-GR/PR mediated toxicity emerges from impaired ribosome biogenesis or the loss of active ribosomes which might even differ *in vitro* and *in vivo*. On the one hand, my study provides strong evidence for the inhibition of ribosome biogenesis: ribosomal protein levels are reduced, ribosome biogenesis factors are interactors of poly-GR/PR and the structure as well as dynamics of the ribosome assembly associated nucleolus is disturbed. On the other hand, the neuronal interactome of poly-GR indicates that the entire ribosome is assembled, suggesting that the existing ribosomes may not be functional. It has previously been shown that comprised function of amino acyl tRNA synthetases (ARS) leads to repression of protein synthesis and neurodegeneration (Latour et al., 2010; Lee et al., 2006; Storkebaum, 2016). Thus, it is also possible, that poly-GR and poly-PR dysfunctionalize the ribosome by affecting these amino acid transferases. For the future, it would be rewarding investigate direct interaction of poly-GR/PR with ribosomes using electron microscopy experiments in order to clarify these hypotheses. Identifying the exact binding site of the DPR proteins on the ribosome would shed light on the interference. It is possible that poly-GR/PR are blocking the sites important for the assembly of the ribosome with the mRNA or that the two DPR species are binding to the E, P or A site which are for example needed for ARS docking and subsequent maturation of the polypeptide chain. In this scenario, poly-GR/PR would impair ribosome activity. However, the two DPR protein species might only bind the ribosomal subunits at multiple sites and thus, hinder

ribosome assembly. Regardless, both scenarios would lead to the same outcome, namely less translation.

Analysis of the whole proteome of poly-PR cell lysates suggests that neurons try to compensate for this translational repression through upregulation of ribosome biogenesis factors such as NSA2, RRP1, BRIX1, NOC2L, WDR77, TSR and as mentioned earlier also BOP1 and PES1. This effect could be validated in immunoblotting experiments for BOP1, but not PES1. Quantitative PCR experiments only showed non-significant trends. The reason for this might be that this method is not sensitive enough and that subtle effects can only be seen by mass spectrometry which allows detection of analytes at concentrations in the attomolar range (Annesley et al., 2009).

Although neurons transduced with poly-PR appeared to counteract translational repression, poly-PR still reduced net ribosomal protein expression and caused pronounced cellular toxicity. Therefore, I hypothesized that the overexpression of poly-GR/PR interactors involved in ribosome biogenesis, which might be sequestered by the DPR proteins and thereby prevented from performing their regular function, should boost protein synthesis and reduce poly-PR mediated toxicity. However, expression of neither of the nucleolar proteins NOP56, NPM1, GTBP4, and BRIX1 could obviate neuronal death. NOP56 is participating in rRNA methylation, NPM1 is a ribosomal chaperone facilitating interactions between ribosomal proteins and rRNA and GTPBP4 as well as BRIX1 are involved in the biogenesis of the 60S subunit. Despite covering several pathways of ribosome biogenesis, none of the proteins alone was sufficient to restore reduced translation. Possibly, the combination of more ribosome biogenesis factors would be more effective. In a previous study in yeast, overexpression of the ribosome biogenesis factors NOB1 (human ortholog: NOB1) and STM1 (no human ortholog) suppressed poly-PR toxicity (Jovicic et al., 2015).

Thus, I overexpressed constitutively active MEK1 as an upstream regulator of translation. It is one of the main components of the MAPK/ERK pathway. It is activated by RAF and further phosphorylates its many downstream targets, thereby promoting cell growth and proliferation (McCubrey et al., 2007). By indirect phosphorylation of eIF4E and RPS6, MEK1 triggers translation initiation. Therefore, overexpression of the constitutive active form of MEK1 represents a more general approach to enhance protein synthesis. Indeed, MEK1 not only rescued translational repression but also prevented cellular toxicity in poly-PR expressing neurons. Furthermore, RPS6 protein expression was elevated upon MEK1 transduction. These findings suggest that inhibition of protein synthesis is connected to RPS6 levels as well as neuronal death, and that restoration of translation be neuroprotective.

However, MEK1 is a protein known to have carcinogenic properties as it can drive ERK1/ERK2 activation and lead to inappropriate cell proliferation and survival, precluding its therapeutic utility in patients. Alternatively, it might be advantageous to block the interaction of poly-GR and poly-PR with

the ribosome directly. Again, the exact binding site determined by electron microscopy might help for further elucidation of therapeutic strategies.

Overall, this study proposes direct binding of poly-GR and poly-PR proteins to the ribosome, disturbed nucleolar organization and accompanied ribosomal biogenesis as the most relevant toxic mechanisms of the two examined DPR protein species. Although the processes occurring *in vitro* represent a very acute situation, my co-aggregation data in *C9orf72*-FTD/ALS patients suggests a similar mechanism may contribute to human pathogenesis. As DPR proteins are present long before symptom onset and brain atrophy, these processes might trigger toxicity less obtrusively. It is unquestionable that the ribosome is physiologically significant as patients show colocalization of all tested ribosomal subunits with 30% of poly-GR aggregates. The next important step will be to directly show translation repression in patient tissue due to poly-GR/PR.

6.2. The role of poly-GR and poly-PR toxicity in disease

6.2.1. Translation centered model of poly-GR and poly-PR mediated neurodegeneration

The discovery of five DPR proteins species translated from the *C9orf72* repeat expansion had major impact on ALS and FTD research. Extensive studies investigated the mechanisms by which the two DPR proteins poly-GR and poly-PR trigger neurodegeneration. The present study convincingly shows that the nucleolus, stress granules, and protein synthesis are the main targets of poly-GR/PR. These results emerged from proteomic analysis as well as validation experiments *in vitro* and, in contrast to most other groups, *post mortem* brains. From my data, I propose the following model for poly-GR/PR related ALS/FTD pathomechanisms (Figure 6-1).

Poly-GR and poly-PR toxicity could inhibit protein translation by interfering with three parallel cellular pathways. RAN translation of the *C9orf72* repeat leads to formation of cytoplasmic poly-GR and poly-PR inclusions. These protein aggregates are causing cellular stress, thereby triggering the assembly of stress granules. Colocalization of poly-GR/PR with the membrane-less compartments impairs stress granule dynamics and disassembly. SGs are made from RNA and RNA-binding proteins and keep the messenger ribonucleoproteins in stalled translation pre-initiation complexes in order to protect them from harmful conditions. Consequently, the accumulation of SGs reduces overall protein synthesis. (Figure 6-1**A**). A parallel toxic mechanism is initiated by poly-GR/PR mediated sequestration of ribosomal subunits. I hypothesize that direct binding of the two DPR protein species to ribosomal proteins leads to a lack of ribosome components at the site where ribosome assembly takes place, namely the nucleolus. Additionally, poly-GR/PR might also bind whole ribosomes. As a result, fewer ribosomes are available finally causing impaired ribosomal assembly and subsequently, less translation. The sequestration of key factors associated with ribosome biogenesis might support this

mechanism of toxicity (Figure 6-1**B**). Furthermore, the interference of poly-GR and poly-PR with the nucleolus might pose a more direct link to reduced protein synthesis. In this situation, disorganization of the nucleolus, possibly emerging from binding to nucleolar proteins, would lead to nucleolar dysfunction (Figure 6-1**C**). As ribosome assembly occurs within the outer layers of the nucleolus, again, ribosome biogenesis is likely to be altered. Ultimately, all three pathways impair translation.
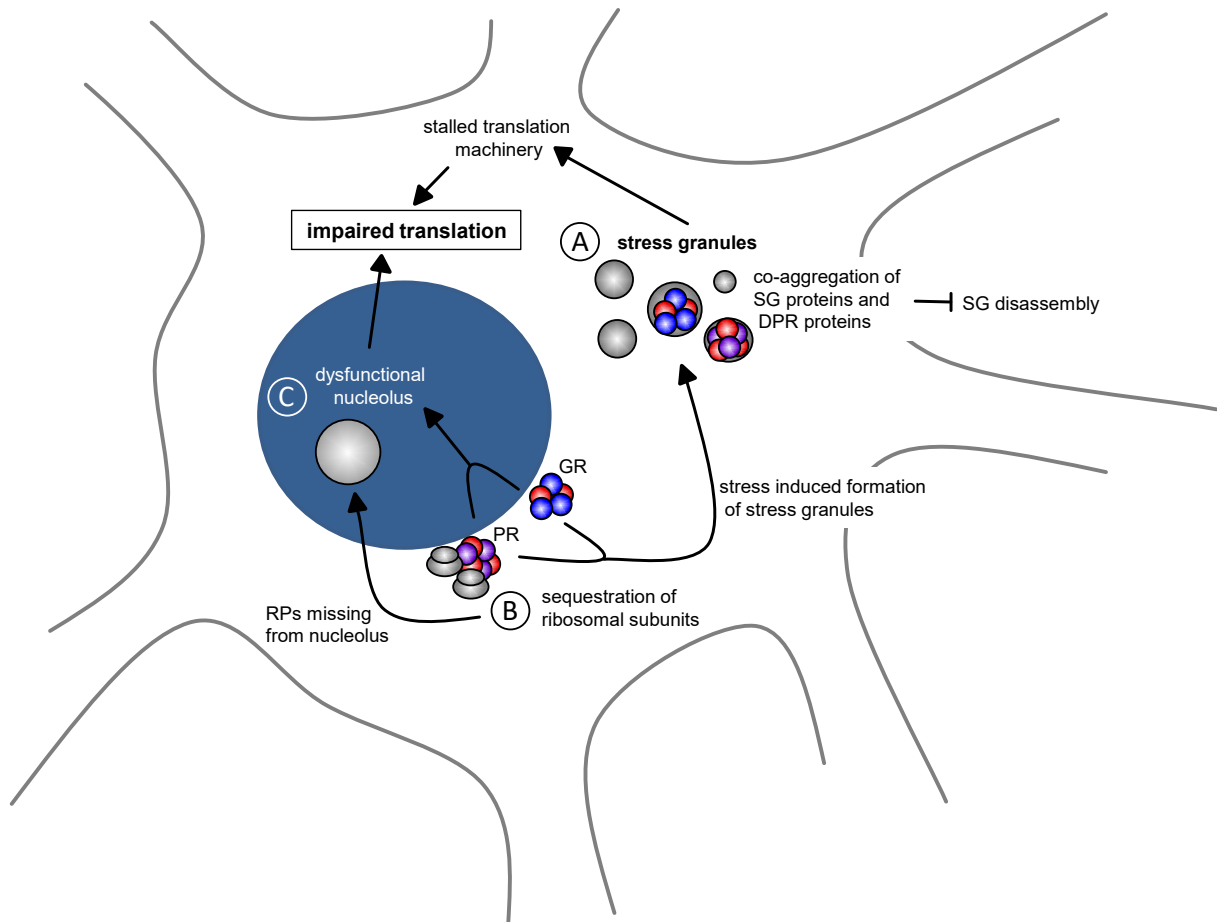

Figure 6-1: Schematic model of poly-GR/PR induced toxicity in *C9orf72*-ALS/FTD

The two arginine-rich DPR protein species poly-GR and poly-PR (glycine depicted in blue, proline in violet and arginine in red) are found in the cytoplasm of *C9orf72*-patient neurons and initiate three potential toxic pathways: (**A**) Stress-induced assembly of stress granules might lead to co-aggregation of poly-GR/PR and stress granule proteins. (**B**) Sequestration of ribosomal subunits (depicted as two grey ovals) in the cytoplasm potentially results in a lack of ribosomes in the nucleolus. (**C**) Poly-GR/PR bind nucleolar components leading to dysfunction of the nucleolus (grey circle in blue background (nucleus)). Ultimately, all three mechanisms comprise translation.

6.2.2.   **Concluding remarks and future directions**

This work importantly contributes to the understanding of pathological mechanisms underlying *C9orf72*-associated ALS/FTD. My data is consistent with parallel reports by other groups showing the association of poly-GR/PR with stress granules, the nucleolus and, most importantly, inhibition of

protein translation. It is the first study successfully validating poly-GR/PR interacting proteins in patient tissue and highlights the importance of the ribosome in disease pathogenesis. Furthermore, this work represents the first interactome study performed in neurons and thereby reflects the patient situation most accurately.

Since neither individual poly-GR expression nor C9orf72 knockout in mice is sufficient to mimic all features of ALS/FTD, synergistic effects of the *C9orf72*-associated pathomechanisms are most likely. For example, the other DPR proteins may contribute to toxicity. Notably, poly-GA and poly-GP are the most abundant DPR species in ALS/FTD brains harboring the *C9orf72* repeat and although poly-PR was shown to be the most toxic one *in vitro*, it is extremely rare (Schludi et al., 2015a). An explanation for this disconnect might be that rapid poly-PR-induced neurodegeneration may preclude its detection. However, RAN-translation of the anti-sense strand seems to be less efficient than from the sense strand as the inert poly-PA is also low abundance (Mori et al., 2013a; Mori et al., 2013c). Analysis of a poly-PR mouse model could be rewarding. In contrast, poly-GA toxicity, comprising nucleocytoplasmic transport (Khosravi et al., 2017) and proteasome function (Guo et al., 2018; May et al., 2014), seems to be slower. Furthermore, the repeat RNA itself is known to bind to several RNA-binding proteins, but a clear loss-of-function of any of these proteins has not been reported. Moreover, C9orf72 haploinsufficiency, particularly in immune cells, might play a crucial role.

As besides DPR protein pathology, *post mortem C9orf72* ALS/FTD patient brains harbor characteristic cytoplasmic TDP-43 inclusions, additional pathomechanisms leading to neurodegeneration exist. Strikingly, the regional distribution of TDP-43 inclusions strongly correlates with neurodegeneration and the clinical phenotype (ALS vs. FTD). In contrast, DPR protein inclusions are also present in several non-degenerating brain regions (Mackenzie et al., 2013). This disconnect between DPR protein pathology (as well as RNA foci and reduced C9orf72 expression) and TDP-43 pathology is the main open question in *C9orf72*-ALS/FTD research. Previous findings suggest that DPR proteins precede TDP-43 inclusions in cellular models as well as patient brains: Occasionally, poly-GA is surrounded by phosphorylated TDP-43 and C9orf72 patients who died of other conditions before reaching end stage of ALS/FTD show abundant DPR pathology while TDP-43 aggregates are rare (Mackenzie et al., 2013; Nonaka et al., 2018; Vatsavayai et al., 2016). And the finding that poly-GA partially reroutes nuclear TDP-43 into cytoplasmic granules in primary neurons and HeLa cells additionally supports a causal role of DPR proteins in TDP-43 pathology (Khosravi et al., 2017). In the end, neuronal death in *C9orf72* mediated ALS/FTD likely results from the interplay of the two types of pathological inclusions and various toxic mechanisms. Thus, the relative contribution of the DPR proteins, particularly of poly-GR and poly-PR, and the synergistic effects remain to be defined. Ultimately, only a drug targeting specific DPR protein species, other pathological inclusions, RNA-

toxicity or C9orf72 haploinsufficiency in patients can tell which pathway is most critical for *C9orf72*-ALS/FTD pathogenesis.

Taken together, my work provides strong evidence that poly-GR and poly-PR contribute to disease pathogenesis by direct binding of the ribosome in *C9orf72*-ALS/FTD patients probably leading to chronic toxicity, which may ultimately trigger a second disease stage with TDP-43 pathology (Edbauer and Haass, 2016). In cellular models, nucleolar poly-GR/PR reduce expression of ribosomal proteins as well as overall protein synthesis. Boosting translation and expression of ribosomal proteins using MEK1 overexpression rescued cellular toxicity *in vitro*. Hence, restoring chronically impaired translation, ribosome biogenesis or related pathways could serve as a novel therapeutic strategy in patients. Since overactivation of the MEK1/MAPK pathways would likely promote cancer, inhibiting the interaction of poly-GR and poly-PR with ribosomes might be a less harmful therapeutic strategy. As mentioned earlier, electron microscopy of ribosomes could help discover specific poly-GR binding sites, thereby unraveling the mode of action leading to rational drug design.

7. APPENDIX

7.1. Supplementary Tables

Table S1: Proteins enriched in the neuronal interactome, T-test difference poly-GR vs GFP

Welch's T-test s0=1, fdr=5%	PR-enriched?	protein ID	protein name
Difference LFQ intensity pGR_LFQ intensity GFP			
11.21805954	PR-enriched	O35796	C1qbp
10.14376736	PR-enriched	Q4QR85;Q7TPI7	Wdr77
9.776339531		D4A0E8	Prmt5
7.359214306		A0A0G2JUV5;M0RBW5	Ccdc40
6.141866207		F1LRU1;Q9JIL3-2	Ilf3
5.795619965		P13383;Q5U328	Ncl
5.287992477	PR-enriched	F1M403	Ube2o
5.082045078	PR-enriched	B5DF95;A0A0G2K782	Zc2hc1a
4.955165863	PR-enriched	A0A0G2K9I8	Prmt1
4.936328411	PR-enriched	G3V7R1;O08587	Nup50
4.934625626	PR-enriched	Q4V898	Rbmx
4.810759544	PR-enriched	D3ZXH7	Alyref
4.55553627	PR-enriched	P15865	Hist1h1e
4.25990057	PR-enriched	P62961;F1LPL7	Ybx1
4.255776405	PR-enriched	P21707;P29101	Syt1
4.249275684	PR-enriched	D3ZBN0	Hist1h1b
4.193473339		P84586;A0A0G2K8K9	Rbmxrtl
4.117208958		D3ZXF9	Mrpl12
3.950805664	PR-enriched	P43278	H1f0
3.944224834	PR-enriched	P55770;H7C5X3	Nhp2l1
3.841823101		F1LNK0;P15146	Map2
3.822192192		A0A0G2JY73;D4A554	Eif4g3
3.754371643		P61314;D3ZXA2	Rpl15
3.735926628	PR-enriched	Q6AY68	Aurkaip1
3.627151489		P19944;A0A0G2K4Q1	Rplp1
3.609757423	PR-enriched	Q63827;F1LM54	Fgfr1
3.590438366		A0A0G2K1R5;F1LR80	Camkv
3.587795258	PR-enriched	D3ZVA5	Fbll1
3.582002163		D3ZIF0	Zfp512
3.532605171		P02401;D4A4D5	Rplp2

Table S2: Proteins enriched in the neuronal interactome, T-test difference poly-PR vs GFP

Welch's T-test s0=1, fdr=5%	GR-enriched?	protein ID	protein name
Difference LFQ intensity pPR_LFQ intensity GFP			
8.999781132	GR-enriched	A0A0G2JUV5;M0RBW5	Ccdc40
8.753255844	GR-enriched	O35796	C1qbp
5.80452919		Q925Q9;Q925Q9-2	Sh3kbp1
5.536819935	GR-enriched	P15865	Hist1h1e
5.257129669	GR-enriched	D3ZXF9	Mrpl12
5.249002934	GR-enriched	P19139	Csnk2a1
5.138173103	GR-enriched	F1LRJ2;A0A0G2K2M9	Srrm2
4.720638752	GR-enriched	D3ZBN0	Hist1h1b
4.530203819	GR-enriched	P43278	H1f0
4.521471024		P04218	Cd200
4.518064976		Q27W01	Rbm8a
4.401230335	GR-enriched	P55770;H7C5X3	Nhp2l1
4.318847179		Q5M7V8;F1M3X4	Thrap3
4.27340889	GR-enriched	P62961;F1LPL7	Ybx1
4.254295826		M0R907;M0R8M3	Snrpd3
4.130423546	GR-enriched	Q68SB1-2;Q68SB1	Stau2
4.084741592	GR-enriched	D4A3K5	Hist1h1a
4.065413952	GR-enriched	P13383;Q5U328	Ncl
4.05639267	GR-enriched	Q4V898	Rbmx
3.973850727		D3ZTW8	Mrpl27
3.90845108		Q5BJX1;D3ZH23	Mrpl41
3.899531841		B5DES0;M0R8K2	Snrpd2
3.853073597		P63170;A0A0G2JU43	Dynll1
3.726355076		D3ZFQ8	Cyc1
3.698761463	GR-enriched	P84586;A0A0G2K8K9	Rbmxrtl;Rbmxl1
3.552656651	GR-enriched	D3ZJY1	Mrpl28
3.538584709	GR-enriched	M0R7B4	LOC684828
3.514945984	GR-enriched	A0A0G2K654;P06349	
3.481257439		D3ZGM1;A0A0G2JU15	Ptcd3
3.480280876		Q3B8Q2	Eif4a3

Table S2: Proteins enriched in the neuronal interactome, T-test difference poly-PR vs GFP

Table S3: Proteins enriched in the HEK293 cell interactome, T-test difference poly-GR vs GFP

Welch's T-test s0=1, fdr=5%	PR-enriched?	protein ID	protein name
Difference LFQ intensity pGR_LFQ intensity GFP			
9.33267212		O14744;O14744-2	PRMT5
8.64189434	PR-enriched	Q9HCE1;Q5JR04	MOV10
7.17884731		Q9BQA1;H0Y711	WDR77
7.06018829	PR-enriched	Q5T653;C9IY40	MRPL2
6.6750226	PR-enriched	Q07021	C1QBP
6.49605656	PR-enriched	Q96A35;X6RJ73	MRPL24
6.41339779	PR-enriched	P09001;H0Y9G6	MRPL3
6.40069199	PR-enriched	Q9H9J2	MRPL44
6.36713791	PR-enriched	Q8IXM3	MRPL41
6.28270912	PR-enriched	Q9P015;E5RIZ4	MRPL15
6.27818775	PR-enriched	Q9BYD2;Q5SZR1	MRPL9
6.26837015	PR-enriched	Q9BYD3;K7ES61	MRPL4
6.13568354	PR-enriched	Q9NRX2;E9PKV2	MRPL17
5.85481071	PR-enriched	Q8N5N7;Q8N5N7-2	MRPL50
5.8260293	PR-enriched	Q9BZE1;S4R369	MRPL37
5.76797581	PR-enriched	Q9NYK5;Q9NYK5-2	MRPL39
5.74533319	PR-enriched	Q13405;H0YDP7	MRPL49
5.69108677		Q7L2E3-2;Q7L2E3	DHX30
5.67733049	PR-enriched	Q96DV4;Q96DV4-2	MRPL38
5.66948223	PR-enriched	Q9BYD6;H0Y8N7	MRPL1
5.61673355	PR-enriched	Q8N983-4;Q8N983	MRPL43
5.57176733	PR-enriched	O95793;O95793-2	STAU1
5.52799082	PR-enriched	Q9Y2S7;B4DEM9	POLDIP2
5.51922655	PR-enriched	Q9NP92;A0A087WV52	MRPS30
5.42335987	PR-enriched	Q16540;A6NJD9	MRPL23
5.2685895	PR-enriched	Q8TAE8	GADD45GIP1
5.20731497	PR-enriched	Q96GQ7;B7Z6D5	DDX27
5.19266939		O15234;J3KSY7	CASC3
5.16271877	PR-enriched	Q13084;A2IDC6	MRPL28
5.14378309		Q14690;S4R3Q4	PDCD11

Table S4: Proteins enriched in the HEK293 cell interactome, T-test difference poly-PR vs GFP

Welch's T-test s0=1, fdr=5%	GR-enriched?	protein ID	protein name
Difference LFQ intensity pPR_LFQ intensity GFP			
5.06309128	GR-enriched	Q5T653;C9IY40	MRPL2
4.91249514	GR-enriched	Q07021	C1QBP
4.88959026	GR-enriched	P09001;H0Y9G6	MRPL3
4.80967426	GR-enriched	Q9H9J2	MRPL44
4.66591167	GR-enriched	Q9BYD3;K7ES61	MRPL4
4.63696957	GR-enriched	Q96A35;X6RJ73	MRPL24
4.50121355	GR-enriched	Q8IXM3	MRPL41
4.29837513		Q9Y5K6	CD2AP
4.23110867	GR-enriched	Q9BYD2;Q5SZR1	MRPL9
4.0637455	GR-enriched	Q13405;H0YDP7	MRPL49
3.97548103	GR-enriched	Q9BYD6;H0Y8N7	MRPL1
3.65711308	GR-enriched	Q9NYK5;Q9NYK5-2	MRPL39
3.64774752	GR-enriched	Q16540;A6NJD9	MRPL23
3.41399431	GR-enriched	Q9P015;E5RIZ4	MRPL15
3.25861359	GR-enriched	Q9NRX2;E9PKV2	MRPL17
3.19250822	GR-enriched	Q9H0U6	MRPL18
3.18459654	GR-enriched	Q8N983-4;Q8N983	MRPL43
3.18127441	GR-enriched	Q9BRJ2;A0A087X2D5	MRPL45
3.16544533	GR-enriched	Q96DV4;Q96DV4-2	MRPL38
3.04626703	GR-enriched	Q8TAE8	GADD45GIP1
3.01187754	GR-enriched	Q9BYD1;E5RJI7	MRPL13
3.01071358	GR-enriched	Q9NWU5;E7ESL0	MRPL22
2.97999954	GR-enriched	Q9BZE1;S4R369	MRPL37
2.95969963	GR-enriched	P68431	HIST1H3A
2.91059303	GR-enriched	Q13084;A2IDC6	MRPL28
2.8484726	GR-enriched	Q9P0M9;D6RAN8	MRPL27
2.80497026	GR-enriched	Q9NP92;A0A087WV52	MRPS30
2.65388632	GR-enriched	Q8N5N7;Q8N5N7-2	MRPL50
2.62585402	GR-enriched	Q14197;J3KS15	ICT1
2.62239504	GR-enriched	Q9HD33;Q9HD33-2	MRPL47

7.2. Table of Abbreviations

abbreviation	explanation
°C	degree Celsius
µg	micro gram
µL	micro liter
µM	micro molar
A	adenine
AA	amino acid
ALS	Amyotrophic Lateral Sclerosis
ARS	amino acyl tRNA synthetase
ASO	antisense oligo nucleotide
ATP	adenosine tri-phosphate
BAC	bacterial artificial chromosome
BOP1	block of proliferation 1
bp	base pairs
bp	base pairs
BSA	bovine serum albumin
bvFTD	Behavioral FTD
C	cytosine
c	concentration
C1QBP	Complement 1q binding protein
C9orf72	Chromosome 9 open reading frame 72
Cas	CRISPR associated
CCDC40	Coiled-coil domain containing 40
CD2AP	CD2 associated protein
cDNA	complementary deoxyribonucleic acid
ChIP	chromatin immunoprecipitation
CHMP2b	Charged multivesicular body protein 2b
CIP	calf intestine phosphatase
CLP1	Cleavage And Polyadenylation Factor 1
cm	centi meter
CMT	Charcot Marie Tooth (disease)
CNS	central nervous system
COX16	cyclooxygenase 16
CRISPR	clustered regulatory intersperse short palindromic repeats
CSF	cerebrospinal fluid
DAPI	4',6-Diamidin-2-phenylindol
DBA	Diamond Backfan Anemia
dd	double destilled
DENN	Differentially expressed in normal and neoplastic cells
DFC	dense fibrillar compartment
DIV	days in vitro
DNA	deoxyribonucleic acid

dNTP	deoxyribonucleotides
DPR	Dipeptide repeat
DTT	dithiothreitol
EAAT2	excitatory amino acid transporter 2
EDTA	Ethylenediaminetetraacetic acid
eIF	eukaryotic initiation factor
ELISA	enzyme-linked immunosorbent assay
ER	Endoplasmic Reticulum
ERK	extracellular signal-regulated kinase
FC	fibrillar core
FCCP	Mesoxalonitrile 4-trifluoromethoxyphenylhydrazone
FCS	fetal calf serum
fig.	Figure
FMRP	fragile X mental retardation protein
FTD	Frontotemporal Dementia
FUS	Fused in sarcoma
G	guanine
G3BP	Ras GTPase-activating protein-binding protein 1
GA	glycine-alanine
GADD45A	DNA damage inducible 45A
GAPDH	glycerinaldehyd-3-phosphat-dehydrogenase
GC	granular compartment
GDP	Guanosine di-phosphate
GEF	Guanosine exchange factor
GFP	green fluorescent protein
GO	gene ontology
GP	glycine-proline
GR	glycine-arginine
GRN	progranulin
GTP	Guanosine tri-phosphate
GTPBP4	GTP binding protein 4
h	hour
HA	hemaglutinin tag
HEK	human embryonic kidney
hnRNP	heterogeneous nuclear ribonucleoprotein
HRP	horseradish peroxidase
IF	immunofluorescence
IgG	immunoglobulin G
iPSC	induced pluripotent stem cell
IP	immunoprecipitation
kb	kilo base pairs
kDa	kilo Dalton

KEOPS-EKC	Endopeptidase and Other Proteins of small Size (KEOPS)/Endopeptidase-like and Kinase associated to transcribed Chromatin
KO	knock out
L	liter
LB	lysogeny broth
LCD	low complexity domain
LC-MS/MS	liquid chromatography mass spectrometry
LDH	lactate dehydrogenase
LLPS	liquid liquid phase separation
M	molarity (mol/L)
mA	milli ampere
MAGOHB	mago nashi
MAPT	Microtubule-associated protein Tau
MBNL1	muscleblind-like protein 1
MEK1	mitogen-activated protein kinase kinase (MAP2K)
min	minute(s)
mL	milli liter
mm	milli meter
mRNA	messenger RNA
MRPL	mitochondrial ribosomal protein large subunit
MRPS	mitochondrial ribosomal protein small subunit
MTCO1	mitochondrially encoded Cytochrome C oxidase I
n	quantity
NACA	nascent polypeptide-associated complex subunit alpha
NCL	nucleolin
NEAA	non-essential amino acid
NES	nuclear export sequence
ng	nano gram
NLS	nuclear localization signal
nm	nano meter
NOC2L	nucleolar complex protein 2 homolog
NOP56	NucleOlar protein of 56.8 kDa
NP-40	Nonidet-P40, nonylphenylpolyethylenglycol
NPC	nuclear pore complex
NPM1	nucleophosmin 1
NSC34	Neuroblastoma hybrid cell line 34
nt	nucleotides
Nup	nucleoporin
OCR	oxygen consumption rate
OPT	optineurin
p	probability value

PA	proline-alanine
PAGE	poly-acrylamide gel electrophoresis
PBS	phosphate buffered saline
PCH	Pontocerebellar Hypoplasia
PCR	polymerase chain reaction
PES1	Pescadillo homolog
pH	measure of the activity of the solvated hydrogen ion
PNFA	Progressive non-fluent aphasia
pNFH	phosphorylated neurofilament heavy chain
Pom121	nuclear pore membrane protein 121 kDa
PPA	Primary progressive aphasia
PR	proline-arginine
PRMT	protein arginine methyltransferase
Pur-a	purine-riche element binding alpha
qRT-PCR	quantitative real time polymerase chain reaction
Rab	Ras-related in brain
Ran	RAs-related nuclear
RanGAP	GTPase-activating protein
RBP	RNA binding protein
RCC1	regulator of chromosome condensation 1
RNA	ribonucleic acid
ROS	reactive oxygen species
RPL	ribosomal protein large subunit
rpm	revolution per minute
RPS	ribosomal protein small subunit
rRNA	ribosomal RNA
RRP1	ribosomal RNA processing protein 1
RT	room temperature
SCA8	Spinocerebellar ataxia type 8
SDS	sodium dodecyl sulfate
sec	second(s)
SF3	splicing factor 3
SG	stress granule
SMCR8	Smith-Magenis syndrome chromosomal region candidate gene 8
SNRPB2	U2 small nuclear ribonucleoprotein B
SOD1	Superoxide dismutase 1
SQSTM1	Sequestome 1
SRSF	Serine and arginine rich splicing factors
STAU	Staufen
SUnSET	surface sensing of translation
T	thymidine
TAR	Transactive response

TCOF1	treacle ribosome biogenesis factor 1
TDP	Tar DNA binding protein
TEMED	N,N,N',N'-tetramethylethylenediamine
TIA1	T-cell-restricted intracellular antigen-1
TIMM9	translocase of the inner mitochondrial membrane
TMP	3,3',5,5' tetramethylbenzidine
TMX2	thioredoxin protein 2
TNPO1	transportin 1
TRA2	transformer 2 protein
TREM2	Triggered receptor expressed on myeloid cells
tRNA	transfer RNA
TSEN	tRNA splicing endonuclease
UBQLN	Ubiquilin
ULK1	Unc51-like kinase
UPS	Ubiquitin proteasome system
UV	ultraviolet
V	volt
V	Volt
VCP	Valosin-containing protein
WB	western blot
WDR	WD repeat domain
wt	wild type
YBX1	Y-box binding protein 1
YWHAZ	Tyrosine 3-Monooxygenase/Tryptophan 5-Monooxygenase Activation Protein Zeta

8. REFERENCES

Abrahams, S., Goldstein, L.H., Simmons, A., Brammer, M., Williams, S.C., Giampietro, V., and Leigh, P.N. (2004). Word retrieval in amyotrophic lateral sclerosis: a functional magnetic resonance imaging study. Brain *127*, 1507-1517.

Al-Chalabi, A., Jones, A., Troakes, C., King, A., Al-Sarraj, S., and van den Berg, L.H. (2012). The genetics and neuropathology of amyotrophic lateral sclerosis. Acta Neuropathol *124*, 339-352.

Al-Sarraj, S., King, A., Troakes, C., Smith, B., Maekawa, S., Bodi, I., Rogelj, B., Al-Chalabi, A., Hortobagyi, T., and Shaw, C.E. (2011). p62 positive, TDP-43 negative, neuronal cytoplasmic and intranuclear inclusions in the cerebellum and hippocampus define the pathology of C9orf72-linked FTLD and MND/ALS. Acta Neuropathol *122*, 691-702.

Anderson, P., and Kedersha, N. (2009). Stress granules. Curr Biol *19*, R397-398.

Anderson, S.L., Coli, R., Daly, I.W., Kichula, E.A., Rork, M.J., Volpi, S.A., Ekstein, J., and Rubin, B.Y. (2001). Familial dysautonomia is caused by mutations of the IKAP gene. Am J Hum Genet *68*, 753-758.

Annesley, T., Majzoub, J., Hsing, A., Wu, A., Rockwood, A., and Mason, D. (2009). Mass spectrometry in the clinical laboratory: how have we done, and where do we need to be? Clin Chem *55*, 1236-1239.

Antonellis, A., Ellsworth, R.E., Sambuughin, N., Puls, I., Abel, A., Lee-Lin, S.Q., Jordanova, A., Kremensky, I., Christodoulou, K., Middleton, L.T.*, et al.* (2003). Glycyl tRNA synthetase mutations in Charcot-Marie-Tooth disease type 2D and distal spinal muscular atrophy type V. Am J Hum Genet *72*, 1293-1299.

Ash, P.E., Bieniek, K.F., Gendron, T.F., Caulfield, T., Lin, W.L., Dejesus-Hernandez, M., van Blitterswijk, M.M., Jansen-West, K., Paul, J.W., 3rd, Rademakers, R.*, et al.* (2013). Unconventional translation of C9ORF72 GGGGCC expansion generates insoluble polypeptides specific to c9FTD/ALS. Neuron *77*, 639-646.

Atanasio, A., Decman, V., White, D., Ramos, M., Ikiz, B., Lee, H.C., Siao, C.J., Brydges, S., LaRosa, E., Bai, Y.*, et al.* (2016). C9orf72 ablation causes immune dysregulation characterized by leukocyte expansion, autoantibody production, and glomerulonephropathy in mice. Sci Rep *6*, 23204.

Baborie, A., Griffiths, T.D., Jaros, E., Perry, R., McKeith, I.G., Burn, D.J., Masuda-Suzukake, M., Hasegawa, M., Rollinson, S., Pickering-Brown, S.*, et al.* (2015). Accumulation of dipeptide repeat proteins predates that of TDP-43 in frontotemporal lobar degeneration associated with hexanucleotide repeat expansions in C9ORF72 gene. Neuropathol Appl Neurobiol *41*, 601-612.

Bang, J., Spina, S., and Miller, B.L. (2015). Frontotemporal dementia. Lancet *386*, 1672-1682.

Beck, J., Poulter, M., Hensman, D., Rohrer, J.D., Mahoney, C.J., Adamson, G., Campbell, T., Uphill, J., Borg, A., Fratta, P.*, et al.* (2013). Large C9orf72 hexanucleotide repeat expansions are seen in multiple neurodegenerative syndromes and are more frequent than expected in the UK population. Am J Hum Genet *92*, 345-353.

Belzil, V.V., Bauer, P.O., Prudencio, M., Gendron, T.F., Stetler, C.T., Yan, I.K., Pregent, L., Daughrity, L., Baker, M.C., Rademakers, R.*, et al.* (2013). Reduced C9orf72 gene expression in c9FTD/ALS is caused by histone trimethylation, an epigenetic event detectable in blood. Acta Neuropathol *126*, 895-905.

Boeynaems, S., Bogaert, E., Kovacs, D., Konijnenberg, A., Timmerman, E., Volkov, A., Guharoy, M., De Decker, M., Jaspers, T., Ryan, V.H.*, et al.* (2017). Phase Separation of C9orf72 Dipeptide Repeats Perturbs Stress Granule Dynamics. Mol Cell *65*, 1044-1055 e1045.

Boeynaems, S., Bogaert, E., Michiels, E., Gijselinck, I., Sieben, A., Jovicic, A., De Baets, G., Scheveneels, W., Steyaert, J., Cuijt, I.*, et al.* (2016). Drosophila screen connects nuclear transport genes to DPR pathology in c9ALS/FTD. Sci Rep *6*, 20877.

Boisvert, F.M., van Koningsbruggen, S., Navascues, J., and Lamond, A.I. (2007). The multifunctional nucleolus. Nat Rev Mol Cell Biol *8*, 574-585.

Borroni, B., Ferrari, F., Galimberti, D., Nacmias, B., Barone, C., Bagnoli, S., Fenoglio, C., Piaceri, I., Archetti, S., Bonvicini, C.*, et al.* (2014). Heterozygous TREM2 mutations in frontotemporal dementia. Neurobiol Aging *35*, 934 e937-910.

Boylan, K. (2015). Familial Amyotrophic Lateral Sclerosis. Neurol Clin *33*, 807-830.

Braun, D.A., Rao, J., Mollet, G., Schapiro, D., Daugeron, M.C., Tan, W., Gribouval, O., Boyer, O., Revy, P., Jobst-Schwan, T.*, et al.* (2017). Mutations in KEOPS-complex genes cause nephrotic syndrome with primary microcephaly. Nat Genet *49*, 1529-1538.

Breuss, M.W., Sultan, T., James, K.N., Rosti, R.O., Scott, E., Musaev, D., Furia, B., Reis, A., Sticht, H., Al-Owain, M.*, et al.* (2016). Autosomal-Recessive Mutations in the tRNA Splicing Endonuclease Subunit TSEN15 Cause Pontocerebellar Hypoplasia and Progressive Microcephaly. Am J Hum Genet *99*, 228-235.

Buchan, J.R., and Parker, R. (2009). Eukaryotic stress granules: the ins and outs of translation. Mol Cell *36*, 932-941.

Budde, B.S., Namavar, Y., Barth, P.G., Poll-The, B.T., Nurnberg, G., Becker, C., van Ruissen, F., Weterman, M.A., Fluiter, K., te Beek, E.T.*, et al.* (2008). tRNA splicing endonuclease mutations cause pontocerebellar hypoplasia. Nat Genet *40*, 1113-1118.

Burberry, A., Suzuki, N., Wang, J.Y., Moccia, R., Mordes, D.A., Stewart, M.H., Suzuki-Uematsu, S., Ghosh, S., Singh, A., Merkle, F.T.*, et al.* (2016). Loss-of-function mutations in the C9ORF72 mouse ortholog cause fatal autoimmune disease. Sci Transl Med *8*, 347ra393.

Byrne, S., Elamin, M., Bede, P., Shatunov, A., Walsh, C., Corr, B., Heverin, M., Jordan, N., Kenna, K., Lynch, C.*, et al.* (2012). Cognitive and clinical characteristics of patients with amyotrophic lateral sclerosis carrying a C9orf72 repeat expansion: a population-based cohort study. Lancet Neurol *11*, 232-240.

Cantara, W.A., Crain, P.F., Rozenski, J., McCloskey, J.A., Harris, K.A., Zhang, X., Vendeix, F.A., Fabris, D., and Agris, P.F. (2011). The RNA Modification Database, RNAMDB: 2011 update. Nucleic Acids Res *39*, D195-201.

Chang, Y.J., Jeng, U.S., Chiang, Y.L., Hwang, I.S., and Chen, Y.R. (2016). The Glycine-Alanine Dipeptide Repeat from C9orf72 Hexanucleotide Expansions Forms Toxic Amyloids Possessing Cell-to-Cell Transmission Properties. J Biol Chem *291*, 4903-4911.

Chio, A., Borghero, G., Restagno, G., Mora, G., Drepper, C., Traynor, B.J., Sendtner, M., Brunetti, M., Ossola, I., Calvo, A.*, et al.* (2012). Clinical characteristics of patients with familial amyotrophic lateral sclerosis carrying the pathogenic GGGGCC hexanucleotide repeat expansion of C9ORF72. Brain *135*, 784-793.

Chio, A., Logroscino, G., Traynor, B.J., Collins, J., Simeone, J.C., Goldstein, L.A., and White, L.A. (2013). Global epidemiology of amyotrophic lateral sclerosis: a systematic review of the published literature. Neuroepidemiology *41*, 118-130.

Chiriboga, C.A., Swoboda, K.J., Darras, B.T., Iannaccone, S.T., Montes, J., De Vivo, D.C., Norris, D.A., Bennett, C.F., and Bishop, K.M. (2016). Results from a phase 1 study of nusinersen (ISIS-SMN(Rx)) in children with spinal muscular atrophy. Neurology *86*, 890-897.

Ciura, S., Lattante, S., Le Ber, I., Latouche, M., Tostivint, H., Brice, A., and Kabashi, E. (2013). Loss of function of C9orf72 causes motor deficits in a zebrafish model of amyotrophic lateral sclerosis. Ann Neurol *74*, 180-187.

Conlon, E.G., Lu, L., Sharma, A., Yamazaki, T., Tang, T., Shneider, N.A., and Manley, J.L. (2016). The C9ORF72 GGGGCC expansion forms RNA G-quadruplex inclusions and sequesters hnRNP H to disrupt splicing in ALS brains. Elife *5*.

Cooper-Knock, J., Higginbottom, A., Stopford, M.J., Highley, J.R., Ince, P.G., Wharton, S.B., Pickering-Brown, S., Kirby, J., Hautbergue, G.M., and Shaw, P.J. (2015). Antisense RNA foci in the motor neurons of C9ORF72-ALS patients are associated with TDP-43 proteinopathy. Acta Neuropathol *130*, 63-75.

Cooper-Knock, J., Walsh, M.J., Higginbottom, A., Robin Highley, J., Dickman, M.J., Edbauer, D., Ince, P.G., Wharton, S.B., Wilson, S.A., Kirby, J.*, et al.* (2014). Sequestration of multiple RNA recognition motif-containing proteins by C9orf72 repeat expansions. Brain *137*, 2040-2051.

DeJesus-Hernandez, M., Mackenzie, I.R., Boeve, B.F., Boxer, A.L., Baker, M., Rutherford, N.J., Nicholson, A.M., Finch, N.A., Flynn, H., Adamson, J.*, et al.* (2011). Expanded GGGGCC hexanucleotide repeat in noncoding region of C9ORF72 causes chromosome 9p-linked FTD and ALS. Neuron *72*, 245-256.

Dixon, M.J. (1996). Treacher Collins syndrome. Hum Mol Genet *5 Spec No*, 1391-1396.

Donnelly, C.J., Zhang, P.W., Pham, J.T., Haeusler, A.R., Mistry, N.A., Vidensky, S., Daley, E.L., Poth, E.M., Hoover, B., Fines, D.M.*, et al.* (2013). RNA toxicity from the ALS/FTD C9ORF72 expansion is mitigated by antisense intervention. Neuron *80*, 415-428.

Draptchinskaia, N., Gustavsson, P., Andersson, B., Pettersson, M., Willig, T.N., Dianzani, I., Ball, S., Tchernia, G., Klar, J., Matsson, H.*, et al.* (1999). The gene encoding ribosomal protein S19 is mutated in Diamond-Blackfan anaemia. Nat Genet *21*, 169-175.

Ebert, B.L., Pretz, J., Bosco, J., Chang, C.Y., Tamayo, P., Galili, N., Raza, A., Root, D.E., Attar, E., Ellis, S.R.*, et al.* (2008). Identification of RPS14 as a 5q- syndrome gene by RNA interference screen. Nature *451*, 335-339.

Edbauer, D., and Haass, C. (2016). An amyloid-like cascade hypothesis for C9orf72 ALS/FTD. Curr Opin Neurobiol *36*, 99-106.

Elden, A.C., Kim, H.J., Hart, M.P., Chen-Plotkin, A.S., Johnson, B.S., Fang, X., Armakola, M., Geser, F., Greene, R., Lu, M.M.*, et al.* (2010). Ataxin-2 intermediate-length polyglutamine expansions are associated with increased risk for ALS. Nature *466*, 1069-1075.

Ferrari, R., Kapogiannis, D., Huey, E.D., and Momeni, P. (2011). FTD and ALS: a tale of two diseases. Curr Alzheimer Res *8*, 273-294.

Fiesel, F.C., Weber, S.S., Supper, J., Zell, A., and Kahle, P.J. (2012). TDP-43 regulates global translational yield by splicing of exon junction complex component SKAR. Nucleic Acids Res *40*, 2668-2682.

Fratta, P., Poulter, M., Lashley, T., Rohrer, J.D., Polke, J.M., Beck, J., Ryan, N., Hensman, D., Mizielinska, S., Waite, A.J.*, et al.* (2013). Homozygosity for the C9orf72 GGGGCC repeat expansion in frontotemporal dementia. Acta Neuropathol *126*, 401-409.

Freibaum, B.D., Lu, Y., Lopez-Gonzalez, R., Kim, N.C., Almeida, S., Lee, K.H., Badders, N., Valentine, M., Miller, B.L., Wong, P.C.*, et al.* (2015). GGGGCC repeat expansion in C9orf72 compromises nucleocytoplasmic transport. Nature *525*, 129-133.

Frick, P., Sellier, C., Mackenzie, I.R.A., Cheng, C.Y., Tahraoui-Bories, J., Martinat, C., Pasterkamp, R.J., Prudlo, J., Edbauer, D., Oulad-Abdelghani, M.*, et al.* (2018). Novel antibodies reveal presynaptic localization of C9orf72 protein and reduced protein levels in C9orf72 mutation carriers. Acta Neuropathol Commun *6*, 72.

Fromont-Racine, M., Senger, B., Saveanu, C., and Fasiolo, F. (2003). Ribosome assembly in eukaryotes. Gene *313*, 17-42.

Gazda, H.T., Kho, A.T., Sanoudou, D., Zaucha, J.M., Kohane, I.S., Sieff, C.A., and Beggs, A.H. (2006). Defective ribosomal protein gene expression alters transcription, translation, apoptosis, and oncogenic pathways in Diamond-Blackfan anemia. Stem Cells *24*, 2034-2044.

Gendron, T.F., Bieniek, K.F., Zhang, Y.J., Jansen-West, K., Ash, P.E., Caulfield, T., Daughrity, L., Dunmore, J.H., Castanedes-Casey, M., Chew, J.*, et al.* (2013). Antisense transcripts of the expanded C9ORF72 hexanucleotide repeat form nuclear RNA foci and undergo repeat-associated non-ATG translation in c9FTD/ALS. Acta Neuropathol *126*, 829-844.

Gendron, T.F., Chew, J., Stankowski, J.N., Hayes, L.R., Zhang, Y.J., Prudencio, M., Carlomagno, Y., Daughrity, L.M., Jansen-West, K., Perkerson, E.A.*, et al.* (2017a). Poly(GP) proteins are a useful pharmacodynamic marker for C9ORF72-associated amyotrophic lateral sclerosis. Sci Transl Med *9*.

Gendron, T.F., Group, C.O.N.S., Daughrity, L.M., Heckman, M.G., Diehl, N.N., Wuu, J., Miller, T.M., Pastor, P., Trojanowski, J.Q., Grossman, M.*, et al.* (2017b). Phosphorylated neurofilament heavy chain: A biomarker of survival for C9ORF72-associated amyotrophic lateral sclerosis. Ann Neurol *82*, 139-146.

Gerrard, G., Valganon, M., Foong, H.E., Kasperaviciute, D., Iskander, D., Game, L., Muller, M., Aitman, T.J., Roberts, I., de la Fuente, J.*, et al.* (2013). Target enrichment and high-throughput sequencing of 80 ribosomal protein genes to identify mutations associated with Diamond-Blackfan anaemia. Br J Haematol *162*, 530-536.

Gerstberger, S., Hafner, M., and Tuschl, T. (2014). A census of human RNA-binding proteins. Nat Rev Genet *15*, 829-845.

Gijselinck, I., Van Mossevelde, S., van der Zee, J., Sieben, A., Engelborghs, S., De Bleecker, J., Ivanoiu, A., Deryck, O., Edbauer, D., Zhang, M.*, et al.* (2016). The C9orf72 repeat size correlates with onset

age of disease, DNA methylation and transcriptional downregulation of the promoter. Mol Psychiatry *21*, 1112-1124.

Goldman, J.S., Farmer, J.M., Wood, E.M., Johnson, J.K., Boxer, A., Neuhaus, J., Lomen-Hoerth, C., Wilhelmsen, K.C., Lee, V.M., Grossman, M.*, et al.* (2005). Comparison of family histories in FTLD subtypes and related tauopathies. Neurology *65*, 1817-1819.

Guo, Q., Lehmer, C., Martinez-Sanchez, A., Rudack, T., Beck, F., Hartmann, H., Perez-Berlanga, M., Frottin, F., Hipp, M.S., Hartl, F.U.*, et al.* (2018). In Situ Structure of Neuronal C9orf72 Poly-GA Aggregates Reveals Proteasome Recruitment. Cell *172*, 696-705 e612.

Haeusler, A.R., Donnelly, C.J., Periz, G., Simko, E.A., Shaw, P.G., Kim, M.S., Maragakis, N.J., Troncoso, J.C., Pandey, A., Sattler, R.*, et al.* (2014). C9orf72 nucleotide repeat structures initiate molecular cascades of disease. Nature *507*, 195-200.

Hayano, T., Yanagida, M., Yamauchi, Y., Shinkawa, T., Isobe, T., and Takahashi, N. (2003). Proteomic analysis of human Nop56p-associated pre-ribosomal ribonucleoprotein complexes. Possible link between Nop56p and the nucleolar protein treacle responsible for Treacher Collins syndrome. J Biol Chem *278*, 34309-34319.

Heiss, N.S., Knight, S.W., Vulliamy, T.J., Klauck, S.M., Wiemann, S., Mason, P.J., Poustka, A., and Dokal, I. (1998). X-linked dyskeratosis congenita is caused by mutations in a highly conserved gene with putative nucleolar functions. Nat Genet *19*, 32-38.

Henras, A.K., Plisson-Chastang, C., O'Donohue, M.F., Chakraborty, A., and Gleizes, P.E. (2015). An overview of pre-ribosomal RNA processing in eukaryotes. Wiley Interdiscip Rev RNA *6*, 225-242.

Henras, A.K., Soudet, J., Gerus, M., Lebaron, S., Caizergues-Ferrer, M., Mougin, A., and Henry, Y. (2008). The post-transcriptional steps of eukaryotic ribosome biogenesis. Cell Mol Life Sci *65*, 2334-2359.

Hsiung, G.Y., DeJesus-Hernandez, M., Feldman, H.H., Sengdy, P., Bouchard-Kerr, P., Dwosh, E., Butler, R., Leung, B., Fok, A., Rutherford, N.J.*, et al.* (2012). Clinical and pathological features of familial frontotemporal dementia caused by C9ORF72 mutation on chromosome 9p. Brain *135*, 709-722.

Isaacs, A.M., Johannsen, P., Holm, I., Nielsen, J.E., and consortium, F.R. (2011). Frontotemporal dementia caused by CHMP2B mutations. Curr Alzheimer Res *8*, 246-251.

Jain, S., Wheeler, J.R., Walters, R.W., Agrawal, A., Barsic, A., and Parker, R. (2016). ATPase-Modulated Stress Granules Contain a Diverse Proteome and Substructure. Cell *164*, 487-498.

Jordanova, A., Irobi, J., Thomas, F.P., Van Dijck, P., Meerschaert, K., Dewil, M., Dierick, I., Jacobs, A., De Vriendt, E., Guergueltcheva, V.*, et al.* (2006). Disrupted function and axonal distribution of mutant tyrosyl-tRNA synthetase in dominant intermediate Charcot-Marie-Tooth neuropathy. Nat Genet *38*, 197-202.

Josephs, K.A., Whitwell, J.L., Vemuri, P., Senjem, M.L., Boeve, B.F., Knopman, D.S., Smith, G.E., Ivnik, R.J., Petersen, R.C., and Jack, C.R., Jr. (2008). The anatomic correlate of prosopagnosia in semantic dementia. Neurology *71*, 1628-1633.

Jovicic, A., Mertens, J., Boeynaems, S., Bogaert, E., Chai, N., Yamada, S.B., Paul, J.W., 3rd, Sun, S., Herdy, J.R., Bieri, G.*, et al.* (2015). Modifiers of C9orf72 dipeptide repeat toxicity connect nucleocytoplasmic transport defects to FTD/ALS. Nat Neurosci *18*, 1226-1229.

Jung, J., Nayak, A., Schaeffer, V., Starzetz, T., Kirsch, A.K., Muller, S., Dikic, I., Mittelbronn, M., and Behrends, C. (2017). Multiplex image-based autophagy RNAi screening identifies SMCR8 as ULK1 kinase activity and gene expression regulator. Elife *6*.

Kanekura, K., Yagi, T., Cammack, A.J., Mahadevan, J., Kuroda, M., Harms, M.B., Miller, T.M., and Urano, F. (2016). Poly-dipeptides encoded by the C9ORF72 repeats block global protein translation. Hum Mol Genet *25*, 1803-1813.

Karaca, E., Weitzer, S., Pehlivan, D., Shiraishi, H., Gogakos, T., Hanada, T., Jhangiani, S.N., Wiszniewski, W., Withers, M., Campbell, I.M.*, et al.* (2014). Human CLP1 mutations alter tRNA biogenesis, affecting both peripheral and central nervous system function. Cell *157*, 636-650.

Khosravi, B., Hartmann, H., May, S., Mohl, C., Ederle, H., Michaelsen, M., Schludi, M.H., Dormann, D., and Edbauer, D. (2017). Cytoplasmic poly-GA aggregates impair nuclear import of TDP-43 in C9orf72 ALS/FTLD. Hum Mol Genet *26*, 790-800.

Kramer, N.J., Haney, M.S., Morgens, D.W., Jovicic, A., Couthouis, J., Li, A., Ousey, J., Ma, R., Bieri, G., Tsui, C.K., *et al.* (2018). CRISPR-Cas9 screens in human cells and primary neurons identify modifiers of C9ORF72 dipeptide-repeat-protein toxicity. Nat Genet *50*, 603-612.

Kressler, D., Hurt, E., and Bassler, J. (2010). Driving ribosome assembly. Biochim Biophys Acta *1803*, 673-683.

Kumar, D.R., Aslinia, F., Yale, S.H., and Mazza, J.J. (2011). Jean-Martin Charcot: the father of neurology. Clin Med Res *9*, 46-49.

Kunst, C.B., Mezey, E., Brownstein, M.J., and Patterson, D. (1997). Mutations in SOD1 associated with amyotrophic lateral sclerosis cause novel protein interactions. Nat Genet *15*, 91-94.

Kwon, I., Xiang, S., Kato, M., Wu, L., Theodoropoulos, P., Wang, T., Kim, J., Yun, J., Xie, Y., and McKnight, S.L. (2014). Poly-dipeptides encoded by the C9orf72 repeats bind nucleoli, impede RNA biogenesis, and kill cells. Science *345*, 1139-1145.

Lagier-Tourenne, C., Baughn, M., Rigo, F., Sun, S., Liu, P., Li, H.R., Jiang, J., Watt, A.T., Chun, S., Katz, M., *et al.* (2013). Targeted degradation of sense and antisense C9orf72 RNA foci as therapy for ALS and frontotemporal degeneration. Proc Natl Acad Sci U S A *110*, E4530-4539.

Latour, P., Thauvin-Robinet, C., Baudelet-Mery, C., Soichot, P., Cusin, V., Faivre, L., Locatelli, M.C., Mayencon, M., Sarcey, A., Broussolle, E., *et al.* (2010). A major determinant for binding and aminoacylation of tRNA(Ala) in cytoplasmic Alanyl-tRNA synthetase is mutated in dominant axonal Charcot-Marie-Tooth disease. Am J Hum Genet *86*, 77-82.

Le Ber, I. (2013). Genetics of frontotemporal lobar degeneration: an up-date and diagnosis algorithm. Rev Neurol (Paris) *169*, 811-819.

Lee, J.W., Beebe, K., Nangle, L.A., Jang, J., Longo-Guess, C.M., Cook, S.A., Davisson, M.T., Sundberg, J.P., Schimmel, P., and Ackerman, S.L. (2006). Editing-defective tRNA synthetase causes protein misfolding and neurodegeneration. Nature *443*, 50-55.

Lee, K.H., Zhang, P., Kim, H.J., Mitrea, D.M., Sarkar, M., Freibaum, B.D., Cika, J., Coughlin, M., Messing, J., Molliex, A., *et al.* (2016a). C9orf72 Dipeptide Repeats Impair the Assembly, Dynamics, and Function of Membrane-Less Organelles. Cell *167*, 774-788 e717.

Lee, S., Shang, Y., Redmond, S.A., Urisman, A., Tang, A.A., Li, K.H., Burlingame, A.L., Pak, R.A., Jovicic, A., Gitler, A.D., *et al.* (2016b). Activation of HIPK2 Promotes ER Stress-Mediated Neurodegeneration in Amyotrophic Lateral Sclerosis. Neuron *91*, 41-55.

Lee, Y.B., Chen, H.J., Peres, J.N., Gomez-Deza, J., Attig, J., Stalekar, M., Troakes, C., Nishimura, A.L., Scotter, E.L., Vance, C., *et al.* (2013). Hexanucleotide repeats in ALS/FTD form length-dependent RNA foci, sequester RNA binding proteins, and are neurotoxic. Cell Rep *5*, 1178-1186.

Lehmer, C., Oeckl, P., Weishaupt, J.H., Volk, A.E., Diehl-Schmid, J., Schroeter, M.L., Lauer, M., Kornhuber, J., Levin, J., Fassbender, K., *et al.* (2017). Poly-GP in cerebrospinal fluid links C9orf72-associated dipeptide repeat expression to the asymptomatic phase of ALS/FTD. EMBO Mol Med *9*, 859-868.

Levine, T.P., Daniels, R.D., Gatta, A.T., Wong, L.H., and Hayes, M.J. (2013). The product of C9orf72, a gene strongly implicated in neurodegeneration, is structurally related to DENN Rab-GEFs. Bioinformatics *29*, 499-503.

Lin, Y., Mori, E., Kato, M., Xiang, S., Wu, L., Kwon, I., and McKnight, S.L. (2016). Toxic PR Poly-Dipeptides Encoded by the C9orf72 Repeat Expansion Target LC Domain Polymers. Cell *167*, 789-802 e712.

Ling, S.C., Polymenidou, M., and Cleveland, D.W. (2013). Converging mechanisms in ALS and FTD: disrupted RNA and protein homeostasis. Neuron *79*, 416-438.

Lipfert, J., Doniach, S., Das, R., and Herschlag, D. (2014). Understanding nucleic acid-ion interactions. Annu Rev Biochem *83*, 813-841.

Liu-Yesucevitz, L., Bilgutay, A., Zhang, Y.J., Vanderweyde, T., Citro, A., Mehta, T., Zaarur, N., McKee, A., Bowser, R., Sherman, M., *et al.* (2010). Tar DNA binding protein-43 (TDP-43) associates with stress granules: analysis of cultured cells and pathological brain tissue. PLoS One *5*, e13250.

Lopez-Gonzalez, R., Lu, Y., Gendron, T.F., Karydas, A., Tran, H., Yang, D., Petrucelli, L., Miller, B.L., Almeida, S., and Gao, F.B. (2016). Poly(GR) in C9ORF72-Related ALS/FTD Compromises Mitochondrial Function and Increases Oxidative Stress and DNA Damage in iPSC-Derived Motor Neurons. Neuron *92*, 383-391.

Lu, Z., and Xu, S. (2006). ERK1/2 MAP kinases in cell survival and apoptosis. IUBMB Life *58*, 621-631.

Mackenzie, I.R., Arzberger, T., Kremmer, E., Troost, D., Lorenzl, S., Mori, K., Weng, S.M., Haass, C., Kretzschmar, H.A., Edbauer, D.*, et al.* (2013). Dipeptide repeat protein pathology in C9ORF72 mutation cases: clinico-pathological correlations. Acta Neuropathol *126*, 859-879.

Mackenzie, I.R., and Feldman, H.H. (2005). Ubiquitin immunohistochemistry suggests classic motor neuron disease, motor neuron disease with dementia, and frontotemporal dementia of the motor neuron disease type represent a clinicopathologic spectrum. J Neuropathol Exp Neurol *64*, 730-739.

Mackenzie, I.R., Nicholson, A.M., Sarkar, M., Messing, J., Purice, M.D., Pottier, C., Annu, K., Baker, M., Perkerson, R.B., Kurti, A.*, et al.* (2017). TIA1 Mutations in Amyotrophic Lateral Sclerosis and Frontotemporal Dementia Promote Phase Separation and Alter Stress Granule Dynamics. Neuron *95*, 808-816 e809.

Maggi, L.B., Jr., Kuchenruether, M., Dadey, D.Y., Schwope, R.M., Grisendi, S., Townsend, R.R., Pandolfi, P.P., and Weber, J.D. (2008). Nucleophosmin serves as a rate-limiting nuclear export chaperone for the Mammalian ribosome. Mol Cell Biol *28*, 7050-7065.

Majounie, E., Renton, A.E., Mok, K., Dopper, E.G., Waite, A., Rollinson, S., Chio, A., Restagno, G., Nicolaou, N., Simon-Sanchez, J.*, et al.* (2012). Frequency of the C9orf72 hexanucleotide repeat expansion in patients with amyotrophic lateral sclerosis and frontotemporal dementia: a cross-sectional study. Lancet Neurol *11*, 323-330.

Mann, D.M., Rollinson, S., Robinson, A., Bennion Callister, J., Thompson, J.C., Snowden, J.S., Gendron, T., Petrucelli, L., Masuda-Suzukake, M., Hasegawa, M.*, et al.* (2013). Dipeptide repeat proteins are present in the p62 positive inclusions in patients with frontotemporal lobar degeneration and motor neurone disease associated with expansions in C9ORF72. Acta Neuropathol Commun *1*, 68.

May, S., Hornburg, D., Schludi, M.H., Arzberger, T., Rentzsch, K., Schwenk, B.M., Grasser, F.A., Mori, K., Kremmer, E., Banzhaf-Strathmann, J.*, et al.* (2014). C9orf72 FTLD/ALS-associated Gly-Ala dipeptide repeat proteins cause neuronal toxicity and Unc119 sequestration. Acta Neuropathol *128*, 485-503.

McCubrey, J.A., Steelman, L.S., Chappell, W.H., Abrams, S.L., Wong, E.W., Chang, F., Lehmann, B., Terrian, D.M., Milella, M., Tafuri, A.*, et al.* (2007). Roles of the Raf/MEK/ERK pathway in cell growth, malignant transformation and drug resistance. Biochim Biophys Acta *1773*, 1263-1284.

Miller, J.W., Urbinati, C.R., Teng-Umnuay, P., Stenberg, M.G., Byrne, B.J., Thornton, C.A., and Swanson, M.S. (2000). Recruitment of human muscleblind proteins to (CUG)(n) expansions associated with myotonic dystrophy. EMBO J *19*, 4439-4448.

Mizielinska, S., Gronke, S., Niccoli, T., Ridler, C.E., Clayton, E.L., Devoy, A., Moens, T., Norona, F.E., Woollacott, I.O.C., Pietrzyk, J.*, et al.* (2014). C9orf72 repeat expansions cause neurodegeneration in Drosophila through arginine-rich proteins. Science *345*, 1192-1194.

Mizielinska, S., Lashley, T., Norona, F.E., Clayton, E.L., Ridler, C.E., Fratta, P., and Isaacs, A.M. (2013). C9orf72 frontotemporal lobar degeneration is characterised by frequent neuronal sense and antisense RNA foci. Acta Neuropathol *126*, 845-857.

Mizielinska, S., Ridler, C.E., Balendra, R., Thoeng, A., Woodling, N.S., Grasser, F.A., Plagnol, V., Lashley, T., Partridge, L., and Isaacs, A.M. (2017). Bidirectional nucleolar dysfunction in C9orf72 frontotemporal lobar degeneration. Acta Neuropathol Commun *5*, 29.

Molliex, A., Temirov, J., Lee, J., Coughlin, M., Kanagaraj, A.P., Kim, H.J., Mittag, T., and Taylor, J.P. (2015). Phase separation by low complexity domains promotes stress granule assembly and drives pathological fibrillization. Cell *163*, 123-133.

Mori, K., Arzberger, T., Grasser, F.A., Gijselinck, I., May, S., Rentzsch, K., Weng, S.M., Schludi, M.H., van der Zee, J., Cruts, M.*, et al.* (2013a). Bidirectional transcripts of the expanded C9orf72 hexanucleotide repeat are translated into aggregating dipeptide repeat proteins. Acta Neuropathol *126*, 881-893.

Mori, K., Lammich, S., Mackenzie, I.R., Forne, I., Zilow, S., Kretzschmar, H., Edbauer, D., Janssens, J., Kleinberger, G., Cruts, M.*, et al.* (2013b). hnRNP A3 binds to GGGGCC repeats and is a constituent of p62-positive/TDP43-negative inclusions in the hippocampus of patients with C9orf72 mutations. Acta Neuropathol *125*, 413-423.

Mori, K., Weng, S.M., Arzberger, T., May, S., Rentzsch, K., Kremmer, E., Schmid, B., Kretzschmar, H.A., Cruts, M., Van Broeckhoven, C., *et al.* (2013c). The C9orf72 GGGGCC repeat is translated into aggregating dipeptide-repeat proteins in FTLD/ALS. Science *339*, 1335-1338.

Nonaka, T., Masuda-Suzukake, M., Hosokawa, M., Shimozawa, A., Hirai, S., Okado, H., and Hasegawa, M. (2018). C9ORF72 dipeptide repeat poly-GA inclusions promote: intracellular aggregation of phosphorylated TDP-43. Hum Mol Genet.

O'Rourke, J.G., Bogdanik, L., Yanez, A., Lall, D., Wolf, A.J., Muhammad, A.K., Ho, R., Carmona, S., Vit, J.P., Zarrow, J., *et al.* (2016). C9orf72 is required for proper macrophage and microglial function in mice. Science *351*, 1324-1329.

Onyike, C.U., and Diehl-Schmid, J. (2013). The epidemiology of frontotemporal dementia. Int Rev Psychiatry *25*, 130-137.

Pang, Y.L., Poruri, K., and Martinis, S.A. (2014). tRNA synthetase: tRNA aminoacylation and beyond. Wiley Interdiscip Rev RNA *5*, 461-480.

Prudencio, M., Belzil, V.V., Batra, R., Ross, C.A., Gendron, T.F., Pregent, L.J., Murray, M.E., Overstreet, K.K., Piazza-Johnston, A.E., Desaro, P., *et al.* (2015). Distinct brain transcriptome profiles in C9orf72-associated and sporadic ALS. Nat Neurosci *18*, 1175-1182.

Rayaprolu, S., Mullen, B., Baker, M., Lynch, T., Finger, E., Seeley, W.W., Hatanpaa, K.J., Lomen-Hoerth, C., Kertesz, A., Bigio, E.H., *et al.* (2013). TREM2 in neurodegeneration: evidence for association of the p.R47H variant with frontotemporal dementia and Parkinson's disease. Mol Neurodegener *8*, 19.

Renton, A.E., Chio, A., and Traynor, B.J. (2014). State of play in amyotrophic lateral sclerosis genetics. Nat Neurosci *17*, 17-23.

Renton, A.E., Majounie, E., Waite, A., Simon-Sanchez, J., Rollinson, S., Gibbs, J.R., Schymick, J.C., Laaksovirta, H., van Swieten, J.C., Myllykangas, L., *et al.* (2011). A hexanucleotide repeat expansion in C9ORF72 is the cause of chromosome 9p21-linked ALS-FTD. Neuron *72*, 257-268.

Rohrer, J.D., Guerreiro, R., Vandrovcova, J., Uphill, J., Reiman, D., Beck, J., Isaacs, A.M., Authier, A., Ferrari, R., Fox, N.C., *et al.* (2009). The heritability and genetics of frontotemporal lobar degeneration. Neurology *73*, 1451-1456.

Rohrmoser, M., Holzel, M., Grimm, T., Malamoussi, A., Harasim, T., Orban, M., Pfisterer, I., Gruber-Eber, A., Kremmer, E., and Eick, D. (2007). Interdependence of Pes1, Bop1, and WDR12 controls nucleolar localization and assembly of the PeBoW complex required for maturation of the 60S ribosomal subunit. Mol Cell Biol *27*, 3682-3694.

Rosso, S.M., Donker Kaat, L., Baks, T., Joosse, M., de Koning, I., Pijnenburg, Y., de Jong, D., Dooijes, D., Kamphorst, W., Ravid, R., *et al.* (2003). Frontotemporal dementia in The Netherlands: patient characteristics and prevalence estimates from a population-based study. Brain *126*, 2016-2022.

Ryan, M.M., Cooke-Yarborough, C.M., Procopis, P.G., and Ouvrier, R.A. (2000). Anterior horn cell disease and olivopontocerebellar hypoplasia. Pediatr Neurol *23*, 180-184.

Sareen, D., O'Rourke, J.G., Meera, P., Muhammad, A.K., Grant, S., Simpkinson, M., Bell, S., Carmona, S., Ornelas, L., Sahabian, A., *et al.* (2013). Targeting RNA foci in iPSC-derived motor neurons from ALS patients with a C9ORF72 repeat expansion. Sci Transl Med *5*, 208ra149.

Schaffer, A.E., Eggens, V.R., Caglayan, A.O., Reuter, M.S., Scott, E., Coufal, N.G., Silhavy, J.L., Xue, Y., Kayserili, H., Yasuno, K., *et al.* (2014). CLP1 founder mutation links tRNA splicing and maturation to cerebellar development and neurodegeneration. Cell *157*, 651-663.

Schludi, M.H., May, S., Grasser, F.A., Rentzsch, K., Kremmer, E., Kupper, C., Klopstock, T., German Consortium for Frontotemporal Lobar, D., Bavarian Brain Banking, A., Arzberger, T., *et al.* (2015a). Distribution of dipeptide repeat proteins in cellular models and C9orf72 mutation cases suggests link to transcriptional silencing. Acta Neuropathol *130*, 537-555.

Schludi, M.H., May, S., Grasser, F.A., Rentzsch, K., Kremmer, E., Kupper, C., T., K., Degeneration, G.C.f.F.L., Alliance, B.B.B., Arzberger, T., *et al.* (2015b). Distribution of dipeptide repeat proteins in cellular models and C9orf72 mutation cases suggests link to transcriptional silencing. Acta Neuropathol *130*, 537-555.

Seeley, W.W., Bauer, A.M., Miller, B.L., Gorno-Tempini, M.L., Kramer, J.H., Weiner, M., and Rosen, H.J. (2005). The natural history of temporal variant frontotemporal dementia. Neurology *64*, 1384-1390.

Sellier, C., Campanari, M.L., Julie Corbier, C., Gaucherot, A., Kolb-Cheynel, I., Oulad-Abdelghani, M., Ruffenach, F., Page, A., Ciura, S., Kabashi, E.*, et al.* (2016). Loss of C9ORF72 impairs autophagy and synergizes with polyQ Ataxin-2 to induce motor neuron dysfunction and cell death. EMBO J *35*, 1276-1297.

Shi, Y., Lin, S., Staats, K.A., Li, Y., Chang, W.H., Hung, S.T., Hendricks, E., Linares, G.R., Wang, Y., Son, E.Y.*, et al.* (2018). Haploinsufficiency leads to neurodegeneration in C9ORF72 ALS/FTD human induced motor neurons. Nat Med *24*, 313-325.

Simone, R., Balendra, R., Moens, T.G., Preza, E., Wilson, K.M., Heslegrave, A., Woodling, N.S., Niccoli, T., Gilbert-Jaramillo, J., Abdelkarim, S.*, et al.* (2018). G-quadruplex-binding small molecules ameliorate C9orf72 FTD/ALS pathology in vitro and in vivo. EMBO Mol Med *10*, 22-31.

Sobala, A., and Hutvagner, G. (2013). Small RNAs derived from the 5' end of tRNA can inhibit protein translation in human cells. RNA Biol *10*, 553-563.

Stewart, H., Rutherford, N.J., Briemberg, H., Krieger, C., Cashman, N., Fabros, M., Baker, M., Fok, A., DeJesus-Hernandez, M., Eisen, A.*, et al.* (2012). Clinical and pathological features of amyotrophic lateral sclerosis caused by mutation in the C9ORF72 gene on chromosome 9p. Acta Neuropathol *123*, 409-417.

Storkebaum, E. (2016). Peripheral neuropathy via mutant tRNA synthetases: Inhibition of protein translation provides a possible explanation. Bioessays *38*, 818-829.

Su, Z., Zhang, Y., Gendron, T.F., Bauer, P.O., Chew, J., Yang, W.Y., Fostvedt, E., Jansen-West, K., Belzil, V.V., Desaro, P.*, et al.* (2014). Discovery of a biomarker and lead small molecules to target r(GGGGCC)-associated defects in c9FTD/ALS. Neuron *83*, 1043-1050.

Swaminathan, A., Bouffard, M., Liao, M., Ryan, S., Callister, J.B., Pickering-Brown, S.M., Armstrong, G.A.B., and Drapeau, P. (2018). Expression of C9orf72-related dipeptides impairs motor function in a vertebrate model. Hum Mol Genet *27*, 1754-1762.

Talbot, K. (2009). Motor neuron disease: the bare essentials. Pract Neurol *9*, 303-309.

Tao, Z., Wang, H., Xia, Q., Li, K., Li, K., Jiang, X., Xu, G., Wang, G., and Ying, Z. (2015). Nucleolar stress and impaired stress granule formation contribute to C9orf72 RAN translation-induced cytotoxicity. Hum Mol Genet *24*, 2426-2441.

Taylor, J.P., Brown, R.H., Jr., and Cleveland, D.W. (2016). Decoding ALS: from genes to mechanism. Nature *539*, 197-206.

Thomas, M.G., Martinez Tosar, L.J., Desbats, M.A., Leishman, C.C., and Boccaccio, G.L. (2009). Mammalian Staufen 1 is recruited to stress granules and impairs their assembly. J Cell Sci *122*, 563-573.

Tyanova, S., Temu, T., Sinitcyn, P., Carlson, A., Hein, M.Y., Geiger, T., Mann, M., and Cox, J. (2016). The Perseus computational platform for comprehensive analysis of (prote)omics data. Nat Methods *13*, 731-740.

Uversky, V.N., Kuznetsova, I.M., Turoverov, K.K., and Zaslavsky, B. (2015). Intrinsically disordered proteins as crucial constituents of cellular aqueous two phase systems and coacervates. FEBS Lett *589*, 15-22.

Van Damme, P., and Robberecht, W. (2009). Recent advances in motor neuron disease. Curr Opin Neurol *22*, 486-492.

Vatsavayai, S.C., Yoon, S.J., Gardner, R.C., Gendron, T.F., Vargas, J.N., Trujillo, A., Pribadi, M., Phillips, J.J., Gaus, S.E., Hixson, J.D.*, et al.* (2016). Timing and significance of pathological features in C9orf72 expansion-associated frontotemporal dementia. Brain *139*, 3202-3216.

Vieira, R.T., Caixeta, L., Machado, S., Silva, A.C., Nardi, A.E., Arias-Carrion, O., and Carta, M.G. (2013). Epidemiology of early-onset dementia: a review of the literature. Clin Pract Epidemiol Ment Health *9*, 88-95.

Webster, C.P., Smith, E.F., Bauer, C.S., Moller, A., Hautbergue, G.M., Ferraiuolo, L., Myszczynska, M.A., Higginbottom, A., Walsh, M.J., Whitworth, A.J.*, et al.* (2016). The C9orf72 protein interacts with Rab1a and the ULK1 complex to regulate initiation of autophagy. EMBO J *35*, 1656-1676.

Wen, X., Tan, W., Westergard, T., Krishnamurthy, K., Markandaiah, S.S., Shi, Y., Lin, S., Shneider, N.A., Monaghan, J., Pandey, U.B.*, et al.* (2014). Antisense proline-arginine RAN dipeptides linked to C9ORF72-ALS/FTD form toxic nuclear aggregates that initiate in vitro and in vivo neuronal death. Neuron *84*, 1213-1225.

Xu, Z., Poidevin, M., Li, X., Li, Y., Shu, L., Nelson, D.L., Li, H., Hales, C.M., Gearing, M., Wingo, T.S., *et al.* (2013). Expanded GGGGCC repeat RNA associated with amyotrophic lateral sclerosis and frontotemporal dementia causes neurodegeneration. Proc Natl Acad Sci U S A *110*, 7778-7783.

Yamakawa, M., Ito, D., Honda, T., Kubo, K., Noda, M., Nakajima, K., and Suzuki, N. (2015). Characterization of the dipeptide repeat protein in the molecular pathogenesis of c9FTD/ALS. Hum Mol Genet *24*, 1630-1645.

Yang, M., Liang, C., Swaminathan, K., Herrlinger, S., Lai, F., Shiekhattar, R., and Chen, J.F. (2016). A C9ORF72/SMCR8-containing complex regulates ULK1 and plays a dual role in autophagy. Sci Adv *2*, e1601167.

Yin, S., Lopez-Gonzalez, R., Kunz, R.C., Gangopadhyay, J., Borufka, C., Gygi, S.P., Gao, F.B., and Reed, R. (2017). Evidence that C9ORF72 Dipeptide Repeat Proteins Associate with U2 snRNP to Cause Mis-splicing in ALS/FTD Patients. Cell Rep *19*, 2244-2256.

Zhang, D., Iyer, L.M., He, F., and Aravind, L. (2012). Discovery of Novel DENN Proteins: Implications for the Evolution of Eukaryotic Intracellular Membrane Structures and Human Disease. Front Genet *3*, 283.

Zhang, K., Donnelly, C.J., Haeusler, A.R., Grima, J.C., Machamer, J.B., Steinwald, P., Daley, E.L., Miller, S.J., Cunningham, K.M., Vidensky, S., *et al.* (2015). The C9orf72 repeat expansion disrupts nucleocytoplasmic transport. Nature *525*, 56-61.

Zhang, Y., Burberry, A., Wang, J.Y., Sandoe, J., Ghosh, S., Udeshi, N.D., Svinkina, T., Mordes, D.A., Mok, J., Charlton, M., *et al.* (2018a). The C9orf72-interacting protein Smcr8 is a negative regulator of autoimmunity and lysosomal exocytosis. Genes Dev *32*, 929-943.

Zhang, Y.J., Gendron, T.F., Ebbert, M.T.W., O'Raw, A.D., Yue, M., Jansen-West, K., Zhang, X., Prudencio, M., Chew, J., Cook, C.N., *et al.* (2018b). Poly(GR) impairs protein translation and stress granule dynamics in C9orf72-associated frontotemporal dementia and amyotrophic lateral sclerosis. Nat Med.

Zhang, Y.J., Gendron, T.F., Grima, J.C., Sasaguri, H., Jansen-West, K., Xu, Y.F., Katzman, R.B., Gass, J., Murray, M.E., Shinohara, M., *et al.* (2016). C9ORF72 poly(GA) aggregates sequester and impair HR23 and nucleocytoplasmic transport proteins. Nat Neurosci *19*, 668-677.

Zhang, Y.J., Jansen-West, K., Xu, Y.F., Gendron, T.F., Bieniek, K.F., Lin, W.L., Sasaguri, H., Caulfield, T., Hubbard, J., Daughrity, L., *et al.* (2014). Aggregation-prone c9FTD/ALS poly(GA) RAN-translated proteins cause neurotoxicity by inducing ER stress. Acta Neuropathol *128*, 505-524.

Zu, T., Gibbens, B., Doty, N.S., Gomes-Pereira, M., Huguet, A., Stone, M.D., Margolis, J., Peterson, M., Markowski, T.W., Ingram, M.A., *et al.* (2011). Non-ATG-initiated translation directed by microsatellite expansions. Proc Natl Acad Sci U S A *108*, 260-265.

Zu, T., Liu, Y., Banez-Coronel, M., Reid, T., Pletnikova, O., Lewis, J., Miller, T.M., Harms, M.B., Falchook, A.E., Subramony, S.H., *et al.* (2013). RAN proteins and RNA foci from antisense transcripts in C9ORF72 ALS and frontotemporal dementia. Proc Natl Acad Sci U S A *110*, E4968-4977.

9. ACKNOWLEDGEMENT

haben die gute alte Zeit im 7. Stock mit spontanen Freitagen entscheidend geprägt an die ich noch heute schmunzelnd zurückdenke.

Vielen lieben Dank auch an alle *Behrendsbrüder*. Sie haben neuen erfrischenden Wind in die Bude gebracht und wesentlich zur tollen Atmosphäre beigetragen. Danke, dass ich mit euch kollaborieren und selbst nach der 100sten LC3B-Frage noch vorbeikommen durfte!

Ich möchte hier auch die *Rolling Stones* nicht vergessen. Danke, dass ihr des Diskutierens nie müde wurdet und für ununterbrochene Unterhaltung gesorgt habt. Danke auch für die Organisation sämtlicher doktorandischer Veranstaltungen. Wenn ihr das lest, dann meckert nicht ob der Deutschen Grammatik, ihr wisst, ich bin Ausländer.

Nicht zu vergessen sind hier auch *Sabine und Marcel* sowie alle Sekretärinnen. Danke, dass ihr meine Bestellungen und den Papierkram gleichermaßen immer im Griff hattet.

Ich danke auch allen *Kollaborationspartnern* für unkomplizierte gemeinsame Projekte. Danke Daniel Hornburg, Jakob Bader, Qiang Guo, Ruben Fernandez-Busnadiego, Marc Suarez, Thomas Arzberger, Irina Pigur, Aga und Susa!

Ein ganz besonderes Dankeschön gilt auch meinen wunderbaren Freunden. Danke an die fetzigen Senioren, die schon seit 10 Jahren in Big Hadern mit mir Freud' und Leid teilen. Danke, dass ihr immer noch mit mir in der Mensa esst, immer noch meine Laborgeschichten anhört, immer noch Feierabend-Bier mit mir trinkt, immer noch meine Verrücktheit aushaltet, einfach immer noch stets für mich da seid. Meinen drei Mädels aus der tollsten Stadt der Welt danke ich dafür, dass sie immer an mich glauben.

Meiner kleinen Familie, Mama, Papa und Harry, danke ich für die unerschöpfliche Unterstützung, das Gut-zu-Reden und den Halt den sie mir geben.

Ich könnte jetzt noch ewig so weiter machen, da es so viele Menschen gibt, denen ich gerne Danke sagen will, aber das würde wohl den Rahmen sprengen. Deshalb möchte ich abschließend einfach allen danken, die mich während meiner Arbeit als Doktorandin in irgendeiner Weise unterstützt haben.

‚Leider läßt sich eine wahrhafte Dankbarkeit mit Worten nicht ausdrücken.'

- Johann Wolfgang von Goethe

10. PUBLICATIONS

Parts of this thesis have already been published.